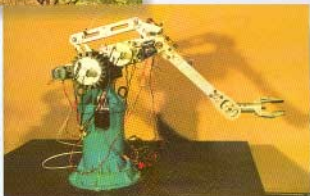
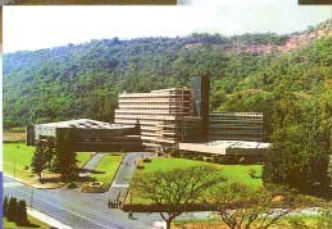


BARC

N E W S L E T T E R

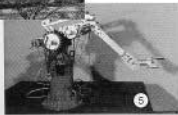
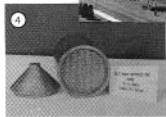
NO 189

OCTOBER 1999



BHABHA ATOMIC RESEARCH CENTRE

BARC
FOUNDER'S
DAY
SPECIAL
ISSUE



- 1) Mass spectrometer for isotopic ratio measurement.
- 2) A view of Central Complex building, BARC.
- 3) High level waste transport cask/placement of vitrified canister in a location at SSSF Tarapur.
- 4) Nb-Ti multifilamentary billet assembly developed at AFD, BARC. It shall produce a 3km single length superconducting wire.
- 5) 5-Axis robot.



The Visionary

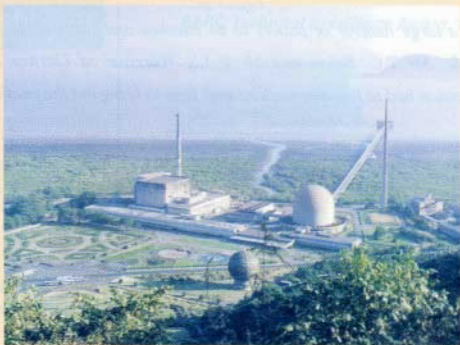
A Homage

The Department of Atomic Energy owes a great debt of gratitude to Dr Homi J. Bhabha whose foresight and vision were responsible for our country reaching an enviable position on the world map of atomic energy. Within a decade of launching its atomic energy programme in 1948, India became one of the first ten most advanced countries in this new and complex technology.

India achieved the distinction of commissioning Asia's first research reactor Apsara in 1956. This reactor was built with indigenous know-how excepting the fuel elements.

(Contd...)

and his vision come true



Today there are 10 nuclear power reactors in operation in India, which totally produce about 1800 MW(e) of power. Although it represents about 3% of the country's total electrical power generation, work is on hand to increase it to about 10% by the year 2020. With the advent of breeder reactors, nuclear power generation is bound to increase significantly in the coming years.

Generating electricity is only one of the many applications of nuclear energy. Radioisotopes produced by our nuclear reactors are widely used in medicine, industry, hydrology, agriculture, healthcare, water resources development and management.

Dr Homi Bhabha was born on October 30, 1909. His birthday every year is observed as the Founder's Day in BARC. On this occasion, the entire fraternity of DAE family remembers with gratitude this great Son of India and a distinguished scientist.

This special issue of BARC Newsletter is being brought out as a homage to the great visionary Dr Homi Bhabha, the architect and founder of India's atomic energy programme.

This issue contains some of the research papers authored by BARC scientists and engineers, and which have won awards on various occasions in the earlier years. A few papers which won awards in 1999 are also included.

With a large number of papers to be checked and re-formatted within a tight time-schedule, Mr T.C. Balan and Mr P.A.S. Warriyar of Library & Information Services Division had to literally work against time to bring out the publication in time.



(Dr Vijai Kumar)

*Head, Library & Information Services Division
Bhabha Atomic Research Centre*

CHIEF EDITOR
Dr Vijai Kumar

MANAGING EDITOR
T.C. Balan

COMPUTER GRAPHICS & LAYOUT
P.A.S. Warriyar

BARC NEWSLETTER

October
1999
No. 189

*BARC Founder's Day
Special Issue*

Bhabha
Atomic
Research
Centre

CONTENTS

- 1 In-house advanced research in material damage modelling
B.K. Dutta
Homi Bhabha Science & Technology Award, 1997
- 22 Uranium recovery from phosphoric acid
Harvinderpal Singh
Homi Bhabha Science & Technology Award, 1997
- 29 Dual sites of electron solvation in microheterogeneous media : a new observation
Hirendra Nath Ghosh
INSA Young Scientist Medal, 1998
- 39 BARCIS (BARC Channel Inspection System)
Manjit Singh
BARC Technical Excellence Award, 1997

BARC NEWSLETTER

on
the
web

Link up with
science!

Available at

URL: <http://www.barc.ernet.in>



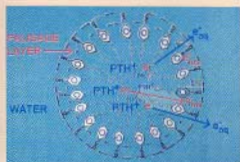
Page 20



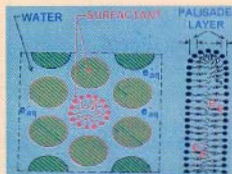
Page 22

CONTENTS (contd...)

- 50 Estimation of transient hydraulic load during Loss of Coolant Accident (LOCA) of a nuclear reactor
D. Mukhopadhyay, Satish K. Gupta and V. Venkat Raj
Dr Wille Memorial Award, 1998 (Best Paper at 1st International Conference on Fluid Mechanics & Fluid Power)
- 62 Concentration of dilute sewage sludge slurry using EB crosslinked fast response temperature sensitive poly (vinyl methyl ether) hydrogel
S. Sabharwal, Y.K. Bhardwaj and A.B. Majali
Best Paper Award at International Conference on Applications of Radiation and Radioisotopes in Industrial Development, 1998
- 66 Evaluation of locally manufactured polyester film (Garfilm-EM) as a dosimeter in radiation processing
R.M. Bhat, U.R. Kini and B.L. Gupta
Best Paper Award at International Conference on Applications of Radiation and Radioisotopes in Industrial Development, 1998
- 69 Characterisation and evaluation of airborne dust associated with mining operation
D.K. Ghosh
Britannia Award, 1998 (International Conference on Occupational Health)
- 75 Measurement traceability in brachytherapy
K.N. Govinda Rajan et al.
Best Paper Award at International Conference on Medical Physics, 1998
- 77 Proposed quality assurance protocol for mammography X-ray system
Kanta Chhokra et al.
Best Paper Award at International Conference on Medical Physics, 1998



Page 31



Page 35

CONTENTS (contd...)

- 79 Tritium in Water Monitor for measurement of tritium activity in the process water
M. Rathnakaran et al.
Best Paper Award at 24th IARP Annual Conference, 1999
- 86 Nondestructive characterisation of MOX fuel rods using Gamma Autoradiography (GAR)
J.P. Panakkal et al.
Best Technical Paper in R&D Award, 1998 (published in Journal of Nondestructive Evaluation)
- 90 Observation of double pulsing in a single mode TEA CO₂ laser caused by the effect of mode pulling and pushing
J. Padma Nilaya and Dhruba J. Biswas
Second Best Presentation Award at XVII Young Physicists Colloquium, 1999
- 95 Elemental analysis of gel grown rare earth crystals by energy dispersive X-ray fluorescence
Daisy Joseph, Madan Lal and P.K. Patra
Best Presentation Award at VIth National Seminar on X-ray Spectrometry and Allied Areas, 1997
- 98 Development of Bedside Vaso-screen at BARC
Shweta Joshi et al.
Second Best Student Paper Award at Conference on Biomedical Engineering, 1999
- 103 Thermal investigations on N,N'dihexyl octanamide complex of uranyl nitrate
P.B. Ruikar et al.
Third Prize at 11th National Symposium on Thermal Analysis, 1998
- 107 Detection of blister formation and evaluation of pressure tube / calandria tube contact location by ultrasonic velocity ratio measurement technique
J.L. Singh et al.
Best Paper Award at 14th World Conference on NDT, 1996

In-house advanced research in material damage modelling

B.K.Dutta

Reactor Safety Division
Bhabha Atomic Research Centre

Introduction

THE SAFETY OF A PLANT IS A STRONG function of the integrity of its structural components. Beside normal operating loads, the structural components experience a significant increase in loading under anomalous scenarios, such as, plant accidents, seismic events, explosions, etc. The structural designers identify the loading histories corresponding to each case to be considered under design specifications. The combinations of loading histories are recommended many times as a part of design specifications. The design is generally carried out using design codes, e.g., ASME Boiler & Pressure Vessel Codes. Some of the limitations of such codal design are that it is not possible to

- i. Exactly quantify the inherent factor of safety available from the point of complete failure of the structural material.
- ii. Ascertain integrity of pressure boundary under large scale loading and deformations.
- iii. Know the mechanical response of a component under the presence of defects of various types subjected to normal operating and accidental loads.

To overcome some of the above limitations, it is necessary to understand the mechanism of material damage under extreme loading scenario and also under the presence of flaws. In the subsequent sections, in-house work carried out in the area of material damage modelling is described.

Material damage modelling during ductile fracture

The general theory of elastic-plastic analysis is based on the theory of material incompressibility during plastic deformations. It means total volume of the material remains constant during the yielding process. Mathematically this is expressed as the sum of the incremental plastic strains in all the three coordinate directions is zero. However, experimental evidences show that such theory is invalid during large-scale damage of the material leading to ductile fracture. The following are the four stages during such phenomena.

- i. The initiation of a large number of voids in the material during initial phase of the damage. Such initiations occur either from the existing micro voids or from the cracking/matrix-detachment of the secondary particles. Such process of void

initiation tends to get saturated after some amount of material damage.

- ii. The next phase is the growth of voids up to a critical value till the adjoining voids become too close.
- iii. The third stage is the coalescence of adjoining voids. This stage leads to the formation of macro voids, which have a tendency to grow rapidly.
- iv. The fourth and the last stage is the fracture of material when the size of macro voids reaches a critical value.

There are number of constitutive models available in the literature to address such mechanism. One of these models is due to Gurson. The modified version of this model is popularly known as Gurson-Tvergaard-Needleman model. Based on the work of Berg (which shows that a porous medium is governed by the normality rule), Gurson derived approximate yield functions for materials containing either cylindrical or spherical voids. For the case of spherical voids with void volume fraction V , the yield function ϕ is given by:

$$\phi(\sigma_{ij}, \sigma_M, f) = \frac{\sigma_{eq}^2}{\sigma_M^2} + 2 \cdot f \cdot q_1 \cosh\left\{\frac{q_2 \sigma_k^k}{2\sigma_M}\right\} - \left\{1 + q_3 (f^*)^2\right\} = 0$$

where $\sigma_{eq} = \left(\frac{3}{2} s_{ij} s_{ij}\right)^{1/2}$ is the macroscopic

effective stress and $s_{ij} = \sigma_{ij} - \frac{1}{3} \sigma_{kk} \delta_{ij}$

represents the stress deviator. The actual microscopic (defect free) stress state in the matrix material is represented by an equivalent flow stress ' σ_M '. The above yield function reduces to von-mises flow criterion for f equals to zero. The function f is given by

$$f = f \quad \text{for } f < f_c$$

$$= f_c + \frac{f^* - f_c}{f_f - f_c} (f - f_c) \quad \text{for } f \geq f_c$$

The second form of f is introduced to artificially model rapid increase in void volume fraction after void coalescence. The constant q_1 , q_2 and q_3 are adjusted to have better agreement with the experimental values.

The increase in void volume fraction f consists of the nucleation of new voids and the growth of existing voids. Hence

$$\dot{f} = \dot{f}_{\text{nucleation}} + \dot{f}_{\text{growth}}$$

The increase in void fraction due to growth can be calculated by using plastic incompressibility condition of the matrix material. This is given by

$$\dot{f}_{\text{growth}} = (1 - f) \delta_{ij} \eta^{p}_{ij}$$

where δ_{ij} is the kronecker delta function and η^{p}_{ij} is the plastic strain tensor. For calculating the void growth due to nucleation, an empirical relation was proposed by Needleman and Rice. This is given by

$$\dot{f}_{\text{nucleation}} = A \sigma_M + 1/3 B \sigma'_{kk}$$

where σ_M is the actual flow stress of the matrix material and σ'_{kk} is the first stress invariant. Due to the interaction effects between particles and the scatter in the

size, shape and spacing of the particles, statistical distributions were used to describe the nucleation of voids. Chu and Needleman[8] proposed a normal distribution for the rate of void nucleation where A and B are as given below. Assuming that nucleation only depends

$$A = B = \left(\frac{1}{E_t} - \frac{1}{E} \right) \frac{f_N}{s_N \sigma_y \sqrt{2\pi}} \exp \left[-\frac{1}{2} \left(\frac{\sigma_M + \frac{1}{3} \sigma_t^k - \sigma_N}{s_N \sigma_y} \right)^2 \right]$$

Here f_N is the volume fraction of void nucleating particles, σ_y is the yield stress of the matrix material and s_N is standard deviation of stress over which most of the voids nucleate. It is important to note that this criterion which is derived on the basis of a critical stress at the interface of the particle is a function of the plastic strain in the material as the stress is produced by local work hardening. So this failure criterion refers fundamentally to strain. Therefore a similar idealization can be made for the mean equivalent plastic strain ' ε_N ' at which nucleation occurs. For strain controlled nucleation,

$$A = \left(\frac{1}{E_t} - \frac{1}{E} \right) \frac{f_N}{s_N \sqrt{2\pi}} \exp \left[-\frac{1}{2} \left(\frac{\varepsilon_M^p - \varepsilon_N}{s_N} \right)^2 \right] ; B=0$$

where s_N is standard deviation of the mean equivalent plastic strain and ε_M^p is equivalent plastic strain of the matrix material.

By decomposing stresses into hydrostatic and deviatoric parts and plastic strain increment into volumetric and deviatoric parts, one may write the following relations

on the stress transmitted across the particle-matrix interface, there exists a mean critical stress for nucleation, ' σ_N ' and the nucleation stress is normally distributed.

- For stress controlled nucleation,

$$\sigma_{n+1} = -P_{n+1} I + S_{n+1} = -P_{n+1} I + \frac{2}{3} q n_{n+1}$$

$$\Delta \varepsilon^p = \Delta \varepsilon_v^p + \Delta \varepsilon_D^p$$

Here 'P' is the first stress invariant, 'q' is the second stress invariant, ' n_{n+1} ' is the unit vector in the deviatoric space normal to the yield surface, S is the deviatoric stress, $\Delta \varepsilon_v^p$ and $\Delta \varepsilon_D^p$ are the volumetric and deviatoric parts of plastic strain increment respectively. A formula for explicitly calculating the consistent tangent moduli for mid-point algorithms has been given by Zhang. We have implemented this algorithm in our code and it has been used to solve the problems with Euler's backward algorithm. This method does not encounter convergence difficulty when the void volume fraction at a gauss point experiences complete damage. Another significant advantage of this methodology is that no matrix inversion is required to obtain consistent tangent moduli expression. The explicit expression of consistent tangent moduli at the end of the solution step t_{n+1} is based on Zhang's seven constant formula. This is given as:

$$D^{consistent} = \left(\frac{\partial \sigma}{\partial \varepsilon} \right)_{n+1} = d_0 J + d_1 I \otimes I + n_{n+a} \otimes (d_2 n_{n+a} + d_3 n_{n+1}) + d_4 n_{n+a} \otimes I + I \otimes (d_5 n_{n+a} + d_6 n_{n+1})$$

where the seven constants are given by:

$$d_0 = \frac{2G}{1 + 3G\alpha\Delta\varepsilon_q / q_n}, d_1 = K - \frac{d_0}{3} - 3K^2 D_{11}, d_2 = -d_0^2 \frac{q_{n+a}}{q_n} D_{22}, d_3 = -d_0^2 \frac{q_{n+a}}{q_n} D_{23},$$

$$d_4 = -3d_0 K D_{21} \frac{q_{n+a}}{q_n}, d_5 = -d_0 K D_{12}, d_6 = -d_0 K D_{13}$$

Here 'G' is the shear modulus of elasticity, 'K' is the bulk modulus, ' $\Delta\varepsilon_q$ ' is deviatoric part of strain increment, D_{11} , D_{12} , D_{13} , D_{21} , D_{22} , and D_{23} are constants.

An in-house finite element based code *MADAM* (MAterial DAamage Modeling) has been developed based on the above principles of continuum damage mechanics [1-2]. The code has the ability to solve both two and three-dimensional structures. The geometric non-linearity is considered by using the updated *Lagrangian* formulation. The deformation and rotation in elastic-plastic analysis is considered by transforming the computed *cauchy* stress to *Jaumann* stress rate using the corresponding *spin rate tensor*. The *frontal* solution technique is used for solving linear set of simultaneous equations. The load-deformation equilibrium conditions are obtained by using *Modified-Riks* Algorithm. An element in the finite element model is considered damaged when the void volume fractions at its gauss points reach the experimental void volume fraction at rupture. For integrating the elastic-plastic constitutive equation with the pressure dependent Gurson-Tvergaard yield model, the *generalised mid-point* algorithm formulated by Zhang has been used.

The code has been tested analyzing number of tensile, C-T and other fracture specimens. This code has recently been used in an international round robin exercise on 'Round Robin on Micro-Mechanical Models, Phase II, Task A', conducted by European Structural Integrity Society. As a part of this exercise, tensile and C-T specimens of two German materials were analyzed to obtain load-displacement and J-R curves. The computed values showed excellent agreement with the experimental data. Fig. 1 shows the load-displacement data of two grooved ($r=4\text{mm}$ and $r=10\text{mm}$) tensile specimens up to the point of complete rupture for a German material designated as DIN StE 460. The load-displacement and J-R curves of a C-T specimen of the same material are shown in Fig. 2. A comparison between computed J-R curves of various fracture specimens is shown in Fig. 3. The effect of stress triaxiality on J-R curve is demonstrated in this figure.

Analysis of cleavage fracture of reactor structural material

The mechanism of a cleavage fracture in reactor structural material is significantly different from ductile

fracture. The cleavage fracture in a material usually originates from the micro-cracks, which are formed by different mechanisms. The micro-cracks are formed due to an inhomogeneous distribution of plastic deformation within the grains, called slip-initiated cleavage. In mild steels, the cracked grain boundary carbides also originate the micro-cracks. This occurs when the stress normal to the planes of carbide particles is sufficiently high. Based on the weakest link assumption and *Weibull statistics*, *Beremin* developed a model for analysing brittle fracture process by local approach. The two parameters of the model are material properties and can be determined from notched tensile tests at low temperatures and their finite element analysis. Once these parameters are determined, these can be used to predict probability of cleavage fracture initiation in a component. The fracture probability of the entire structure follows a two-parameter distribution function given by

$$P_f(\sigma_w) = 1 - \exp\left[-\left(\frac{\sigma_w}{\sigma_w}\right)^m\right]$$

where σ_w is the scaling parameter to describe the point of distribution function on the stress axis at $\ln[1/(1-P_f)]=0$. This gives $P_f=0.632$, i.e. 63.2 % failure probability. The 'm' is the Weibull exponent or Weibull modulus or the shape parameter which describes the scatter of the distribution. The Weibull stress, σ_w , is defined as follows by a summation of the maximum principal stresses σ_i ,

$$\sigma_w = \sqrt[m]{\sum_{i=1}^n (\sigma_i^{(i)})^m} \frac{V_i}{V_0}$$

Since plastic deformations are a prerequisite for cleavage fracture, the summation is taken over the plastically deformed part of the volume only. Hence, n_{pl} is the number of elements experienced plastic deformations. The Weibull parameter σ_w depends on the choice of reference volume V_0 .

The values of 'm' and σ_w are generally determined using *Maximum Likelihood Method*. In this approach, the values of the two parameters are adjusted such that there is 'most likely' representation of experimental data by Weibull function. The maximum likelihood function is the product of all fracture probabilities of experimental data. This is given by

$$F_L = \prod_{i=1}^N f(\sigma_{w_i})$$

This function is maximised to obtain Weibull parameters. This is done equating the partial derivatives of F_L with respect to 'm' and σ_w to zero. One obtains the following two equations by this exercise.

$$\sigma_w = \sqrt[m]{\frac{1}{N} \sum_{i=1}^N (\sigma_{w_i})^m}$$

$$\frac{N}{m} + \sum_{i=1}^N \ln(\sigma_{w_i}) - N \frac{\sum_{i=1}^N (\sigma_{w_i})^m \ln(\sigma_{w_i})}{\sum_{i=1}^N (\sigma_{w_i})^m} = 0$$

These two nonlinear equations are solved iteratively to obtain the values of 'm' and σ_w . A post-processor has been developed to calculate Weibull parameters based on above theory [3]. The inputs to the processor are the experimental and finite element analysis data and outputs are the Weibull parameters. As a part of International round robin exercise, conducted by ESIS, we have used this

post-processor to calculate Weibull parameters for number of cases. The notched tensile tests at -150°C were carried out at *GKSS Institute for Material Research, Germany*. The data were available to us as a part of this round robin exercise. Thirty-two numbers of specimens were tested in all. The specimens were machined from a forged ring segment. The specimens were subjected to a quasi-static displacement controlled loading in axial direction. The loading rate was $0.2\text{mm}/\text{min}$. All specimens failed by unstable fracture and the fracture surfaces show pure cleavage facets. The load v/s reduction in diameter (ΔD) curves of the specimens up to the point of fracture were made available. The notched tensile specimens were numerically analysed in order to determine the two critical parameters for cleavage fracture at low temperature. The finite element analyses of all the tensile specimens were done using an in-house code *THESIS*. Eight-noded iso-parametric quadratic elements with reduced order integration were used in the analysis. Loading is applied as homogeneously prescribed displacements in axial direction at the top edge of the model. A large strain analysis based on updated Lagrangian formulation is used in the code. The task was divided into two parts. Part-I is concerned with the application of Beremin's model to a set of seven numbers of specimens taken out of a limited region of the material block and which show a nearly identical load deformation behaviour up to their respective fracture points. Hence, these specimens were analysed using one representative true stress-strain curve. The specimens were ranked separately according to both the load as well as ΔD at fracture points. The Weibull parameters

were then calculated using the above post processor. The values of the parameters were $m=68.15$ and $\sigma_v=1859.98\text{ MPa}$ when diametral contraction was taken as ranking parameter. The same values were $m=48.0$, $\sigma_v=1975.0\text{ MPa}$ in case of load at fracture was taken as ranking parameter. Fig. 4 shows a comparison between experimental and numerical load- ΔD curves. Fig.5 shows a comparison of probability of failure between experimental and numerical values for ' m '=48.0.

Part-II deals with the entire set of experimental results (32 specimens). All the specimens were analysed separately with separate stress-strain data in order to match the numerical load- ΔD curves with experimental ones. In this case the computed Weibull parameters were $m=18.15$ and $\sigma_v=2875.5\text{ MPa}$.

Two parameter characterisation of the crack tip

Crack initiation and stable crack growth in a ductile material are usually described by J-R curves obtained from standard fracture specimens. Such theory is based on that a single parameter (J-integral) can be used to characterize the crack tip and a single fracture resistance curve is sufficient to characterize the material. However, there is growing evidence to show that J-R curves are geometry dependent. Therefore, the transferability of specimen J-R curve to component level is an unresolved issue, which is currently receiving a lot of attention among structural researchers. The influence of crack tip constraint or stress triaxiality on ductile fracture emphasized recently in explaining the geometry dependent fracture resistance of

specimens and structures to ductile tearing.

In most cases, standard ASTM specimens maintain high constraint even up to high load levels. The ASTM standards require sufficient thickness of the specimen to ensure predominantly plane strain conditions at the crack tip and a crack depth of at least half of the specimen width. Within certain limits on load level and crack growth, these restrictions ensure the existence of high constraint conditions for fracture as described by the HRR field equation and satisfy the validity of single parameter characterization. However, real structures may be low constraint geometries. This difference between crack tip constraint between specimens and structures indicates that structures can often carry greater loads without failure than predicted using fracture toughness values measured from high constraint specimens. This introduces a high degree of conservatism into the design. On the other hand, the application of toughness data from low constraint specimen geometry to structural applications with high constraint crack geometry makes the design unsafe.

Although there is no doubt that the resistance against ductile tearing depends on the crack tip constraint, the issue still to be addressed is how to define and quantify this parameter. Different definitions and measures are in use and the two parameter fracture mechanics has emerged as the most acceptable theory. Most of these approaches involve the introduction of a second parameter to characterize the crack tip constraint conditions.

THEORY-I One of the theories utilizes the elastic T-stress as the second parameter

for predicting fracture. This J-T approach has limited use in the elastic-plastic region as it is based on elasticity theory.

THEORY-II A physically significant definition of the triaxiality of the stress-state resulting from a crack tip constraint is given by the triaxiality factor (h). This is defined as the ratio of hydrostatic stress (σ_h) to the von-Mises stress (σ_e). Hence $h = \sigma_m / \sigma_e$. If σ_1 , σ_2 & σ_3 are the three principal stresses then

$$\sigma_m = (\sigma_1 + \sigma_2 + \sigma_3) / 3.0 \quad \text{and} \\ \sigma_e = \{(\sigma_1 - \sigma_2)^2 + (\sigma_2 - \sigma_3)^2 + (\sigma_3 - \sigma_1)^2\}^{1/2} / \sqrt{2}.$$

The physical meaning of this ratio was that the growth rate of cavities in perfectly plastic material is mainly influenced by 'h'. High constraint is associated with the high value of 'h'. It was found that the slopes of the J-R curve decreases with the increase in stress triaxiality.

THEORY-III The stress triaxiality or crack tip constraint can also be quantified by the multiaxiality quotient 'q'. This is defined as $q = \sqrt{3} \sigma_e / \sigma$. Low 'q' value signifies according to this definition for a high degree of stress triaxiality. This quotient can be determined from finite element calculations for specimen and component. A Comparison of the 'q' values helps to assess the similarity between the fracture characteristics of a specimen and component.

THEORY-IV Another theory introduces a parameter 'Q' to quantify the crack tip constraint. As per this theory, the laboratory specimen must match the constraint of the component i.e. two geometries must have the same Q-value at failure in order to have the same fracture resistance. The non-dimensional parameter, 'Q' is defined as,

$$Q = [\sigma_{\theta\theta} - (\sigma_{\theta\theta})_{ref}] / \sigma_0 \text{ at } \theta = 0^\circ\text{-}90^\circ, \\ r = 2J / \sigma_0.$$

Here, r and θ are polar co-ordinates at the crack-tip. $\sigma_{\theta\theta}$ is the existing stress field ahead of the crack-tip of the actual geometry, $(\sigma_{\theta\theta})_{ref}$ is the reference solution obtained from the standard plane strain small scale yielding solution $(\sigma_{ij})_{SSY,T=0}$ or HRR field.

A negative Q -value means that the hydrostatic stress is lower than the reference field ($Q = 0$ state) and vice versa. Geometries with negative Q -value show low stress triaxiality ahead of the crack tip and loss of J -dominance. The geometries with $Q \geq 0$ show high triaxiality ahead of crack tip and good agreement with the HRR or SSY fields. Thus, the Q -value provides a framework for quantifying the constraint to plastic flow from small scale yielding to fully yielded conditions. In this present study [4-5], a detailed finite element analyses have been carried out on conventional laboratory specimens like Centred Cracked Panel (CCP), Three Point Bend Bar (TPBB) and Compact Tension (CT) specimen. The characteristics of the crack-tip constraint parameters, ' Q ' and ' h ' have been studied. Fig.6 shows the variation of ' Q ' parameter with loading for two different sizes of crack depths. It is observed that the constraint loss is gradual with the increase in deformation level for CCP irrespective of crack depth. However, the same is true only for shallow cracked TPBB & CT geometries. Conversely, deeply cracked TPBB & CT geometries maintain high degree of constraints to fairly high deformation levels. This figure also shows the crack tip constraints in axisymmetric circumferentially flawed pipe (CFP). The two different loading conditions have been analysed. These are

(i) CFP under axial pull (ii) CFP under internal pressure and axial pull. It is found that axisymmetric CFP under internal pressure exhibits lower constraint than pure axial pull. The radial compressive stresses resulting from internal pressure is believed to reduce the constraint.

Probabilistic material damage modelling under pressurised thermal shock

One of the most important high temperature transients, which may jeopardise the safety of a Pressurised Water Reactor (PWR), is the sudden cooling of the hot reactor vessel under accidental condition. This phenomena is commonly known as Pressurised Thermal Shock (PTS). Such a scenario leads to very high stresses in the component leading to tearing of the vessel wall under the presence of a small flaw at the weld region [6]. The reactor vessel of a PWR may be subjected to such condition during a Loss of Coolant Accident (LOCA) with a delay in the Emergency Core Cooling System (ECCS). The vessel wall just below the ECCS nozzle may experience a large scale PTS. Three conditions appear to be necessary for tearing out of the reactor vessel wall during such a scenario.

(i) A large upward shift in the Nil Ductility Transition (NDT) temperature of the near core weld material due to a combination of nuclear irradiation during service and the presence of high copper and nickel content in the vessel welds. (ii) The existence of an initial flaw on or under the inner surface of the vessel near core weld material. (iii) A severe over-cooling transient caused by the injection of cold water on the inner surface of the vessel by

the activation of the emergency core cooling system during LOCA.

It should be recognised that, while LOCAs have occurred during reactor operation (e.g. Three Mile Island II), no catastrophic fractures of nuclear reactor pressure vessels have been experienced as all these three conditions did not occur simultaneously. Nevertheless, such analyses are very important to demonstrate the vessel integrity under severe abnormal conditions, thus confirming the avoidance of large scale core melt down and release of radioactive materials in public domain. A conservative set of material properties to guard the pressure vessel under such a scenario has been provided in the regulatory guide, i.e., ASME, Boiler and Pressure Vessel Code. However, research work in different parts of the world is being conducted to acquire better insight into this problem.

The pressure vessels used in nuclear industry are exposed to additional hazards due to neutron irradiation. In an operational reactor, the pressure vessel material undergoes neutron embrittlement. Due to this, the toughness of the material decreases. This is further compounded by the increase in the nil ductility transition temperature (NDT) of the material. Both these factors contribute to the reduction in safety margin against brittle failure of the structural material. It is necessary to examine whether such a reduction in safety margin compounded with the sudden cooling due to a LOCA followed by injection of cold water may cause a failure of the pressure vessel, especially in the presence of a flaw. A fracture mechanics based integrity analysis keeping in view of the degraded fracture resistance of the embrittled vessel is required to ensure safety.

The deterministic analysis [7] makes use of a number of inputs, which have certain degrees of uncertainties. The ultimate conclusions drawn from the deterministic analysis may be affected by these uncertainties. Hence it is necessary to calculate the probabilities of occurrence of different events during a PTS scenario. A crack in the high tensile stress zone under such pressurised thermal shock scenario may experience three different states depending upon the initial size of the crack, material properties and severity of the thermal shock. In the first case the propagation of the crack may not initiate throughout the transient. The second state pertains to the initiation followed by arrest after some penetration of the vessel thickness. In the third state, the propagation after initiation is not arrested and leads to the complete penetration of the vessel thickness. The objective of the probabilistics analysis is to compute the conditional probability of crack initiation and the probability of reactor vessel failure considering uncertainties in various inputs.

To calculate probabilities of crack initiation and vessel failure, one has to first carry out the deterministic fracture mechanics analysis of number of cracks having different initial crack lengths for the entire thermal transient history. Such analysis can be done either by using influence technique or by using detailed finite element technique. Outputs of such analysis are the variation of the crack tip temperature and the crack tip stress intensity factor (SIF) with time of the thermal transient. A large number of such tables are generated by varying the initial crack length and serve as input data base for the probabilistic analysis code. In the probabilistic calculations, first an initial crack is assumed on the inner surface of

the vessel. The size of the crack is decided by using a cumulative distribution function. The possibility of crack propagation during the entire period of thermal transient is then checked. The deterministically calculated applied SIF and crack tip temperature are used for this purpose. The material toughness (K_{IC}) is calculated depending upon the crack tip temperature and reference nil ductility temperature transient (RT_{NDT}). The RT_{NDT} in turn depends upon the copper content, nickel content and fluence level. These parameters at the crack tip may be simulated from a normal (Gaussian) distribution with a mean value and standard deviation as shown in Fig. 7. If the applied SIF is found to be less than K_{IC} , the crack is assumed to be stable in the present time step and one may proceed for the next time step of the thermal transient. In case applied SIF is found to be more than the K_{IC} , the crack is assumed to propagate during the present time step. The size of the crack is incremented by a small length and fracture arrest toughness (K_{Ia}) is calculated based on probabilistically simulated RT_{NDT} . If the K_{Ia} is more than the applied SIF, the crack is arrested and one may proceed for the next time step. In case K_{Ia} is less than the applied SIF, the crack length is further incremented in the present time step and rechecked for the crack arrest. Such procedure is repeated for the entire time history. At the end of the time history, the state of the crack in terms of no-initiation, initiation with arrest or propagation throughout the vessel thickness is noted. This methodology is repeated for a large number of simulated initial crack-length. The conditional probability of crack initiation is estimated by dividing the number of cracks that experienced

initiation by the total number of cracks simulated. Similarly, the conditional probability of vessel failure is calculated by dividing the number of cracks that penetrated the entire thickness of the vessel by the total number of cracks simulated. The probabilities are conditional in the sense that the transient is assumed to occur.

As a part of the participation in an International Assessment Study, a computer code 'PARISH' (Probabilistic Assessment of Reactor Integrity under thermal Shock) has been developed based on the above methodology. The code makes use of the Monte Carlo technique to calculate the probabilities of crack initiation and vessel failure. A large number of initial cracks of different length are simulated during each failure assessment. The final probability is calculated dividing the number of cracks that experience an event by the total number of cracks simulated. Some of the salient features of this code are as follows.

Simulation of Initial Flaw Depth : It has been observed that the accuracy with which the conditional probability of initiation and failure are calculated, depend somewhat on the number of discrete points used to describe the initial flaw depth distribution function. However, the results of the analyses showed no appreciable difference in the probability values beyond 15 values of discrete initial flaw depths. Hence, in the present code 15 discrete initial flaw depths are used to describe initial flaw depth distribution. The flaws are assumed to lie on the inner two inches of the vessel wall according to the MARSHALL flaw depth cumulative distribution function given by $CDF(a) = 1.0 - \exp(-4.06 a)$. Here, a is the flaw depth (inches) and $CDF(a)$ is the

cumulative distribution function. A random number varying between 0 to 1 is generated. If value of the number lies between CDF(a) and CDF(a+Δa), then initial flaw depth is assumed to be 'a'.

Fracture Initiation Toughness (K_{IC}): The ASME curve of K_{IC} is used to calculate the material fracture initiation toughness. However, the ASME curve is conservatively defined as 70% of the experimentally determined $(K_{IC})_{mean}$. Hence $(K_{IC})_{mean}$ is calculated by $(K_{IC})_{mean} = 1.43 \times ASME K_{IC}$. The probabilistic variation of $(K_{IC})_{mean}$ at the crack tip is considered by using the expression $K_{IC} = err(K_{IC}) \times (K_{IC})_{mean}$. The $err(K_{IC})$ is sampled from a Gaussian (normal) distribution that has a mean value of 1 and a standard deviation of 0.15. The value is truncated at $\pm 3\sigma$. Therefore, $err(K_{IC})$ varies between 0.55 and 1.45. This value is simulated at each new crack tip position.

Fracture Arrest Toughness (K_{Ia}): The ASME curve of K_{Ia} is used to calculate the material fracture arrest toughness. However, the ASME curve is conservatively defined as 70% of the experimentally determined $(K_{Ia})_{mean}$. Hence, $(K_{Ia})_{mean}$ is calculated by $(K_{Ia})_{mean} = 1.43 \times ASME K_{Ia}$. The probabilistic variation of $(K_{Ia})_{mean}$ at the crack tip is considered by $K_{Ia} = err(K_{Ia}) \times (K_{Ia})_{mean}$. The $err(K_{Ia})$ is sampled from a Gaussian (normal) distribution that has a mean value of 1 and a standard deviation of 0.15. The value is truncated at $\pm 3\sigma$. Therefore, $err(K_{Ia})$ varies between 0.55 and 1.45. This value is simulated at each new crack tip position.

Computation of RT_{NDT} : The simulated value of RT_{NDT} is given by

$$RT_{NDT} = RT_{NDT0} + \Delta RT_{NDT} + err(RT_{NDT}) \times \sqrt{[(\sigma_{RT_{NDT0}})^2 + (\sigma_{\Delta RT_{NDT}})^2]}$$

Here RT_{NDT0} is the mean value of unirradiated RT_{NDT} . ΔRT_{NDT} is the increase in RT_{NDT} due to irradiation induced embrittlement. This value is a function of copper, nickel and the neutron fluence at the crack tip. Procedure to calculate ΔRT_{NDT} is taken from Regulatory Guide 1.99, Revision 2. This is described in the following subsection. The $\sigma_{RT_{NDT0}}$ is the standard deviation for the mean value of RT_{NDT0} and $\sigma_{\Delta RT_{NDT}}$ is the standard deviation for the correction used to predict ΔRT_{NDT} . The $err(RT_{NDT})$ is sampled from a Gaussian distribution with a mean value of zero and a standard deviation of one and is truncated at $\pm 3\sigma$. This value is simulated once per vessel. It may be noted here that due to independency of $\sigma_{RT_{NDT0}}$ and $\sigma_{\Delta RT_{NDT}}$, these values are combined as the square root of their sum.

Procedure to calculate ΔRT_{NDT} from Regulatory Guide 1.99, Rev. 2: As explained above the computation of the RT_{NDT} requires the increase in RT_{NDT} due to irradiation induced embrittlement. This value is calculated using the Regulatory Guide 1.99, Rev.2. The increase in RT_{NDT} is expressed as

$$\Delta RT_{NDT} = C_1 \times \Phi_c^{(0.28 - \log^{0.07} / 10.0)}$$

Here Φ_c is the neutron fluence at the tip of the crack. The coefficient C_1 depends upon the percentage of copper and nickel at the crack tip.

Simulation of neutron fluence: Neutron fluence at the vessel inner surface Φ_v is simulated from a normal distribution with mean values from 0.3 to 3.5 $\times 10^{19}$ neutrons / cm^2 . The value of one standard deviation is equal to 30% of the respective mean value. The simulated value of Φ_v must lie in the range 0.0 to 10 $\times 10^{19}$. The fluence attenuation at the

tip of the crack is calculated by $\Phi_c = \Phi_v \times \exp(-0.24a)$. Here 'a' is the length of the crack.

Simulation of Copper : Copper is simulated at the tip of the crack from a normal distribution with a mean value of 0.3%. The value of one standard deviation is equal to 0.025%. The simulated value of copper must lie in the range $0.0 \leq Cu \leq 0.40$.

Simulation of Nickel : Nickel is simulated at the tip of the crack from a normal distribution with a mean value of 0.75%. The value of one standard deviation is equal to 0.1%. The simulated value of nickel must lie in the range $0.0 \leq Ni \leq 1.20$.

The code 'PARISH' is written using FORTRAN-90 and is commissioned on PC as well as on DEC-ALPHA computers [8]. The code is thoroughly tested against the benchmark cases reported from literature. Reactor Safety Division of BARC recently participated in an International Round Robin exercise PTS-ICAS conducted by GRS (Germany). As a part of this exercise the code 'PARISH' was used for probabilistic assessment of a pressure vessel subjected to PTS. There were four cases in this study. These are designated as PFM-1 to PFM-4. The cases are as follows.

- PFM-1: Axial Crack Experiencing a Simplified Thermal Transient.
- PFM-2 :Circumferential Crack Experiencing the transient of PFM-1.
- PFM-3 : Axial Crack Experiencing Thermal Transient corresponding to a Small Break LOCA
- PFM-4 : Circumferential Crack Experiencing the transient of PFM-3.

The probabilities of crack initiation and vessel failure were calculated for the cases PFM-1 to PFM-4 for surface fluence

level from 0.3×10^{19} to 3.5×10^{19} . The variations of these probabilities are shown in Fig. 8.

Experimental programme on flawed piping components

The in-house advanced research programme on material damage modelling is supported by experimental programme on real life structures. Under this programme, actual PHT piping components are tested with through-the-thickness and part-through flaws under four point bending loads. The 45 tests have been planned on pre-cracked straight pipes and elbows in order to determine the component J-R curves. The sizes of pipes and elbows range from 8 inch to 16 inch in diameter and thickness vary from 0.75 inch to 1.5 inch. The material of the pipes and elbows is SA333Gr6 (or SA106GrB). The notched test specimens are fatigue pre-cracked by small prior to performing the experiment. This ensures a sharp crack tip. During the fatigue pre-crack, sinusoidal cyclic load is applied. The maximum cyclic load is approximately 10% of the collapse load and minimum cyclic load is 10% of the maximum load.

The tests are conducted using computer controlled servo-hydraulic actuator of ± 1000 kN capacity. Fig. 9 shows the test set-up. The pipe is supported over a span of 4 and 5.82 m. in case of 8 and 16 inch diameter pipes respectively. Steel pedestals are used to support the pipes. A distribution beam with rollers is used to apply two concentrated loads on the pipe over a distance of 1.48 m. The servo-hydraulic actuator is fixed to a reaction frame of ± 1000 kN dynamic capacity which is connected to the distribution beam by

suitable plates and tie rods. The actuator system consists of an in-built LVDT for control of displacement. Static monotonic load is applied on the pipe specimens under displacement control. The rate of displacement is fixed at 0.055 mm/sec. In order to facilitate re-arrangement and re-focusing of cameras during the test, the entire fracture test is programmed in such a way that displacement is applied gradually for three minutes followed by three minutes of holding time. A HP computer is interfaced with the controller of the actuator, through which the load history is controlled using block programming. Since the actuator has a maximum displacement of 100 mm, the test is programmed to stop after reaching the maximum displacement using the limit switch of the controller. The test is again continued after adjusting the displacement of the actuator using manual control and by providing packing plates at the loading points. The recorded data are (i) Applied load (ii) Load line displacement (iii) ACPD measurement at the crack tip (iv) Crack opening displacement at various locations of the notch (v) Crack growth and (vi) Deflection of pipe at typical locations. Fig 7 also shows the load v/s COD data for fracture tests of 8" diameter straight pipe with through-wall circumferential crack of 126°. Such experimental results are being used to generate component level J-R curves to obtain transferability relation. These relations are very useful in Leak-Before-Break qualification of PHT piping components [9]. The experimental data are also used to verify analytical calculations of piping components with flaws [10].

On-line material damage monitoring of plant components

Recently the issue of remaining life prediction has attracted considerable attention. The vast interest in the area of remaining life prediction arises from the need to avoid costly forced outages, safety considerations and the necessity to extend the component operation life beyond the original design life. Many of the structural components used in fossil power plant, nuclear industry, chemical process plants, etc. are subjected to cyclic stresses due to the fluctuation of process transients. On the other hand components like steam pipes, super-heater headers, turbine rotors, casings, etc. operate at elevated temperature. The fluctuating stresses at an elevated temperature lead to material damage mechanism due to combined creep and fatigue. It is worth to note that among the various aging effects, fatigue, creep and creep-fatigue interaction are commonly responsible for most of the failures in various industrial components. Thus there is a need to develop a life prediction methodology to address the various aspects of failure mechanisms.

An on-line fatigue-creep monitoring system has been developed to monitor these aging effects of the components used in industries [11]. The system acquires the process transients, such as, pressure, temperature and flow rate, through a data recording system. The recorded data are initially screened based on the severity of the transients. The temperature transients and the thermal stresses of the structure due to the fluctuation of the process transients are computed using the finite element method. The stresses due to mechanical loading (internal pressure) and system

induced loading (piping loads) are computed using a transfer function approach. The stress time history is converted to stress frequency spectrum using rain-flow cycle algorithm. The fatigue usage factor is computed using ASME material fatigue curve. The creep damage index is evaluated from the computed temperature and stress histories and the material creep curve. To account for the combined damage mechanism, the damage accumulation approach is adapted.

The system is implemented at Heavy Water Plant, Kota [12-13] and will be shortly implemented at HWP, Tuticorin. At HWP Kota, the system is monitoring the fatigue degradation of three components. The selected components are shell nozzle junctions connected to hot tower and waste stripper tower. The recorded data are processed everyday to evaluate the fatigue damage. The system at HWP, Tuticorin will monitor the fatigue degradation of the three components of the drier loop. The performance of the system is satisfactory. It is capable of monitoring the degradation of several components of a plant using a single P.C. The information provided by the system is helpful in life extension program of the plants. The system is also found to be useful for thermal power plants, nuclear power plants, chemical process industries, etc. Fig. 10 shows the recorded and the computed data stored by this code over the time of plant operation at HWP Kota.

References

1. Samal M.K., Dutta B.K., Kushwaha H.S., "A study on ductile fracture initiation in the PHT piping material of an Indian PHWR using local approach", *International Journal of Pressure Vessels & Piping*, Vol. 76, 1999, pp.319-330.
2. Samal M.K., Dutta B.K., Kushwaha H.S., "Prediction of J_R curves of various fracture mechanics specimens using Gurson-Tvergaard model", *Engineering Fracture Mechanics (Communicated)*, 1999.
3. Samal M.K., Dutta B.K., Kushwaha H.S., "Determination of critical Weibull parameters for brittle fracture of a ferritic steel at low temperature", *International Journal of Pressure Vessels & Piping (Communicated)*, 1999.
4. T.V.Pavankumar, J.Chattopadhyay, B.K.Dutta and H.S.Kushwaha, "A Study on characteristics of crack tip constraint parameter 'Q' in two dimensional geometries", *International Journal of Pressure Vessels & Piping (Communicated)*, 1999.
5. T.V.Pavankumar, J.Chattopadhyay, B.K.Dutta, H.S.Kushwaha, Manoranjan Sinha and P.K.Kalra, "Crack-tip constraint parameters in two dimensional geometries and the application of artificial neural network to predict 'Q' parameter", *Engineering Fracture Mechanics (Communicated)*, 1999.
6. N.K.Mukhopadhyay, B.K.Dutta, H.S.Kushwaha, S.C.Mahajan and A.Kakodkar, "Numerical investigations on a cylinder with circumferential crack under PTS to characterise experimental observations", *Int. J. of Pres. Vessel & Piping*, 65, pp 97-104, 1996.
7. N.K.Mukhopadhyay, T.Pavankumar, J.Chattopadhyaya, B.K.Dutta, H.S.Kushwaha, V.Venkat Raj, "Deterministic Assessment of reactor pressure integrity under pressurise

- thermal shock", *Int. Jl. of Pres. Vessel & Piping*, 75, pp 1055-1064, 1999.
8. B.K.Dutta, H.S.Kushwaha, V.Venkat Raj, "Probabilistic assessment of reactor pressure vessel integrity under pressurised thermal shock", *International Jl. Press. Vessel and Piping*, 76, pp 445-453, 1999.
 9. J.Chattopadhyay, B.K.Dutta, H.S.Kushwaha, "Leak-before-break qualification of primary heat transport piping of 500 Mwe Tarapur atomic power plant", *International Jl. Press. Vessel and Piping*, Vol. 76, pp 221-243, 1999.
 10. J.Chattopadhyay, D.K.Nathani, B.K.Dutta, H.S.Kushwaha, "Closed-form collapse moment equations of elbows under combined internal pressure and bending moment", *Jl. Of Pressure Vessel Technology (Communicated)*, 1999.
 11. N.K.Mukhopadhyay, B.K.Dutta, H.S.Kushwaha, S.C.Mahajan and A.Kakodkar, "On line fatigue life monitoring methodology for power plant components, *Int. Jl. of Pressure Vessel and Piping*, 60, 297-306 (1994).
 12. N.K.Mukhopadhyay, B.K.Dutta, H.S.Kushwaha & S.C.Mahajan, "Implementation of on-line fatigue monitoring methodology in heavy water plant Kota for remnant life assessment programme", *J. of Transactions of Indian Institute of Metals* (1996).
 13. N.K.Mukhopadhyay, B.K.Dutta, P.Swami Prasad, H.S.Kushwaha, A.Kakodkar, "Implementation of finite element based fatigue monitoring system at heavy water plant Kota", *Nuclear Engineering Design*, 187, pp 153-163, 1999.

Acknowledgement

The author would like to thank his colleagues Mr J.Chattopadhyay, Dr. N.K.Mukhopadhyay, Mr T.Pavankumar and Mr M.K.Samal for their primary contributions in different segments of the present work. He would also like to thank Mr H.S.Kushwaha, Head, Reactor Safety Division, for his keen interest and guidance in pursuing the present package of developmental work.

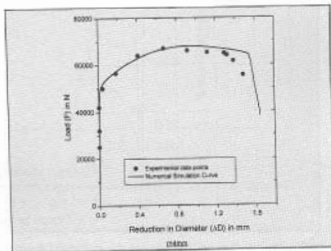
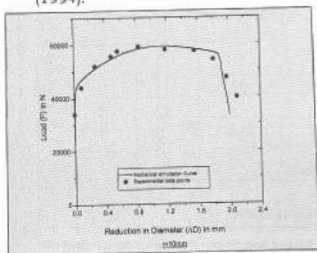


Fig. 1 Load vs Reduction of diameter curve for the notched tensile specimens having notch radii $r=4$ and 10 mm respectively.

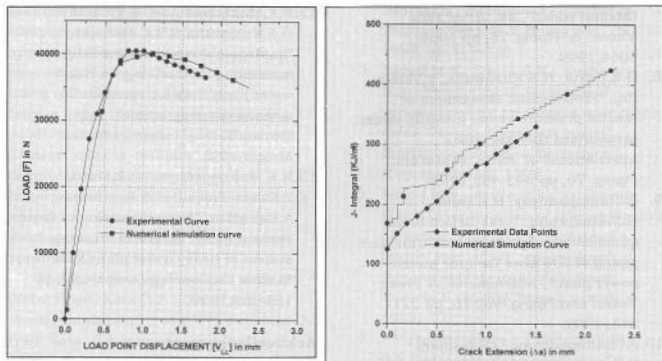


Fig. 2 Comparison of experimental results of a C-T specimen with analytical results calculated using principles of material damage mechanics

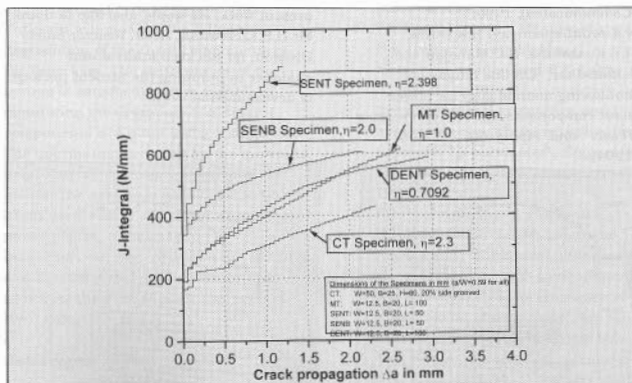


Fig. 3 Analytical J-R curves for different fracture mechanics specimens for the material Ste460

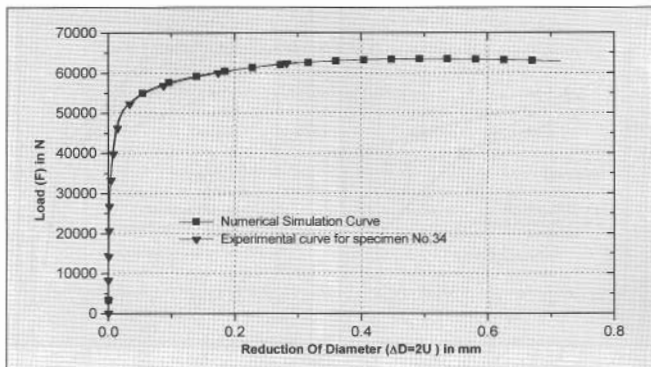


Fig. 4 Experimental and numerical Load vs Reduction in diameter curves for a notched tensile specimen under cleavage fracture

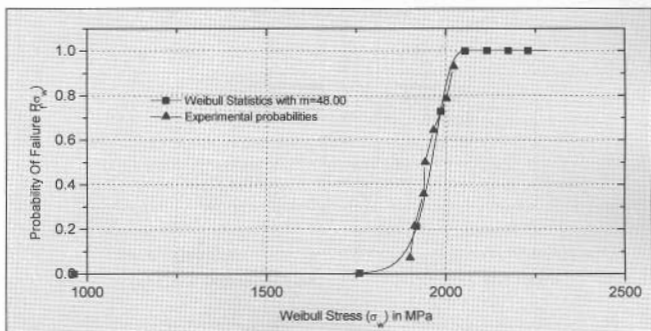


Fig. 5 Fitting of Weibull statistics to experimental data points for $m=48.0$ (taking load as ranking parameter)

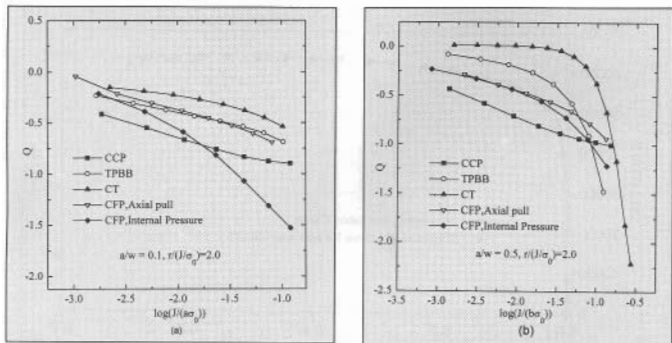


Fig. 6 Variation of 'Q' with deformation level (SA 333 Gr 6) for (a) $a/w=0.1$, (b) $a/w=0.5$

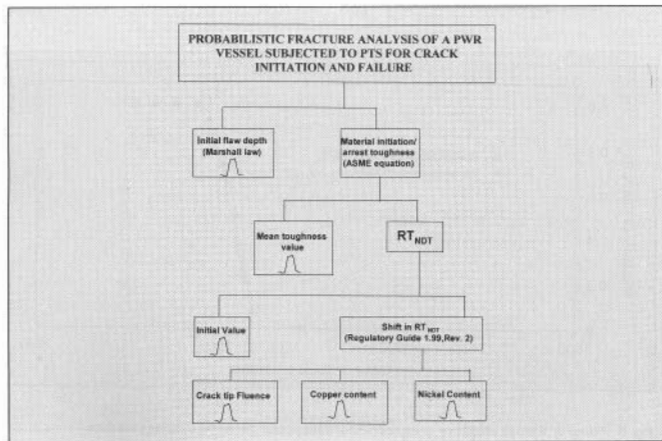


Fig. 7 Sketch showing normal distribution of parameters in probabilistic fracture mechanics assessment

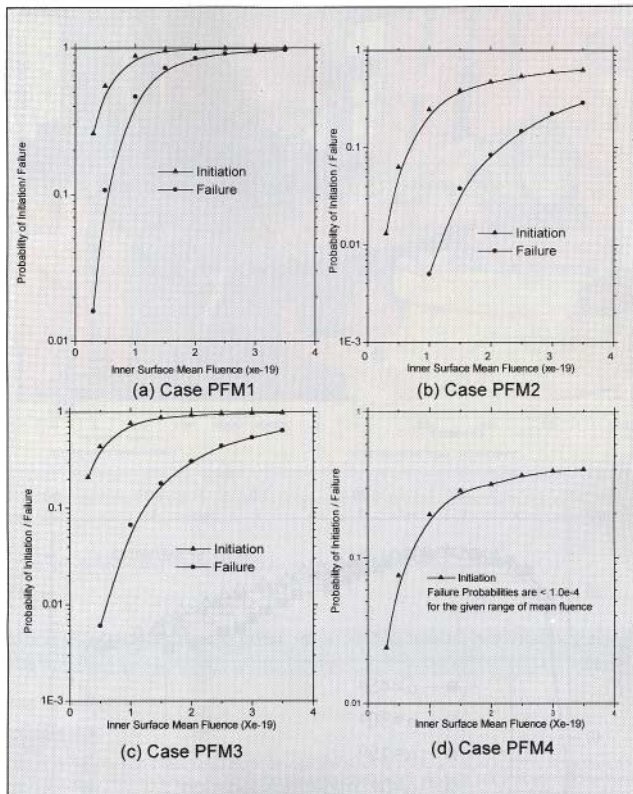


Fig. 8 Probabilities of crack initiation and vessel failure for the four cases (PFM1 to PFM4)

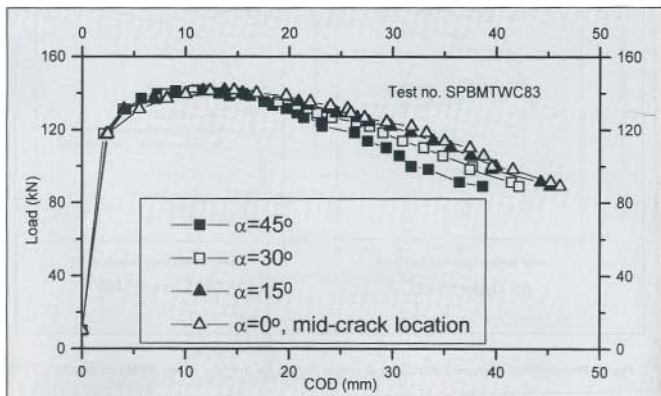
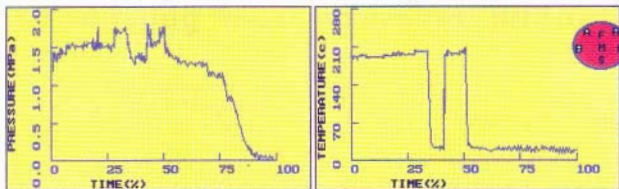


Fig. 9 Load vs COD curves for fracture tests of 8" dia. straight pipe with throughwall circumferential crack of 126°



Recorded Process Parameter fluctuations of nozzle N02 at HWP Kota



Information of Rainflow cycles & fatigue damage history of a selected point of N02

Fig. 10 Recorded and computed data by on line fatigue monitoring system

Dr B.K. Dutta is the recipient of the "Homi Bhabha Science & Technology Award, 1997"

About the author



Dr B.K. Dutta joined BARC through 20th batch of Training School in 1977. Since then, he has been working in the area of reactor structural safety analysis. His primary contributions are the mathematical modelling and solutions of variety of complex problems related to the safety of Indian nuclear reactors. The solutions of such problems have been obtained by using finite element based in-house codes developed by him. He is the recipient of Technical Excellence Award in 1992.

Uranium recovery from phosphoric acid

Harvinderpal Singh

Rare Earth Development Section
Bhabha Atomic Research Centre

ROCK PHOSPHATE IS A VITAL INPUT FOR increased foodgrain production, required to feed the growing populations of the developing countries. India has a number of fertiliser plants which process the rock phosphate into fertiliser, mostly by the sulphuric acid process. In addition, there are two plants using the sulphuric acid process to produce industrial phosphates required for applications as detergent and water softening agents. A number of plants also use commercially available strong phosphoric acid.

Uranium is known to occur in phosphates. The potential for recovery of uranium from the phosphates is substantial, ~1000 t/ year. It is available as a by-product of an industry which is well established and stable. Unlike the conventional sources of uranium such as the mined ore, the phosphatic uranium is amenable for rapid exploitation and its operation is eco-friendly. It is also

economical as it is equivalent to an ore which has been extracted, ground, digested and filtered, ready for wet processing operations of concentrations and purification.

As an energy source, if uranium contained in phosphates is not recovered, it is lost irretrievably with the fertilisers. Besides the spread with fertiliser is of environmental concern due to the radioactive hazards involved. The radioactivity levels in the fertilisers far exceed the new levels prescribed in the revised international standards for safe use of radioactive materials. It is imperative therefore that uranium separation from phosphates is carried out. The know-how developed by BARC in this direction is described in this note. An overall picture of the BARC pilot plant, used for technology demonstration, is shown in Figure 1.



Fig. 1 Set up of the pilot plant

Overall process flowsheet for uranium separation from phosphoric acid

The recovery process consists of basic steps shown in Figure 2. The phosphate ore, as mined, is accompanied by waste rock. Hence upgradation by ore dressing techniques is carried out. Typical results on a sample from a uraniferous Indian phosphate deposit show that subjecting an ore containing $P_2O_5 = 29.6\%$ and $U_3O_8 = 0.043\%$ to the operations of calcination, magnetic separation and froth flotation yields a high acid-grade concentrate fit for fertiliser purpose, containing $P_2O_5 = 36.3\%$ and $U_3O_8 = 0.046\%$. The bulk of uranium values (~75%) are intimately associated in the phosphate mineral and no selective upgradation or leaching is feasible.

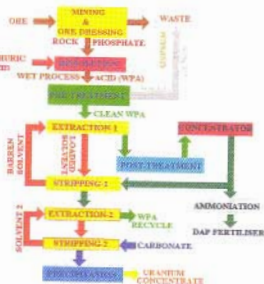


Fig. 2 Schematic flowsheet for uranium separation from phosphoric acid.

The next step in the process is acid dissolution of the rock phosphate. There are several methods of acidulation, but the most common one is the process involving the use of sulphuric acid to reject the calcium in the rock phosphate

as 'dihydrate' gypsum, while yielding phosphoric acid containing 27-32% P_2O_5 - which is called the 'wet process phosphoric acid' (WPA). The strong acid containing ~52% P_2O_5 is obtained by evaporation from WPA is traded as 'merchant grade acid' (MGA).

During acidulation, > 90% of uranium present in the rock can report to the WPA if the operation is carried out under oxidising conditions. This is generally the case since air cooling or flash-cooling of the acid is adopted for removal of the heat produced in the dissolution reaction. If required the operation can be deliberately controlled by monitoring the redox potential, or the e.m.f.

Uranium recovery from WPA involves these steps: (i) phosphoric acid pre-treatment, (ii) uranium extraction, (iii) uranium purification by re-extraction, (iv) product recovery, and (v) post-treatment of uranium depleted acid.

Prior to uranium extraction, WPA must undergo several pre-treatment steps. These include cooling to an optimum processing temperature, clarification to remove both the suspended solids and the organic material present in the acid (called as 'humates'), and adjustment of uranium valency. Depending upon the solvent, uranium is extracted from the acid, after pre-treatment, either in the +4 or +6 oxidation state by solvent extraction. The uranium is recovered from the solvent by another contact with an acid strip solution.

The uranium in the acid strip solution may be precipitated but needs to be purified before conversion to the final product. Purification is accomplished by re-extracting the uranium with a second organic solvent. The uranium loaded

organic in the second circuit is scrubbed to remove the impurities. The pure uranium is stripped from the solvent and precipitated. This precipitate, called 'yellow cake', is dried or calcined, packaged and transferred to uranium fuel conversion facilities. The uranium-barren phosphoric acid, called 'raffinate', is sent to a clean-up step to remove traces of entrained organic before being returned to the fertilizer plant.

Details of these steps are discussed below, based on the experience gained by BARC on acid from several fertiliser plants.

Pre-treatment of phosphoric acid

Pre-treatment of the acid to make it suitable for the uranium extraction is a step of prime importance. Pre-treatment costs in an industrial plant can constitute a third of the total costs. Pre-treatment usually involves three operations of temperature adjustment, valence adjustment, and clarification.

Temperature adjustment

Phosphoric acid fed to a uranium-recovery plant may be hot, up to 65°C. The actual temperature depends upon the surge volume, plant capacity, length of transfer pipe, etc. Lowering of the temperature reduces the fire hazard of the solvent used for extraction and increases the extraction power of solvents. Cooling the phosphoric acid however has some disadvantages. The viscosity of the acid increases with decreased temperature, which in turn necessitates larger and costlier equipment in the solvent extraction circuit, with the additional cost of increased solvent hold-up. A more serious problem with cooling is the crystallization of salts from the acid onto

the heat exchanger surfaces led to increased maintenance of the heat exchanger. Similarly, the added cost of reheating the acid, if processed for concentration before further processing into fertiliser, as is common in many plants, is an additional consideration.

As a compromise, the temperature of the acid is reduced only to some optimum level, depending on the local conditions, usually in the range of 38°C - 55°C.

Valence adjustment

The second unit operation in the acid pre-treatment is the adjustment of the acid valency or the redox potential, as measured by the 'emf', to a value that will be suitable for the particular solvent extraction system being used. There are two types of solvents: one which extracts uranium at lower emf value, and second which extracts uranium at higher emf value.

For systems where oxidation is needed or the emf is to be high, reagents which can be added include: air, oxygen, H_2O_2 , $NaClO_2$ and ozone. The use of chlorate is not acceptable in some plants because of potential additional corrosion that would be caused by introducing the extra chloride ions into the acid. Peroxide is expensive and is used in moderate quantities after use of air or oxygen.

In systems where uranium must be reduced, the reduction can be carried out by using scrap iron. The reduction usually occurs in less than 15 minutes. Reduction tests on acid samples taken from several plants showed scrap iron consumption in the range of 0.2 to 0.8 g/l. Since most acids already contain 4-5 g/l iron, this amount of iron is generally accepted by the fertiliser producers.

Clari-flocculation

The WPA contains 1 - 2 % suspended solids and humic material. Both these need to be reduced to prevent problems of 'crud' build-up in the solvent extraction unit. The 'crud' consists of troublesome solid phase which accumulates at the interphase of the aqueous and organic phase in the solvent extraction equipment. It renders operation difficult and leads to high loss of expensive solvent. The solids contained in WPA can be almost completely removed by flocculation using a high molecular weight polyacrylamide type ionic flocculant and settling in a thickener. The thickener underflow can be returned to the acid plant filter for recovery of contained phosphate and uranium values.

The acid after clari-flocculation may be 'green' or 'black' depending on the 'humate' content. The humate content of the 'green' acids is sufficiently low (<100 ppm) and no special separation operation is required for further removal. Black acids, however, contain high humate levels and a special treatment is required. Troublesome humates in black phosphoric acid are more difficult to remove than gypsum, and several methods have been tested to accomplish this separation. The humates in the wet-process acid consist of either dissolved matter in the acid or are of suspended very fine colloidal particles. A portion of these humates flocculate with the gypsum in the clari-flocculator and the balance need other means to eliminate them.

One efficient method of humate removal is carbon adsorption. However the black acids made from uncalcined rock contain too high, upto 2 g/l, of humates for the method to be industrially feasible. Since the capacity of carbon for adsorption of these humates is limited,

the cycle time is short. Short cycle times and the problem of quick regeneration cause operating problems. In addition, the cost of regeneration, using NaOH, is excessive and the carbon needs to be replaced or thermally reactivated in a calciner after several in-plant regenerations, further adding to the operating costs. Thus carbon adsorption is used only for green or brown acids, low in humic content.

For black acids, BARC has developed a process where the acid is contacted with a viscous liquid hydrocarbon in a specially designed equipment. The humates form a flocculated precipitate. The precipitate and other suspended solids accumulate as an emulsion above the aqueous phase. The emulsion is separated and filtered to remove the organic material and to recover the entrained acid and the hydrocarbon.

Once the phosphoric acid has been cleaned of the undesirable suspended solids and the humates, the acid is filtered to remove residual suspended solids and then re-heated slightly before solvent extraction.

Solvent extraction

Solvent extraction separates uranium from the WPA and concentrates it for the subsequent purification process. WPA is a highly ionic systems and the solvents found to have sufficient extraction power are of a group including phosphate ester, acid, oxide, etc., There are two extractant systems for commercial utilisation. The first system consists of di-2-ethyl hexyl phosphoric acid (D2EHPA) or nonyl phenyl phosphoric acid (NPPA), with a synergistic additive, trioctylphosphine oxide (TOPO), di-butyl butyl phosphonate (DBBP) or tributyl phosphoric acid (TBP). The second system involves a number of

compounds called as octyl phenyl acid phosphate (OPAP). TOPO and TBP are neutral organo-phosphates, whereas OPAP and DEHPA are acidic organophosphates. BARC has developed indigenous synthesis processes for the various solvent extraction reagents. The solvent extraction reagents are used in the extraction circuit as a dilute solution in refined kerosene. In India, a special grade of diluent has been developed to meet the needs of hydrometallurgical extraction.

Di-2-Ethyl hexyl phosphoric acid extractant

D2EHPA has been used in India to extract rare earths and base metals from acidic solutions. D2EHPA alone is, however, not a sufficiently strong extractant to recover uranium from typical wet-process phosphoric acids. D2EHPA/NPPA is effective in synergistic combination with TBP/DBBP/TOPO or for oxidised uranium. TOPO is most effective but is costliest. Stripping of the solvent can be accomplished by using reductive strong phosphoric acid.

Octyl phenyl acid phosphate extractant

OPAP offers some advantages over D2EHPA-TOPO. These are:

1. OPAP extracts tetravalent uranium, which is the prevalent species in many phosphoric acids.
2. Uranium is stripped from the OPAP with phosphoric acid and an oxidant (H_2O_2) and therefore, valence adjustment is not needed to purify the hexavalent uranium in a second cycle.
3. OPAP is a more powerful uranium extractant than D2EHPA-TOPO, thus enabling less number of contact stages and higher concentration ratio.

4. OPAP is cheaper than D2EHPA-TOPO

BARC was the first to report the utility of OPAP in uranium extraction from WPA, even though the early researchers in USA had reported negative results. The chemical stability of OPAP is lower than D2EHPA-TOPO. The commercial OPAP product consists of many components but only two components, the mono and di-isomers of octyl phenyl phosphoric acid, are of interest in the extraction. Differential solubility of the mono and di-isomers in WPA is important since an equi-molar mixture of the two esters has a positive synergistic effect due to which uranium extraction increases several times in comparison with the extraction by either isomer individually. OPAP losses into WPA are higher and it needs to be recovered from the acid after solvent extraction. A further improvement involves a mixture of mono-ester and di-ester forms of NPPA.

Uranium purification by re-extraction

A chemical precipitation method can be used to purify uranium prior to product recovery, but is costly in view of the low concentration of uranium. Elimination of impurities and further concentration of uranium into a solution suitable for uranium recovery is accomplished by a process of re-extraction. Impurities which are separated include phosphate, fluoride, sodium, iron etc. There are many solvents that can be used to control these impurities. The selection of the solvent depends in the part on the solvent used in the first circuit and the reagents used to strip that solvent. In the re-extraction process further purity is obtained by scrubbing the loaded solvent. Sulphuric acid is very effective as it not only removes phosphate

but also separates other contaminants. The acid scrub solution containing the unwanted impurities is used for regeneration of the solvent. The D2EHPA-TOPO gives excellent results in the re-extraction. The OPAP system has also been used in second circuit. But selectivity is not high and purification of the strip solution before precipitation of the yellow cake is important.

Solvent stripping and regeneration

Stripping of the solvents can be accomplished with Na_2CO_3 or ammonium carbonate. Using Na_2CO_3 to strip the solvent yields a solution from which a uranium cake can be precipitated which needs only to be dried before packaging. The use of $(\text{NH}_4)_2\text{CO}_3$ to strip the solvent produces a uranium precipitate that must be calcined to remove ammonia before being packed. The former however gives lower filtration rate.

Stripping uranium with $(\text{NH}_4)_2\text{CO}_3$ and precipitating the uranium in the stripping mixer-settler as a single operation has been tested. The slurry is filtered and the solution recycled after adding NH_3 and CO_2 . However precipitating solids in the SX unit generally increases phase disengagement times, reduces mass transfer rates, and increases solvent losses.

When D2EHPA-TOPO is used in the purification circuit, the sodium or ammonium ions loaded onto the organic during stripping can get recycled to the extraction section causing precipitation of sodium or ammonium fluosilicates. Hence regeneration of the solvent, wherein monovalent ions are replaced with hydrogen ions, is necessary after stripping and before recycle to extraction. The acid used to scrub impurities from the loaded organic can be used to

regenerate the solvent. This reuse of the scrub solution in regeneration also prevents any scrubbed uranium from being lost since it is recovered by the organic during regeneration.

Product uranium recovery

Sodium carbonate stripping of uranium from D2EHPA-TOPO yields a solution containing 40 to 60 g/l U_3O_8 . This solution is acidified to pH 6.5 with sulphuric acid. At this pH a precipitate is formed which contains many impurities that can be removed by filtering. These impurities include phosphate, iron, silica, and heavy metals. The filtration of the impurity precipitate is accomplished by relatively small equipment. After filtration, acidification is continued to eliminate carbon dioxide. Then the pH is raised with NH_3 or NaOH . The precipitate consists of hydrated uranyl salts. An alternate route to precipitate uranium as peroxide has also been developed.

The yellow cake product from the precipitated slurry is obtained by thickening, centrifuging and drying.

Entrained solvent recovery

The WPA from the primary extraction, depleted of uranium, contains traces of entrained solvents (~250ppm) which can add to the costs as well as lead to problems in downstream operations. A limit of 50 ppm of solvent carryover into the raffinate is as a safe level. Therefore, the raffinate clean-up is carried out using packed coalescers (similar to the ones used in petro-chemical industry for oil-water separation) to remove the solvent to ~50ppm. This is followed by separation using flotation cells (similar to the equipment used in ore dressing industry) to further reduce the solvent to less than 40 ppm.

Advantages of uranium separation from phosphoric acid

There are several advantages of uranium separation from WPA. One advantage is that the raffinate acid returned to the fertiliser plant is in an extremely clear state. Physically, it is a practically sparkling, clear, light-brown liquid. Most of its suspended solids, waxes and organics have been either intentionally removed during the pre-treatment step or eliminated as a result of the solvent extraction process. Clarified raffinate acid gives very low scaling in the downstream operations, ~ 20 % of the normal dirty acid. Second advantage is realised during the concentration stage. When the dirty acid is concentrated in the evaporators to 52-54 % P_2O_5 , its solid content gets raised to 2.5-3 %. Through a combination of post-precipitation and cooling, this content may be further get raised so that clarification is necessary to secure a good grade control during the

manufacture of granular triple superphosphate and diammonium phosphate (DAP). The uranium recovery process considerably reduces the requirement of such clarification. Clarification at 40 % and 52 % P_2O_5 is made easier. Third advantage lies in improvement of the grade of DAP by as much as 0.2-0.4 % N and 0.5-1.0% P_2O_5 . Uranium recovery from phosphoric acid and its inherently incorporated acid clean up gives an excellent incentive for acid purification to remove undesirable impurities such as Mg, Fe, Al and produce technical grade acid. Other chemical processes become applicable e.g. fluorine precipitation, alkalisation precipitation of metals.

The rare earth elements present in the WPA can also be recovered. Similarly cadmium present in many of the acids can also be separated after uranium recovery.

Mr H. Singh is the recipient of the "Homi Bhabha Science & Technology Award, 1997."

About the author



Mr Harvinderpal Singh joined the 20th batch of BARC Training School after obtaining a first class first in B.E.(Hons.) in Chemical Engineering from BITS, Pilani. His major achievements in the DAE include process optimisation at UCIL plants (Bihar) and IRE plants (Kerala/Tamil Nadu), scale-up of uranium ingot production at Trombay, rare earth phosphor technology development and technology industrialisation for rare materials separation from phosphates. He has won honours/Awards including the BARC Officers Association Award for Excellence in Nuclear Science & Engineering in 1994 as well as the Homi Bhabha Science & Technology Award, 1996. He has also been nominated for Shanti Swarup Bhatnagar Award and for Metallurgists of the Year Award. He is a member of

Indian Institute of Chemical Engineers, Indian Institute of Metals, Indian Society for Heat & Mass Transfer, Indian Nuclear Society, Materials Research Society of India and vice-president of Rare Earths Association of India. He has participated in IAEA programmes abroad.

Dual sites of electron solvation in microheterogeneous media: a new observation

Hirendra Nath Ghosh

Radiation Chemistry & Chemical Dynamics Division
Bhabha Atomic Research Centre

Introduction

THE PROCESS OF IONIZATION BY THE interaction of high energy radiation with matter or by laser excitation results in creation of an electron and a hole (cation). Following the energy absorption in $< 10^{-16}$ seconds electron is ejected with sufficient kinetic energy to escape the coulombic attraction of its sibling hole. It creates further ionizations and excitations along its path, get thermalised and in the absence of suitable scavengers can polarise and orient solvent molecules around itself to get solvated and is called as "Solvated Electron". When the electron is solvated in water it is known as hydrated electron (e_{aq}). The excess electron is the primordial intermediate in the Radiation Chemistry of liquids. It continues to be of prime importance in chemistry and biology. The characteristic absorption band of solvated electron has been observed in many liquids by using the techniques of pulse radiolysis and flash photolysis. The advancement of technology in the creation and detection of ultrashort optical pulses have made it now possible to follow the absorption spectrum in picosecond (10^{-12} sec) to femtosecond time (10^{-15} sec) scale.

Intensive studies have produced substantial information concerning

reactions between solvated electron and chemical or biological acceptors in homogeneous aqueous solutions. The knowledge of absolute rate constant is of prime importance for a proper understanding of chemical reactions. In particular, the studies of one-electron-transfer reactions in concentrated solutions of biomolecules (coenzymes, nucleic acid components e.g. purines, pyrimidines and amino acids) should permit apprehension of the mechanisms of free radicals occurring in components of living cells.

Amphiphilic molecules which possess both hydrophilic and hydrophobic end group may associate in aqueous media to form dynamic aggregates commonly called micelles. With increasing concentration, the aggregates may take different structure and shapes like spherical and ellipsoidal micelles, microemulsion, bilayer, liquid crystal etc, and are called microheterogeneous media in general. Such systems mimic structures and functions of living body membranes and lipids. To understand the reactivity of electron and electron transfer processes in a living body one can extrapolate studies on microheterogeneous media as a first approximation.

The dynamics of generation and solvation of excess electrons in microheterogeneous systems is a topic of considerable current interest. The photoionization of chromophores embedded in micelles (or vesicles) under pulsed or continuous excitation have provided a wealth of information concerning the dynamics and energetic of excess electron production in closed organized media (COM). The prime interest in the generation of excess electrons and study of electron transfer reactions in the organized media stems from (1) to understand charge separation and charge recombination reactions (2) to increase efficiency of charge separation process with a special interest to improve photochemical utilization of solar energy. It is also of interest to see whether the optical properties of the solvated electron can be exploited to understand the properties of the organized medium itself. In effect, valuable specific properties characterise such heterogeneous assemblies in which surface processes replace bulk reactions and where the

transients and reaction products may become localised in two different phases.

Two commonly used techniques for such studies are 1) pulse radiolysis and 2) flash photolysis (Fig 1) of a suitable chromophore embedded in the micellar medium. A simple schematic diagram is shown in Fig 1. On excitation of the sample by laser light or irradiation by electron pulse, excited species are produced and monitored by light from a Xe lamp through monochromator, PMT and oscilloscope. The spectroscopic properties of the solvated electron have been used to probe the solvent structure, state and surroundings of the solvation site in liquids and microheterogeneous media. Photolysis of nonionic micelles having chromophore group, or a suitable solute solubilised in the nonionic micelles is seen to give rise to the dual sites of electron solvation and these observations are discussed. The observation of dual site solvation of electrons by us has been considered as *pioneering research* by peers and experts in Radiation and Photochemistry.

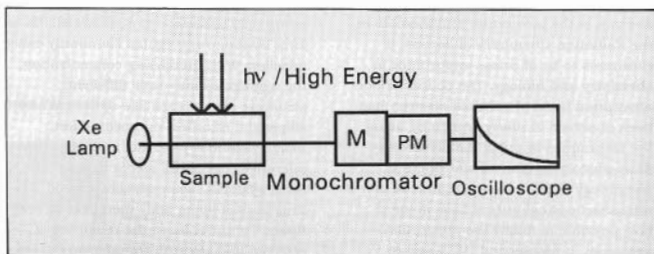


Fig. 1 Schematic diagram of a conventional flash photolysis and pulse radiolysis set-up

Dual sites of solvation of electrons in aqueous micellar solutions

a) Laser flash photolysis of tritons (Tx)

Laser (248 nm) irradiation of Triton X-100 (Tx-100) :

$[(H_3C)_3CCH_2C(CH_3)_2C_6H_4(OCH_2CH_2)_n]$
OH: ($n = 9.5-10.5$) above its critical micellar concentration (CMC) was seen to photoionize the surfactant molecule. Immediately after the 10 ns laser pulse transient optical absorption due to Tx^* ($\lambda_{max} = 480$ nm), triplet ($\lambda_{max} = 420$ nm) and two negatively charged species ($\lambda_{max} = 600$ nm and 720 nm) were observed. Among these the peaks at 630 and 720 nm were seen to be heavily quenched by N_2O , an efficient scavenger of solvated electrons. The optical absorption peak at 420 nm has been assigned to the triplet, based on the scavenging studies in methanol solutions of Tx by β -carotene, an efficient triplet scavenger. The absorption peaks at 630 and 720 nm attributed to either solvated electron or some anionic species.



Since in Tx the phenoxy chromophore is nearly at the center of the surfactant, the photoejected electron has to travel the entire length of POE chain of the micelle to reach the bulk aqueous phase to get solvated and give the characteristic absorption spectrum of hydrated electron (e_{aq}^-) with $\lambda_{max} = 720$ nm. By kinetic and spectral analysis of the transient species it was confirmed that the absorption peak at 630 nm is not due to any negative species like anion radical of Tx (e.g. Tx^- formed by $e_s^- + Tx \rightarrow Tx^-$) and the species is electron solvated in the palisade layer ($e^- \rightarrow e_s^-$) of the micellar structure (Fig. 2).

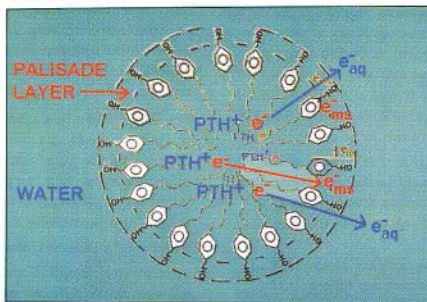


Fig. 2 Dual sites of solvation for electrons in aqueous micellar (Triton X-100) solutions. Solubilising site of the hydrated electron (e_{aq}^-) and palisade electron (e_{ms}^-) are shown in the figure. After photoionization phenothiazine cation (PTH^+) are located inside the core of the micelle.

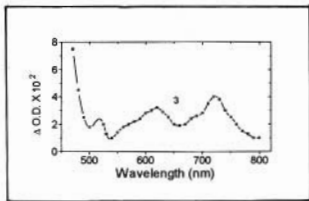
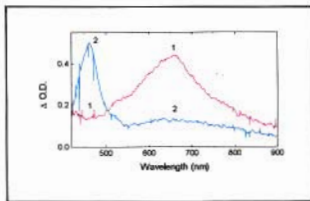


Fig.3 Transient absorption spectra produced on laser flash photolysis of N_2 bubbled solutions of PTH in Triton X-165 : 1. immediately (delay - 0 ps) and 2: 4000 ps after the 35 ps, 355 nm laser pulse. 3: immediately after XeF (351 nm) excimer laser pulse (100ns)

b) Photoionization of phenothiazine (PTH) in nonionic micelles

The above results were confirmed using another interesting system. Photoionization of a suitable probe molecule e.g. PTH incorporated in nonionic micelle gives similar dual electron solvation sites. Due to its low solubility in water, PTH is preferentially solubilized inside the core of the nonionic micelle (Fig 2). Figure 3 (curve 3) shows the transient optical absorption spectrum on 351 nm excitation of PTH in aqueous Triton-X-165 solution. The spectrum shows four absorption peaks at 460 (not shown in the figure), 520, 630 and 720 nm. The peaks at 460 and 520 nm are attributed to the triplet and cation radical of PTH respectively. Both the 630 and 720 nm peaks were found to be efficiently quenched by N_2O and H^+ (i.e. in acidic medium) and could be safely attributed to the solvated electrons arising from two different sites of solvation in these media.

Time evolution of the dual sites of electron solvation : a numerical simulation study

If the probe molecule e.g. PTH solubilized near the core of the micelle undergoes photoionization by a UV

photon (e.g. 355nm, 3.5 eV), the kinetic energy of the photoejected electron is expected to be limited to 0.1-1 eV and the typical thermalization distances for the electrons are expected to be 2.5 - 4 nm similar to the micellar dimensions. The radii of the micelles chosen for the present studies i.e. Tx-100, Tx-165 and Brij-35 are approximately 4 nm and hence a major fraction of the photoejected electrons is expected to get solvated in the palisade region of the nonionic micelles studied. Femtosecond flash photolysis experiments confirmed that solvation time for hydrated electron in micellar system is ~350fs. In the present case, it is expected that the solvation of the electron in the palisade region (e_{ms}^-) is complete within the pulse time i.e. 35 ps. It is possible that during the pulse time some electrons might have travelled the poly oxy ethylene (POE) segment length of the nonionic micelle and become hydrated in the bulk water (e_{aq}^-). However, this fraction appears to be small. Some of the electrons solvated in the palisade region might have also diffused to the bulk water to get hydrated. It was not possible to distinguish between these two possibilities. For this purpose PTH in

Tx-100 was excited by 355 nm, 35 ps laser pulses. On excitation by laser pulse excited singlet state, triplet state and cation radical of PTH are formed and both palisade and hydrated electron have been

observed (Fig 4). The rate constants and the quantum yields of the excited species have been measured and are shown in the scheme.

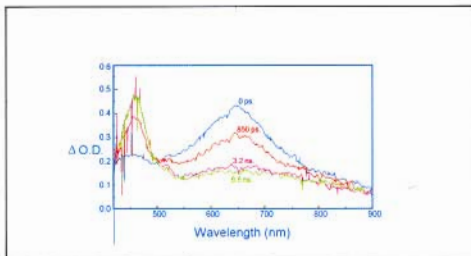
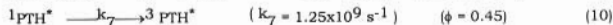
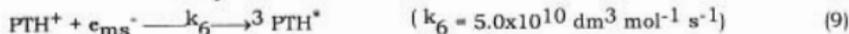
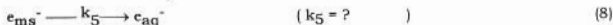
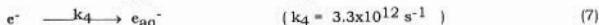
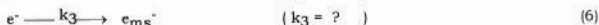
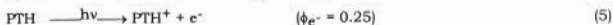
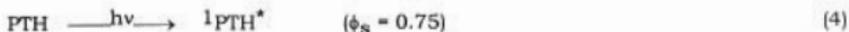


Fig.4 Transient absorption spectra obtained on excitation of PTH in Triton X-100 micellar solution by 355nm laser light at different time scales



(${}^1\text{PTH}^*$ and ${}^3\text{PTH}^*$ represent the excited singlet and triplet state of PTH and e^- represents the unsolvated /dry electron.)

The reactions described in the above scheme lead to various coupled differential equations. To generate the evolution profile for the concentrations of the above transient species, the coupled differential equations are solved

numerically. Initial concentrations of the excited species and the rate constants are fixed as per experimental conditions as described in earlier sections. In the above equations (Eqn 4-10) it has been observed that k_3 and k_5 are unknown and have

been solved by numerical simulation. It is not known what fraction of e^- gets solvated in the palisade layer of the surfactant and what fraction comes out in the bulk aqueous phase without getting solvated in the palisade layer. Moreover, some electrons solubilised in the palisade layer will diffuse out in the bulk aqueous phase and vice versa. It is assumed that approximately 10% of the unsolvated electrons diffuse out to bulk aqueous phase (based on observed yield of e_{aq}^-) and transition of e_{aq}^- to e_{ms}^- is assumed to be negligible. Simulated curves are fitted to observed decays by iterating k_3 and k_5 . The evolution of concentration profiles of different transients obtained from numerical integration are shown in Fig. 5.

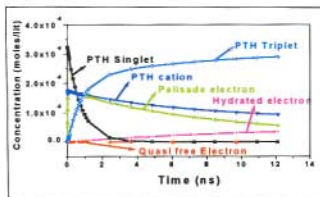


Fig.5 Computer simulation showing the time domain concentration of different species (the concentration traces for PTH singlet and PTH triplet are experimentally observed, and those for quasi free electron, palisade electron, hydrated electron and PTH cation concentration traces are obtained from simulation.)

By comparing the concentration profile of different transient species, as determined by simulation and experiments, the two unknown parameters i.e. solvation time ($1/k_3$) for electron in palisade layer and diffusion

time ($1/k_5$) for e_{ms}^- from micellar phase to the bulk aqueous phase have been estimated and found to be 10 ps and 400 ps respectively.

Dual sites of solvation of electrons in liquid crystalline media

The problem was investigated from another angle. Irradiation by electron is known to ionize the medium and generated electrons. In normal micelles (1% surfactant concentration) most of the e^- are generated in aqueous phase. Under the condition where surfactant concentration is large (>20%) a sizeable number of e^- will be produced in the micellar phase and must diffuse out to get hydrated, and in this process generate dual sites of solvation. For this purpose various compositions of Tx and water mixtures deoxygenated by bubbling with N_2 were irradiated by 50 ns electron pulses and transient absorption spectra were recorded. N_2 bubbling is necessary to remove O_2 which reacts with e^- . Figure 6A shows the transient absorption spectra for 50:50 (v/v) Tx- H_2O mixture, 300ns after the electron pulse. Three absorption peaks at 460, 630 and 720nm are clearly seen. In the presence of N_2O , a good scavenger of solvated electrons, both 630 and 720nm absorption peaks were drastically reduced, indicating that these peaks are due to the solvated electrons. Our earlier work showed clearly that, although the electrons react with Tx, no transient absorption due to Tx^- was seen in the spectral region 300-800nm. The 460nm absorption peak is known to be the cation radical of Tx.

Interestingly at 300 ns after the pulse (Fig-6A), an emission was seen with λ_{max}^- 305nm which decays fast and an

absorption signal grows in $\sim 1\mu\text{s}$ with $\lambda_{\text{max}} = 320\text{nm}$. The species absorbing at 320nm has been identified as the triplet state of Tx. The inset of Fig 6D shows transient absorption spectra obtained in 20% (v/v) Tx-H₂O mixture 300ns after the electron pulse. At this composition, the cation radical and triplet peaks are minor and 630nm peak is not clear. Distinct 630 and 720nm peaks are seen for Tx-100 concentrations between 40-70%.

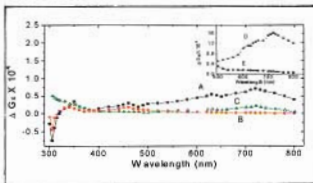


Fig. 6 Transient absorption spectra obtained on irradiation of Triton X-100 : water (50:50 V/V) mixtures by 50ns electron pulses. (A) N₂ bubbled (0.3 μs); (B) N₂O saturated (0.3 μs); (C) N₂ bubbled (1 μs). Inset: Transient absorption spectra of Tx-100 : Water (20:80 v/v) mixtures. (D) N₂ bubbled, (E) N₂O saturated after 0.3 μs .

The widths of the two peaks are not as broad as that for e_{aq}^- in neat water or for e_{S}^- in neat alcohols. In the present case the smaller peak widths probably arise due to the strong influence of the micellar aggregation on the variation of trap depth for both the electron solvation sites. However, as described earlier the 630nm peak does not arise from the anion of Tx. Below 40% of Tx the fraction of electrons generated in Tx fraction would be low and hence 720nm peak due to e_{aq}^- absorption dominates. Between 40-70% of Tx the energy deposited in aqueous and Tx

pseudophases is comparable leading to preferential solvation of electrons in both the phases to give 630 and 720nm peaks. Above 70% of Tx, the water fraction diminishes, hence 720nm peak due to e_{aq}^- reduces and is not clearly observed. The electron yield in Tx pseudophase at 630 nm also reduces drastically in these high concentration of Tx, probably due to the limited hydration of the POE chains, the polarity of the palisade layer is low or the e_{S}^- absorbs beyond the detection limits of our system (>800nm). The increased yields of Tx⁺ cation radicals and increased emission yields suggest that the ionization yield is not diminished at high concentration of Tx. These observations thus support that the above fact that low apparent electron yields (630 nm) must be due to the shift of the electron absorption spectrum beyond 800nm.

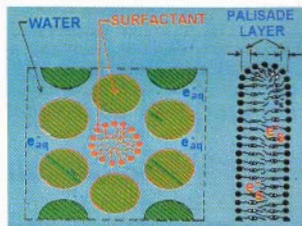


Fig.7 Hexagonal structure of liquid crystal middle phase of water + Triton-X-100 system. Sites of solubilisation for electrons in palisade layer (e_{S}^-) and aqueous pseudophase (e_{aq}^-) are shown.

The nonionic surfactant systems are free from the electric charge effects seen for ionic micellar and microemulsion systems. Further, ionic micelles have

thinner ($\sim 0.5\text{nm}$) Stern layer. Hence absence of charge effects and availability of a thick palisade layer ($3\text{--}4\text{nm}$) which is fairly polar due to heavy hydration, seems to be major reasons for electron solvation in the surfactant pseudophase giving rise to 630nm peak at the present systems.

Studies with electron scavengers

Two electron scavengers were chosen to study their scavenging effect; *viz*: (a) nitrate ion (b) pyrene. Both of these solutes have high reactivities towards solvated electrons. Being charged species, nitrate ions are expected to show a concentration gradient from aqueous phase to the surfactant pseudophase, and are expected to scavenge electrons preferentially from aqueous phase. In accordance with these expectations, addition of nitrate ions was found to scavenge electrons solvated in both the phases, but to different extents.

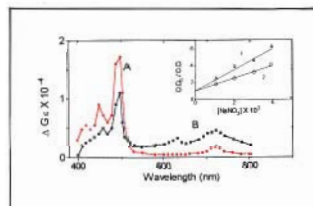


Fig. 8 Transient absorption spectra obtained on irradiation of Triton X-100 - Water (50:50 v/v) mixtures containing pyrene ($2.6 \times 10^{-3} \text{ mol} \cdot \text{dm}^{-3}$) by 50ns electron pulse, after (A) $0.25 \mu\text{s}$; (B) $1 \mu\text{s}$. Inset: Stern-Volmer type plots for the scavenging of solvated electron generated on irradiation of Triton-X-100 - Water (50:50 v/v) in N_2 bubbled solution with nitrate ions monitored at (1) 720nm and (2) at 630nm . (300ns after pulse)

Figure 8 (inset) shows the Stern-Volmer type of plot for the change of optical density (OD) due to the scavenging of electrons by nitrate ions for both 630 and 720nm peaks for pulse radiolysis of Tx-100 and water mixtures (50:50). It is seen that 720nm peak is quenched with higher efficiency as expected.

Pyrene is also a good electron scavenger and due to its low solubility in water it selectively solubilizes in the surfactant pseudophase. So it is expected that pyrene molecules will quench the electron solubilized in surfactant pseudophase more effectively. Figure 8A shows the transient absorption spectrum obtained from nitrogen bubbled Tx-100/ H_2O (50:50 v/v) mixture containing $2.6 \times 10^{-3} \text{ mol} \cdot \text{dm}^{-3}$ pyrene. In the $2\text{--}4 \times 10^{-3} \text{ mol} \cdot \text{dm}^{-3}$ concentration range of pyrene the preferential scavenging of e_{ms}^- was observed prominently. The spectrum obtained $1 \mu\text{s}$ (Fig 8B) after 50ns electron pulse clearly shows preferential scavenging of e_{ms}^- as compared to e_{aq}^- as seen by the heights of 630 and 720nm peaks. Three additional peaks at 420nm , 450nm and 500nm are known to be triplet, cation radical and anion radical of pyrene. Figure 8B clearly shows that the 720nm peak still remains at $1 \mu\text{s}$ time scale where the peak at 630nm is peak totally quenched. This observation again shows the preferential scavenging of e_{ms}^- from surfactant phase. Such preferential scavenging of the electrons in different pseudophase might have far reaching consequences in radiation biology.

Conclusions

Photoionization of aqueous micellar solutions of Triton X or by the photolysis of phenothiazine in Triton X micelles by laser pulse gives two distinct optical absorption peaks at 630 and 720 nm attributable to electrons solvated at two different sites: former in the palisade region of the nonionic micelle and the latter in the bulk aqueous phase. Picosecond laser flash photolysis of PTH in both the micelles show that within the laser pulse a major fraction of the photoelectrons get thermalized and solvated in the palisade region of the nonionic micelles. Within a few tens of nanoseconds, a fraction of them undergo geminate recombination with the sibling cation and some of the electrons diffuse out of the micelle to get hydrated. Numerical integrations are carried out to find out electron solvation processes and in particular the diffusion time for the palisade electron from palisade layer to aqueous phase.

These studies were extended to liquid crystalline mixtures of Tx-100 & water, where the excess electrons were generated radiolytically. The electron solubilized in aqueous pseudophase shows the well known transient optical absorption maximum at 720nm, while the electron solubilized in palisade layer shows absorption maxima at 630nm. Electrons were scavenged using two efficient scavengers namely nitrate ions and pyrene. The former, being ionic, remains in the aqueous pseudophase and preferentially scavenges the electrons solvated in the aqueous phase. Pyrene, on the other hand, scavenges preferentially the electrons solubilized in the surfactant pseudophase.

The reactivity of electron is found to be different in two different phases. Exploiting this property for electron there will be lot of implication in radiation biology. The knowledge of dual sites of solvation will be extremely useful in electron transfer processes in biological system e.g. lipid, bilayer and membranes. The reactivity of electron with biological acceptors in different parts of the living body can be extrapolated using the idea of dual sites of electron solvation.

References

1. H.N.Ghosh, D.K.Palit, A.V.Sapre, K.V.S.Rama Rao and J.P.Mittal. *Chem. Phys. Lett.* 1993, 203, 5.
2. H.N.Ghosh, D.K.Palit, A.V.Sapre, K.V.S.Rama Rao and J.P.Mittal. *Photochem. Photobiol.* 1994, 59, 13.
3. H.N.Ghosh, A.V.Sapre and K.V.S.Rama Rao. *Chem. Phys. Lett.* 1996, 255, 49.
4. H.N.Ghosh, A.V.Sapre, D.K.Palit and J.P.Mittal. *J.Phys.Chem.* 1997, 101, 2315.
5. H.N.Ghosh, A.V.Sapre and J.P.Mittal. *Radt.Phys.Chem.* 1997, 49, No 1, 107.

Acknowledgements

I would like to thank Dr. A.V. Sapre and Dr. D.K. Palit for many fruitful discussions, Dr. T.Mukherjee, Head, Radiation Chemistry & Chemical Dynamics Division, for corrections and Dr. J.P. Mittal, Director, Chemistry Group, for his constant encouragement.

"The observation of dual site solvation of electrons has been considered as pioneering research by peers and experts in Radiation and Photochemistry."

Dr H.N. Ghosh was awarded the "Indian National Science Academy Young Scientist Medal" in 1998 for his outstanding work in chemistry. Dr Ghosh has been the only recipient of this prestigious award so far from BARC in the field of chemistry.

About the author



After obtaining his M.Sc. in Chemistry from IIT, Kharagpur, in 1989, Dr. H.N. Ghosh joined Chemistry Division, BARC, in 1990, through BARC Training School Course (33rd batch). Dr. Ghosh obtained his Ph.D. degree in 1996 from Bombay University for his work on fast photochemical processes in liquid and microheterogeneous media. He did his post-doctoral studies, for the period of 1997-98, with Prof Tim Lian at the Chemistry Department of Emory University, Atlanta, USA, on femtosecond interfacial electron transfer dynamics, using Infrared spectroscopic detection. Dr. Ghosh was awarded the *"INSA Young Scientist*

Medal" in 1998 for his outstanding Ph.D. work. His current research interests include ultrafast interfacial electron transfer and electron solvation dynamics in microheterogeneous media.

BARCIS (BARC Channel Inspection System)

Manjit Singh

Reactor Control Division
Bhabha Atomic Research Centre

IN-SERVICE INSPECTION (ISI) OF COOLANT channels of PHWRs is essential to provide assurance of continued structural integrity of pressure tubes over reactor life-time. A semi-automated remotised channel inspection system known as BARCIS (BARC Channel Inspection System) for ISI of coolant channels has been developed. The system is designed with the objectives of minimising radiation exposure to inspection personnel and completion of inspection with minimum reactor down time.

The inspection is carried out from one end of the channel with the reactor in the shutdown condition and shutdown pumps running. The channel to be inspected is defuelled and the fuel bundles are temporarily stored in the fuelling machine at the other end of the channel. After the inspection, the fuel bundles are put back in the channel to occupy the same old positions. Isolation of the channel from the primary heat transport system is not needed and the fuel bundles need not be discarded.

Coolant channel assembly

The design of PHWRs is characterised by neutral uranium fuel, heavy water moderator, pressure tube containment of primary coolant, bundle fuel and on-power refuelling. The most significant

feature in the design is the use of multiple coolant channels (fuel channels) configuration rather than a single large pressure containment. Each 235 MWe reactor has 306 coolant channels. These are mounted horizontally within a horizontal cylindrical vessel, the calandria and surrounded by low pressure low temperature heavy water moderator. Each coolant channel assembly is made of Zircaloy-2 pressure tube of nominal outside diameter 90.33 mm, wall thickness 3.92 mm and length 5435.6 mm. Each end of the pressure tube is attached by means of a cold rolled joint to a stainless steel end-fitting. Each end-fitting has a coolant piping connection and contains a sealing plug that can be removed by remotised fuelling machines to permit on-power fuelling. External and concentric with the pressure tube is a thinner tube of Zircaloy-2 known as calandria tube, that separates the hot pressure tube from the cool moderator. Dry nitrogen or carbon dioxide gas fills the annular space between the tubes and garter springs keep the tubes from touching each other.

Because of the critically important role of the pressure tube as part of the pressure boundary, it is necessary to confirm their structural integrity and collect data related to changes in their

material properties. Also, changes in the geometry of the pressure tubes and the condition and relative position of other channel components must be monitored in order to predict maintenance requirements. Fig-1 shows a typical coolant channel assembly.

Brief description of BARCIS

The overall system of BARCIS consists of

- an inspection head containing NDE sensors.
- a special sealing plug.
- an in-head calibration plug containing standard references notches for online calibration checking of flaw sensors.
- a remotely operated drive mechanism for positioning the inspection head inside the coolant channel (two-axis drive mechanism for Mark-II system and four-axis drive mechanism for Mark-III system).
- a windows based operator friendly computerised control system.
- a dedicated computer compatible gap measuring instrument with facility for automatic logging of eddy current inspection data.
- a quad CCTV system for remotised alignment of drive tubes and calibration checking of linear and rotary displacement of inspection head.
- NDE instruments.

The existing fuelling machine (FM) has been used to remotely load/unload the assembly of special sealing plug and inspection head into the coolant channel. This has resulted in substantial reduction in cost and complexity of the system.

A drive tube attached to the inspection head carries the transducers cables and passes through seals in the special sealing plug. Once the inspection head and sealing plug are in place, extension drive tubes in drive mechanism are manually coupled to the basic drive tube attached to the inspection head. The joints for extension drive tubes designed to be leak tight and have features for positive locking. The drive mechanism is remotely operated for driving the inspection head inside the coolant channel in the desired test sequence. ISI control station is located outside containment. Seventy metre long cable are provided for operation of BARCIS from ISI control station.

NDE capabilities

BARCIS has the following NDE capabilities:

- Ultrasonic measurement of wall thickness of pressure tube.
- Ultrasonic detection of flaws in longitudinal and circumferential directions in pressure tube.
- Eddy current detection of garter spring location and tilt.
- Eddy current estimation of annular gap between pressure tube and calandria tube.
- Eddy current detection of flaws in longitudinal and circumferential directions on inner surface of pressure tube.
- Inclinator based sag measurement of pressure tube.

BARCIS is capable of inspecting an average of two coolant channel per day with approximately half the time required for defueling the channel, alignment of

drive mechanism and refueling the channel upto inspection.

The successful completion of indigenous channel inspection system marks the development of critical technology and has resulted in substantial savings in foreign exchange. A prototype version of the system was developed in 1992. The prototype system was used for ISI of about 200 coolant channels of RAPS-2, MAPS-1 & MAPS-2. Based on the successful operation of the prototype system, NPC had requested BARC to supply two Mark-II systems for MAPS and one Mark-III system for NAPS at a total cost of Rs 5.50 crores. Mark-II system was supplied to MAPS in July, 97. Mark-III system was supplied to NAPS in Jan 1999. Reference [1] gives description of BARCIS. Figures 2 & 3 show BARCIS Mark-II & III systems respectively.

NDE sensors and instruments

10 MHz ultrasonic normal beam point focussed and angle beam line focussed immersion probes are used for thickness measurement and flaw detection respectively. Eddy current split bobbin probe (7 kHz) is used for detection of garter spring location and tilt. Eddy current pan-cake probe (2.5 kHz) is used for gap measurement. Eddy current focussed differential probe (100 kHz) is used for detecting flaws on inner surface of pressure tubes. All eddy current probes have been specially developed for BARCIS. Standard ultrasonic thickness tester and flaw detector have been utilised. Standard eddy current tester has been utilised for garter spring location and eddy current flaw detection. A dedicated computer compatible eddy current instrument has been developed for gap measurement. The problem of estimation of annular gap

between pressure tube and calandria tube has been quite challenging. All the above sensors have worked satisfactorily upto an integrated radiation dose of about 10^6 Rads which gives about 100 hours of operation in coolant channels having a radiation field of the order of 10^6 Rads per hour. The radiation rating of commercially available servo-inclinometer is limited to 10^7 Rads due to the type of damping oil used.

Reference [2] describes the technique for eddy current estimation of annular gap between pressure tube and calandria tube. Fig-4 shows the salient features of the technique and the instrument developed.

Reference [3] describes the technique for inclinometer based sag measurement.

The reference notches in the in-head calibration plug for calibration of ultrasonic and eddy current flaw detection have depth equal to 3 % of wall thickness of pressure tube.

Advances in BARCIS

Under IX-Plan project "Development of Tools & Techniques" (Power-6) following additional capabilities are being developed at Reactor Control Division:

- Ultrasonic measurement of ID, OD and WD of pressure tubes.
- Ultrasonic imaging of zirconium hydride blisters in pressure tubes.
- Development of miniature underwater radiation resistant CCTV camera for visual inspection.
- Automatic data acquisition and evaluation

Recently, a computer based four channel ultrasonic dimensional measuring system has been developed.

Three nos. of 25 MHz normal beam point focussed immersion probes mounted 120° apart are used for measurement of ID, OD & WT of pressure tube. The fourth probe is used to provide correction for change in ultrasonic velocity with temperature. The system has a resolution of measurement of one micro-meter and overall accuracy of ten micro-meters. Using this system, experiments for detection of zirconium hydride blisters are being conducted. It has been possible to detect one millimeter diameter blister using amplitude of reflected shear wave generated from one of the above mentioned probes. Fig-5 shows the system developed and the image of blister sample. Further experiments to qualify the technique for field use are on hand. Reference [4] describes the methodology for growth of zirconium hydride blisters and their detection.

Prototype optical and electronic components for radiation resistant CCTV camera have been developed and are undergoing irradiation testing. Fig-6 shows the camera components developed and the Gamma Chamber being used for the irradiation testing. The components are being qualified for use in radiation field of 10^6 Rads/hr for an integrated dose of 10^8 Rads. Efforts to extend radiation life of servo-inclinometers by using radiation resistant damping oils are in progress.

Participating agencies

Reactor Control Division has been responsible for the development of inspection head, drive mechanism, computerised control system, eddy

current gap measurement, inclinometer based sag measurement, quad CCTV system and NDE instruments. Atomic Fuels Division has been responsible for the development of inspection techniques. Refueling technology Division has been responsible for the development of special sealing plug and in-head calibration plug

References

1. Manjit Singh et al, "BARCIS-A Semi Automated Tool for In-Service Inspection of Coolant Channel", *IAEA Technical committee Meeting*, Feb '94, Mumbai, India.
2. Manjit Singh et al, "Eddy Current Measurement of Annular Gap Between Pressure Tube and Calandria Tube in Indian PHWRs", *14th World Conference on NDT*, pp 377-380, Dec 8-13, 1996, New Delhi, India.
3. Manjit Singh et al, "Techniques to Measure Deflection of Pressure Tubes in Indian PHWRs", *14th World Conference on NDT*, pp 381-384, Dec 8-13, 1996, New Delhi, India.
4. Manjit Singh et al, "Study of Hydride Blisters in Zirconium Alloy Pressure Tube Spools and their Detection using an Ultrasonic Techniques", *Joint EC-IAEA Specialist Meeting on NDT Methods for Monitoring Degradation*, pp 53-69, March 10-12, 1999, Petten, The Netherlands.

"BARCIS is capable of inspecting an average of two coolant channel per day with approximately half the time required for defueling the channel, alignment of drive mechanism and refueling the channel upto inspection."

Mr Manjit Singh received the "BARC Technical Excellence Award" in 1997 for the development of BARCIS

About the author



Mr Manjit Singh joined 16th batch of BARC Training School in 1972 after graduating in Electrical Engineering from Punjabi University, Patiala. He stood first among successful electrical engineers at BARC Training School. He has specialised in the design and development of remotised control mechanisms and inspection tools for nuclear reactors. He has been responsible for the development of shut-off rod drive mechanisms for Dhruva, Kamini and NAPP reactors. He has also been responsible for the development of BARCIS (BARC Channel Inspection System) for in-service inspection of coolant channels of 220 MWe PHWRs. Presently, he is heading Control Mechanisms & ISI Section of Reactor Control Division, BARC.

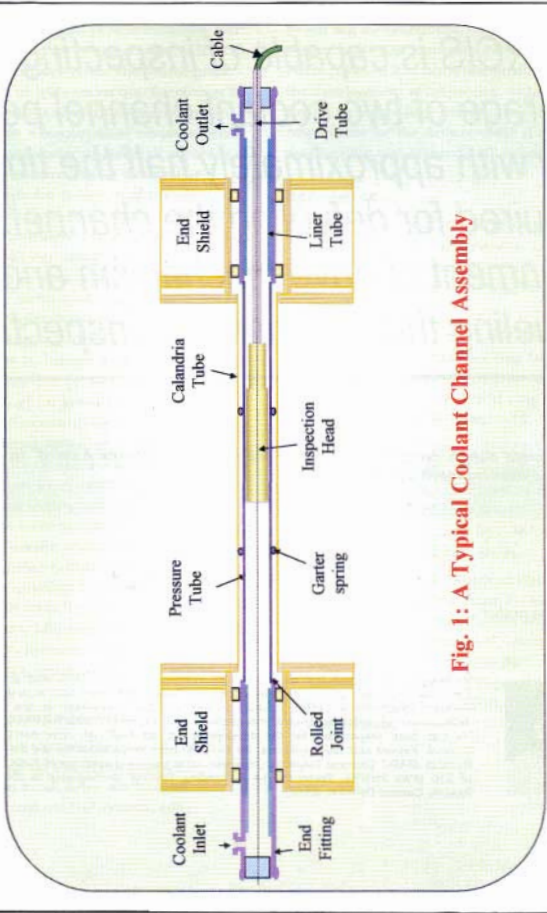
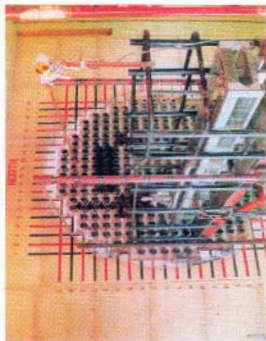
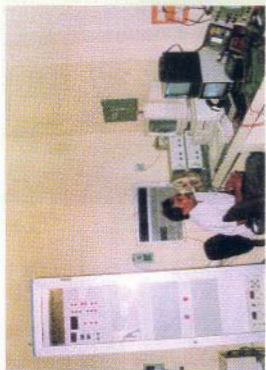


Fig. 1: A Typical Coolant Channel Assembly



Drive Mechanism

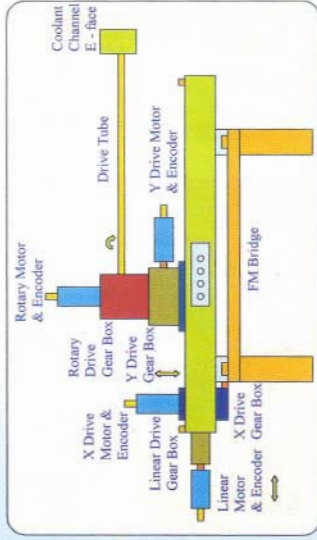


Control Station

Fig. 2: BARCIS Mark-II System for MAPS/RAPS



Assembly of Inspection Head & Special Sealing Plug



Drive Mechanism

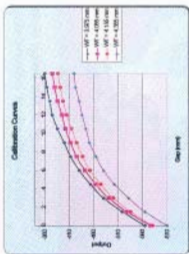


Control Cabinet

Fig. 3: BARCIS Mark-III System for NAPS

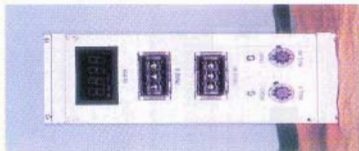
Sensor Specifications

- Type – Pan-cake driver, differential pick-up probe
- Range of gap measurement – 0 – 17 mm
- Pressure – 5 kg/cm²
- Radiation life – 100 Mega Rads



Technique for gap measurement

- Probe lift-off effect is nullified by aligning it in X-axis
- Temperature effect is nullified by using differential pick-up probe
- Measured eddy current signal contains information about wall thickness of PT and PT-CT gap
- PT wall thickness is measured separately using ultrasonic technique
- Calibration curves of eddy current output for change in gap as a function of wall thickness are generated
- From measured eddy current output and wall thickness of PT, PT-CT gap values are generated using calibration curves and gap profile is plotted



Eddy current instrument for gap measurement

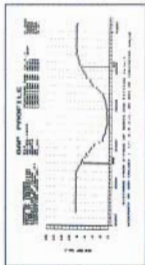
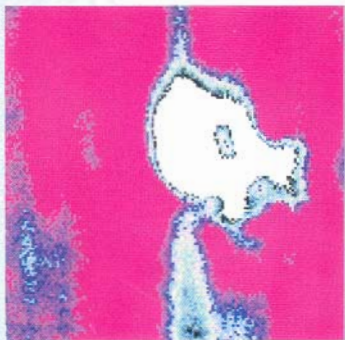
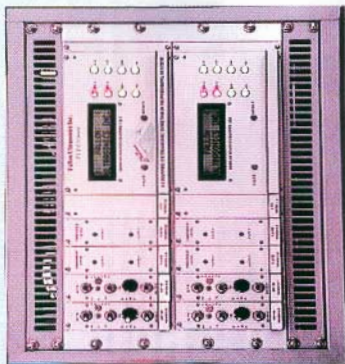


Fig-4: Eddy Current Measurement of Gap between Pressure Tube and Calandria Tube



Ultrasound image of Zirconium Hydride Blister
using amplitude of reflected shear wave



4 channel Dimension Measuring

Fig-5: Advances in Ultrasonic Inspection and Monitoring Techniques

Optical components of Radial viewing head

- Multi-component coated lens
- Two component elliptical mirror
- Transparent tube for encasing light bulbs
- Transparent discs

Camera PCBs

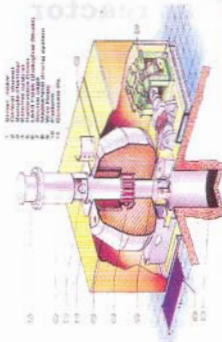
- Pre-amplifier
- Focus Board
- Gate Drive Board
- Video Amplifier and Signal Processor Board
- Vertical Deflection Board
- Horizontal Deflection Board
- Sync Generator
- Voltage Generator Board
- Servo Controller Board



Radiation Resistant CCTV Camera



Internals of Radiation Resistant CCTV Camera



Gamma Chamber 5000 – Sectional View

Fig 6: Development of Miniature Underwater Radiation Resistant CCTV Camera

Estimation of transient hydraulic load during Loss of Coolant Accident (LOCA) of a nuclear reactor

D. Mukhopadhyay, Satish K. Gupta and V. Venkat Raj

Reactor Design and Development Group
Bhabha Atomic Research Centre

Abstract

The RELAP-LOAD code, a post processor of the transient thermal-hydraulic computer code RELAP4/MOD6, has been developed to retrieve relevant data from RELAP4/MOD6 and calculate the time dependent force exerted on the piping system subjected to pipe rupture. The code RELAP4-LOAD forms a tool for piping analysis. Both analytical and experimental data of different fluid conditions were used to verify the RELAP-LOAD code. Code-Data comparison indicated an overall good code performance.

Introduction

A POSTULATED SUDDEN BREAK IN THE pressurised piping network of a nuclear power plant leads to blowdown thrust force on the different components of Primary Heat Transport (PHT) system or the secondary coolant system depending on the break location. The resultant transient pressure fields also impose large forces on the internal components like fuel bundles for the pressure tube type nuclear reactors which may lead to the mechanical failure of the component. This is an important consideration in nuclear safety assessment. The design of restraints, protection devices for nuclear class I and II piping system, Steam Relief Valves mounted on the steam pipe lines and reactor internal structures must consider severe pipe rupture and steam / water hammer loading.

The Indian Pressurised Heavy Water Reactor (PHWR) is a pressure tube type

nuclear reactor which consists of coolant channels (pressure tubes) containing nuclear fuel bundles, steam generators, pumps and a large piping network. A study has been carried out to estimate the blowdown load arising from breaks of different sizes and locations in the primary and secondary heat transport system for PHWRs. Calculation of the blowdown force and unbalanced piping acceleration loads involves information regarding the system behaviour during the transient such as the change of pressure, temperature, fluid density, mass flow rates through the pipe and break mass flow rate as a function of time. The thermal-hydraulic Nuclear Safety Analysis computer code, RELAP4/MOD6 [1] developed by Idaho National Engineering Laboratory (INEL), and modified and adapted by us, is capable of calculating these transients variables in the fluid system subjected to pipe rupture. The RELAP4/MOD6 code uses the node

junction approach by dividing the system into control volumes with connecting flow paths, called junctions. The integrated mass, momentum and energy equations for the control volumes are solved along with water property routine to calculate the average thermal hydraulic properties. The integrated momentum equation with proper loss coefficients is used for calculating mass flow rates in junctions. The temperature distribution in the heated elements like nuclear fuel bundle and steam generator tubes is estimated by solving the conduction equation. The RELAP-LOAD code, a post processor of RELAP4/MOD6 has been developed to retrieve relevant data from RELAP4/OD6 calculation and calculates total blowdown force based on the model developed by Strong [2]. The code RELAP-LOAD calculates the wave force by integrating the momentum equation over the control volumes. The pressure force and the momentum force are calculated from the integrated momentum equation for the break junction. In RELAP-LOAD, for open segment of the broken pipe, a sum of these three forces is considered. For the bounded segment (pipe segment between two bends) only the wave force has been considered.

The RELAP-LOAD code has been validated against series of experiments measuring the hydraulic loads during (i) steam blowdown and (ii) subcooled blowdown followed by saturated blowdown. The code has also been validated with the analytical solution for a steam blowdown problem. The capability of RELAP-LOAD to simulate wave propagation, which is the dominant phenomenon during pipe rupture has been verified. A sensitivity analysis has been carried out by varying control volume length and time step. The ratio of

control volume length to time step is important to capture the wave propagation phenomena correctly. As a part of the sensitivity studies, different critical flow models like Homogeneous Equilibrium Model (HEM), Henry's model, Moody's model or a combination of the two models are employed to calculate the break flow rates for the same experiment. From the validation exercise it is concluded that RELAP-LOAD force prediction is in good agreement with the experimental data.

The paper also describes the application of the RELAP-LOAD for estimating the blowdown force arising from a double ended break (2x100 % Reactor Header flow area) at the Reactor Inlet Header (the largest diameter pipe in PHT) for an Indian PHWR.

Development of Relap-load

Fundamental equation :

The balanced mass, momentum and energy must be satisfied among control volumes and junctions. Eq. (1) shows the Navier-Stokes momentum equation in the integral form:

$$\frac{\partial}{\partial t} \int \rho u dV + \int \rho u(u.n) dS = - \int P n dS - \int \tau dS - \int \rho g dV \quad (1)$$

The following equation can be obtained by applying eq.(1) to the control volume shown in Fig.1[2]

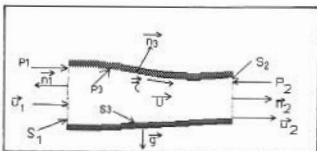


Fig. 1 : Control volume for thrust force calculation

$$\frac{\partial}{\partial t} \int_V \rho u dV + \int_A \rho u(u, n) dS_1 + \int_A \rho u_2(u_2, n_2) dS_2 = - \left[\int_A P_1 n_1 dS_1 + \int_A P_2 n_2 dS_2 + \int_V \rho g dV \right] - \int_A \tau dS_1 - \int_V \rho g dV \quad (2)$$

The only way a fluid can exert a force upon its container is (i) by means of fluid pressure which acts over the wetted surfaces of the container and (ii) by means of friction between the wetted surfaces of the container and the fluid. The thrust force is shown in eq. (3)

$$F = \int_A P_1 n_1 dS_1 + \int_A \tau dS_1 \quad (3)$$

Eq. (2) and (3) lead to the thrust force :

$$-F = \frac{\partial}{\partial t} \int_V \rho u dV + \int_A \rho u(u, n) dS_1 + \int_A \rho u_2(u_2, n_2) dS_2 + \int_A P_1 n_1 dS_1 + \int_A P_2 n_2 dS_2 + g \int_V \rho dV \quad (4)$$

Eq. (4) is now applied to the constant area pipe shown in Fig. 2.

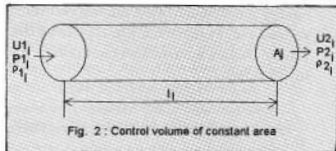


Fig. 2 : Control volume of constant area

The gravitational term in eq. (4) can be neglected because of its low magnitude. The density ρ_i and velocity u_i for the i th control volume can be linearised by introducing arithmetic average value in the volume. Thus eq. (4) can lead to the following expression for the blowdown thrust force of the i th control volume

$$-F = A l_i \left(u_i \frac{\partial \rho}{\partial t} + \rho \frac{\partial u_i}{\partial t} \right) + A l_i (\rho_2 u_2 - \rho_1 u_1) + A (P_2 - P_1) \quad (5)$$

Assemblage of eq. (5) for all the control volume leads to the blowdown thrust force in a single phase flow and homogeneous two phase flow as follows :

$$F = \sum F_i = F_A + F_M + F_P \quad (6)$$

where,

$$\text{Acceleration force: } -F_A = \sum l_i \delta W_i / \delta t \quad (7)$$

$$\text{Momentum force: } -F_M = \sum A_i (\rho_2 u_2 - \rho_1 u_1) \quad (8)$$

$$\text{Pressure force: } -F_P = \sum A_i (P_2 - P_1) \quad (9)$$

and \sum is the summation for all the control volumes.

For the internal forces i, e for bounded segment (section of pipe with bend at both ends) the redundant inclusion of the static pressure differential force and the momentum force are avoided. The force is due to the acceleration force associated with the unsteady flow [2,3]. The expression of blowdown force in the bounded segment is as follows in eq. 10

$$-F_A = \sum l_i \delta W_i / \delta t \quad (10)$$

For an open segment (bend at one end and is open to the atmosphere at the other end) the blowdown force can be given by eq. (11) to (13) [2,3,4]

$$\text{Acceleration force: } -F_A = \sum l_i \delta W_i / \delta t \quad (11)$$

Momentum force :

$$-FM = [A\rho u^2]_e = [W^2/A\rho]_e \quad (12)$$

$$\text{Pressure force: } -FP = A_e (P_e - P_x) \quad (13)$$

When the flow is satisfying the critical flow condition, the exit pressure P_e is assumed to be the critical pressure P_c . The Pressure force for each flow pattern can be expressed as,

$$-FP = A_e (P_c - P_x) \quad (14)$$

In this critical pressure calculation, the Henry-Fauske model [3] is applied to the non-equilibrium state for the LOCA initiation although it is derived for the small ratio of the L/D. According to the Henry-Fauske model, the critical pressure ratio in the subcooled region is expressed as eq. 15

$$\eta = P_c / P_0 = 1 - [G_c^2 / (2\rho_0 P_0)] \quad (15)$$

$$\text{where } G_c = W_c / A_e$$

Coupling with RELAP4/MOD6

The modelling of a piping system with RELAP4/MOD6 is done with the help of control volumes and junctions. A typical example of a RELAP4/MOD6 model for piping system consisting a source tank, bounded segment and an open segment shown in Fig. 3.

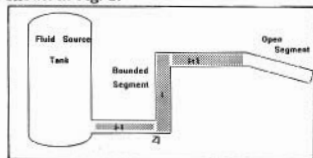


Fig. 3 : Concept of Open and Bounded segment

The control volumes $i-1$ and i is being connected with junction Z_j . To calculate acceleration force for a bounded segment Eq. (11) has been applied on RELAP4/MOD6 specific model over the control volume i . The acceleration force over the control volume of length L is given by,

Acceleration force :

$$-FA = \sum_{i=1,n} L \cdot dW(i,t) / dt \quad (16)$$

where, n is the number of control volumes presenting the bounded segment.

The time dependent force in the open segment for a RELAP4/MOD6 specific model is being calculated with the help of Eq. (11) to (13). The different components of the blowdown force is given by,

Pressure force :

$$-FP = A(Z_j)_e [P_c(Z_j, t)_e - P_x] \quad (17)$$

Momentum force :

$$-FM = W^2(Z_j, t)_e / [A(Z_j)_e \rho(Z_j, t)_e] \quad (18)$$

Acceleration force :

$$-FA = \sum_{i=1,n} L \cdot dW(i,t) / dt \quad (19)$$

where, n is the number of control volumes present in the open segment.

The total force for the open segment is given as,

$$-F = A(Z_j)_e [P_c(Z_j, t)_e - P_x] + W^2(Z_j, t)_e / [A(Z_j)_e \rho(Z_j, t)_e] + L \cdot dW(i,t) / dt \quad (20)$$

P_c , the critical pressure is determined by applying eq. (15)

Calculational method

(i) Pressure force (FP) : Calculation of pressure force involves three steps, they are as following,

step 1. P_o used in the eqn. (15) is determined in the following way,

$$P_o(i,t)_{ev} = P(i,t-\Delta t)_{ev} + [W^2(i,t-\Delta t) / 2A^2 \rho(i,t-\Delta t)]_{ev} \quad (21)$$

Stagnation pressure at the exit volume (break volume) at the current time step, $P_o(i,t)_{ev}$ is being determined from the eq. 21. The exit volume pressure, break volume flowrate and break volume density of the previous time step ($t-\Delta t$) calculated by RELAP4 execution is fed into RELAP-LOAD to calculate the stagnation pressure.

step 2. P_c is being calculated from eq. (15). Replacing W_c and ρ_{10} with the transient data of $W(Z_j,t)_e$, $\rho(Z_j,t)_e$ obtained from RELAP4 execution, geometric parameter (A_e) and stagnation pressure $P_o(i,t)_{ev}$. The down stream condition of the break is considered to be atmospheric.

step 3. The pressure force is estimated with the eq. (17). The critical pressure transient and the break area are used to generate the pressure force time history.

(ii) Momentum Force (FM) : The momentum force is being calculated from eq. (18) with the break discharge mass flow rate $W(Z_j,t)_e$ and the fluid density at the break $\rho(Z_j,t)_e$. Transient data of these two parameters of the break junction are generated from the RELAP4 run and fed into RELAP-LOAD along with the break area to calculate the momentum force.

(iii) Acceleration Force (FA) : Eq. (19) has been used to calculate the acceleration force. Transient parameter of control volume flow rates $W(i,t)$, time step Δt and the control volume length L are the

parameters used to calculate the force. RELAP4 output of transient volume flow rates are used as the input to RELAP-LOAD to calculate the wave force.

Modelling technique

Wave propagation

The RELAP4 code uses the node junction approach by dividing the system into control volumes with connecting flow paths, called junctions. The average thermal hydraulic properties are calculated in each volume. With the proper modelling technique, RELAP4 can simulate the wave propagation during the pipe rupture. The condition is that the combination of the nodalisation and calculation time step must satisfy criteria that the distance travelled by the wave in one time step is less than the length of a volume. This ensures that its effect is properly detected in each volume.

Pipe branching

Pipe branching is common in a nuclear power plant coolant circuit. In RELAP4/MOD6 simulation, the selection of the fluid equation at the branching location is an important consideration. There are five basic fluid momentum equations available.

- (i) compressible single stream flow with momentum flux (MVMIX = 0)
- (ii) compressible two stream flow with one dimensional momentum mixing (MVMIX = 1 or 2)
- (iii) incompressible single stream flow with one dimensional momentum mixing (MVMIX = 3)

This set of equations is designed for different flow patterns and geometries. The choice of the equation in RELAP4/MOD6 is controlled by the junction input parameter MVMIX. Ref. 1

provides detailed discussion on the assumption of each equation and the selection of MVMIX under different geometries.. An example of momentum equation selection is given in Fig. 4.

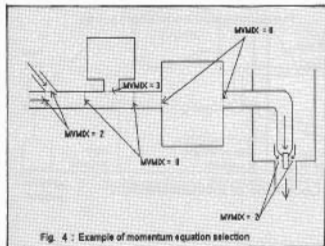


Fig. 4 : Example of momentum equation selection

Critical flow model selection

The depressurisation rate for any system is dependent upon the rate of mass depletion. Critical flow governs the rate at which fluid will be discharged from a system during most of the depressurization and, consequently, it largely controls the time of blowdown. Experience has shown that the simple equation for inertial flow rate is quite accurate at relatively low flows but becomes greatly exaggerated as junction pressure ratio increases and critical conditions are approached. Critical flow criteria are therefore invoked to limit the flow rate through an opening or junction to a more realistic level under these circumstances. From the test runs with different critical flow models, namely inertial flow model, sonic, Moody, Henry-Fauske and HEM models as reported in reference 1, it is found that nearly all the flow models and combinations, with the exception of the inertial model, the sonic model and the HEM model, exhaust about the same amount of water from a system in the same blowdown time. Some exhibit

a higher flow rate during subcooled conditions while for others the reverse is true. These observations along with initial condition of the fluid and blowdown pipe length constitute the basic criteria for critical flow model selection.

Validation exercise

The accuracy and validity of the RELAP-LOAD code have been verified using the following benchmark test data. The experiments produced reasonably good data on hydrodynamic pipe forces resulting from the fluid transient.

Japan Atomic Energy Research Institute (JAERI) Pressurised Water Reactor (PWR) blowdown experiment [3]

The pipe whip experiment was conducted at JAERI with a 4" pipe under the PWR Loss of Coolant Accident (LOCA) conditions. The schematic of test facility is given in Fig. 5. The initial conditions before the break were 15.6 MPa and 320° C in the pressure vessel, test pipe and other component. A 19 control volume test facility specific RELAP4/MOD6 model was developed (Fig. 6). The blowdown thrust force prediction using the Henry-Fauske critical flow model and the experimental data (test no. 5506) are depicted in Fig. 7. The comparison shows a good agreement for the initial subcooled blowdown period but the code underestimate the saturated blowdown load after 0.5 s of the transient.

Electric Power Research Institute (EPRI) / Combustion Engineering (C-E) Safety Relief Valve (SRV) tests. [4]

A full scale Pressurised Water Reactor (PWR) pressuriser SRV test program was carried out at the EPRI, C-E

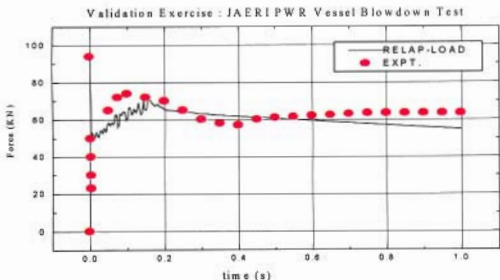
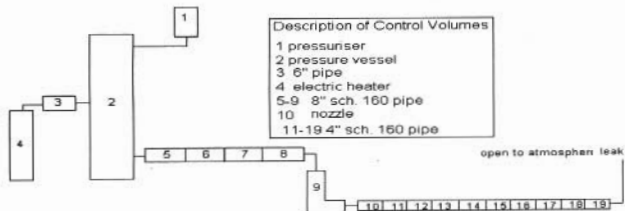
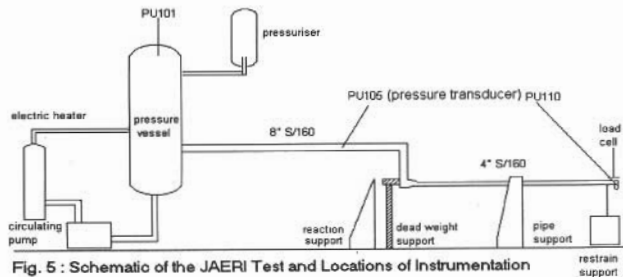


Fig. 7 : Transient Blowdown Force History

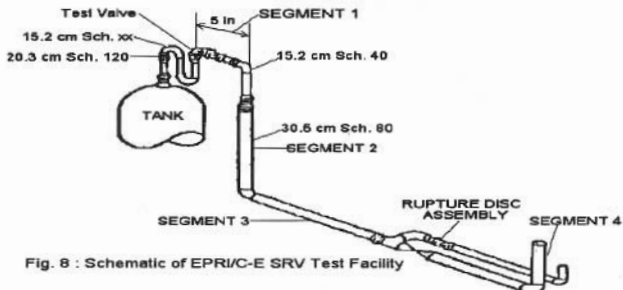


Fig. 8 : Schematic of EPRI/C-E SRV Test Facility

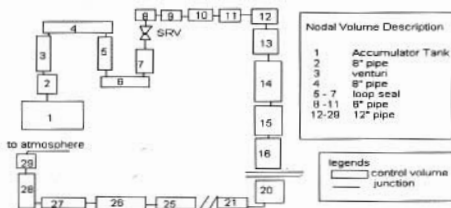


Fig. 9 : Nodalisation Scheme for EPRI SRV Test

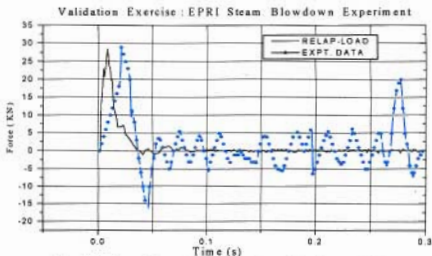


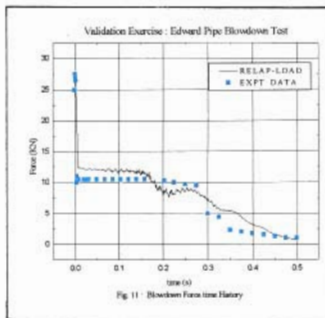
Fig. 10 : Force Transient Comparison for Segment 2

test facilities at Windsor, Connecticut. The schematic is given in Fig. 8. Test 1411 simulates a continuous steam discharge through the safety valve. The valve inlet pressure was regulated by modelling the reservoir pressure ramp from 1.66 MPa to 1.69 MPa in 0.5 s. An instantaneous opening of the SRV has been considered in the analysis compared to 15 ms linear opening as RELAP4 can simulate a linear opening when the valve is located in the flow path. This valve leaked slightly before the test and thus initial downstream air was replaced with steam. Assuming constant enthalpy throttling, a quality of 0.9 is calculated for the downstream piping steam environment. Therefore RELAP4/MOD6 model downstream conditions for this case correspond to 0.9 quality steam at atmospheric pressure and fluid temperature initialised at 100°C. The test segment has been modelled with twentynine control volumes (Fig. 9) and the reservoir is modelled with a time dependent volume option of RELAP4/MOD6, where the boundary condition to the test is given. The critical flow through the valve is modelled with Moody's critical flow model. The segment 2 hydrodynamic piping force calculated with RELAP-LOAD is compared with the test data in Fig. 10. It can be seen that the magnitude and timing of the RELAP-LOAD calculated force agrees reasonably well with the test data. A notable discrepancy occurs near 250 ms, where the test data indicates a force peak not calculated by the code. The difference is apparently due to the accumulation of condensate in the lower horizontal discharge piping leg prior to valve opening. Although an attempt was made to model the downstream steam environment, information on the accumulation of the condensate was not

available to allow reasonable modelling of this condition.

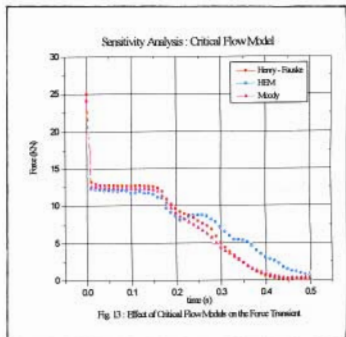
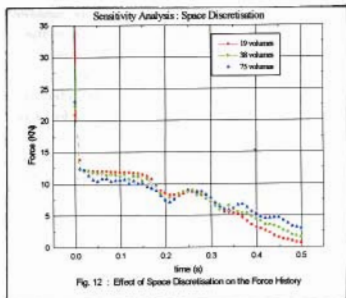
Edward and O'Brien pipe experiment [5]

The pipe blowdown experimental data reported by Edward and O'Brien provide an excellent experimental data base to benchmark the blowdown force calculation of RELAP-LOAD. The experimental test consisted of pressurising the pipe of 4.096 m length and internal diameter of 73 mm with water to the required test pressure (7 MPa and 242°C) and rupturing the glass disk at the end of the pipe with a pellet gun to initiate the blowdown. The load cell was mounted at the end of the pipe to measure the hydraulic load. The same RELAP4/MOD6 model with 26 equal volumes to represent the pipe and a HEM critical flow model was used. A RELAP-LOAD run was made to calculate the thrust force. Since the entire segment is an open one, the force calculated is the sum of the blowdown force at rupture end and the wave force. A comparison between the RELAP-LOAD calculated end thrust load and measured data (Fig. 11), indicates good agreement.



Sensitivity analysis

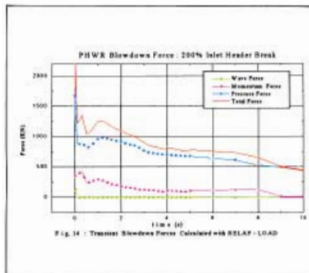
The sensitivity analysis has been carried to see the effect of space discretisation, temporal discretisation and different critical flow model on the hydraulic forces. For this study, Edward's pipe blowdown experiment has been considered. The space discretisation study has been done with 19, 38 and 75 control volumes. Coarse (19 volumes) to finer (75 volume) nodalisation shows an increase in initial peak load (Fig. 12). As increase in number of control volumes helps to capture the wave propagation well, the depressurisation rate as well as the critical flow becomes higher, which lead to higher peak load. It has been observed also that the difference of load calculated for 38 and 75 volumes is very less i.e the critical flow and hydraulic force is not so sensitive to the space discretisation over 38 control volume for this case. A temporal discretisation study involving time step (Δt) of 10^{-4} s, 10^{-5} s and 10^{-6} s shows a rise in load from 10^{-4} s to 10^{-5} s. After 10^{-5} s the decrease in time step becomes insensitive. This is also attributed due to the wave propagation history. Sensitivity analysis with different critical flow model (Homogeneous Equilibrium Model, Moody's model and Henry-Fauske's model) is being depicted in Fig. 13. Henry-Fauske's model predicts the highest peak flow and peak force transient among the three models. The Homogeneous Equilibrium Model predicts the minimum and prediction from Moody's model lies in between the Henry-Fauske model and Homogeneous Equilibrium Model.



Application of RELAP-LOAD

The RELAP-LOAD code has been used for estimating the blowdown force arising from a double ended break at the Reactor Inlet Header (the largest diameter pipe). In this analysis it has been assumed that the load cell is located at any one end of the header. A detailed RELAP4/MOD6 model developed for the Indian PHWRs and the LOCA analysis are described in

Reference 6. The break flow rate, header pressure and density obtained from the LOCA analysis along with geometric details are used by RELAP-LOAD to calculate blowdown force as depicted in Fig. 14. The peak estimated total force is found to be 2126 KN for a maximum break discharge rate of 8000 kg/s using Homogeneous Equilibrium Model as the critical flow model.



Conclusion

Although RELAP4/MOD6 uses a lumped parameter approach and calculates only the average thermal-hydraulic properties inside a volume, it has been demonstrated that with proper modelling RELAP4/MOD6 can simulate wave propagation phenomena during a pipe rupture. The comparison of RELAP-LOAD results experimental data shows a favourable agreement, verifying that RELAP-LOAD has been correctly formulated and the code provides a satisfactory basis for piping analysis.

Nomenclature

A : flow area
 F : blowdown thrust force
 FA : acceleration force

FM : momentum force
 FP : pressure force
 G : mass flow rate per unit area
 L : pipe length
 l : control volume length
 P : pressure
 S : surface area
 u : velocity
 V : volume
 W : mass flow rate
 τ : shear force
 ρ : density

Subscripts

c : critical condition
 e : exit
 ev : break volume
 lo : liq. at stagnation
 o : stagnation
 α : atmosphere

References

- Fischer, S. R., et. al, 1978 RELAP4/MOD6: A computer program for transient thermal-hydraulic analysis of nuclear reactors and related systems, user's manual. *Technical Report no. CDAP TR003*, Idaho National Engineering Laboratory (INEL), USA
- Strong, R. Benjamin and Baschire, J., 1978 Pipe rupture and steam/water hammer design loads for dynamic analysis of piping systems. *J. Nuclear Engineering and Design* 45, 419-428.
- Yano, T., Miyazaki, N. and Isozaki T., 1982 Transient analysis of blowdown thrust force under PWR LOCA, *Nuclear Engg. and Design*, vol. 75, 157-168
- Wheeler, A. J. 1983 Measurement of piping forces in a safety valve discharge, *Technical Report no. EPRI NP-2628*

5. Cajigas, Juan M., 1990 The RELAP5-FORCE MOD2 code: a hydrodynamic forcing function calculation version of RELAP5, *J. Nuclear Technology* 90, 316-325
6. Mukhopadhyay, D., Chatterjee, B. and Gupta K. Satish, 1996 Modelling and simulation of a large break LOCA for Indian PHWRs, *Proceedings of the IChE Golden Jubilee Congress*, vol. 1, 73-83

This paper was presented the "Dr Wille Memorial Award" for the best paper in the industrial section in 25th National and 1st International Conference on Fluid Mechanics and Fluid Power, held at IIT, Delhi, during December 15-17, 1998.

About the authors



Mr D. Mukhopadhyay did his B. Tech. in Chemical Engineering from Calcutta University and joined the 34th batch of BARC Training School. His field of study involves safety analysis and plant transient analysis for nuclear power plants and transient hydraulic load determination for piping, process equipment internals and reactor channel. His work also includes study and simulation of severe accident for PHWRs and AHWR with thermal-hydraulic model, thermo-mechanical model, thermo-chemical model and high temperature reaction model.



Dr. S. K. Gupta at present Head, Core Safety Studies Section, Reactor Safety Division, graduated from IIT Chennai in 1971 and completed his Ph.D in 1992 from IIT Mumbai. He is a 15th batch graduate from Training School, BARC. His work includes computer code development and their application for the safety analysis of nuclear power plants and research reactors. The safety analysis includes Loss of Coolant Accident (LOCA) analysis and various anticipated operational plant transients for Indian PHWRs, BWRs and the proposed AHWR



Dr. V. Venkat Raj is presently the Director of the Health, Safety and Environment Group, BARC. He graduated from the University of Madras in 1963 and is from the 7th batch of the BARC Training School. He obtained his Master's degree from the University of London and Ph.D. from the Indian Institute of Technology, Mumbai. His major areas of research include nuclear reactor thermalhydraulics and safety, single-phase and two-phase flow and heat transfer studies, probabilistic safety assessment, ageing management studies, etc. He is a life member of a number of professional societies. He is Vice-President of the Indian Society for

Heat and Mass Transfer (ISHMT) and the President of Mumbai Chapter of ISHMT. He is a member of the Executive Committee of the Indian Nuclear Society and a member of the Governing Council of the National Society of Fluid Mechanics and Fluid Power. He participates actively in the safety review of Indian nuclear installations through a number of Senior Level Committees of AERB. He is a member of the Nuclear Safety Standards Advisory Committee of the IAEA.

Concentration of dilute sewage sludge slurry using EB crosslinked fast response temperature sensitive poly (vinyl methyl ether) hydrogel

S. Sabharwal, Y.K.Bhardwaj and A.B. Majali

Isotope Division
Bhabha Atomic Research Centre

Abstract

Electron beam (EB) irradiation technique has been utilized to create non-homogeneous fast response temperature sensitive poly (vinyl methyl ether) (PVME) hydrogels. The crosslinked hydrogels were swollen in dilute sewage sludge samples at room temperature and dewatering was achieved by deswelling the hydrogels at 323 K. The results show that 1g gel could remove 9 to 12 g of water from 25 g of sludge, in ten cycles. The effect of various factors such as swelling/deswelling cycle time, solid content of sludge on the removal efficiency of water removal process has been investigated.

Introduction

THE "ENVIRONMENTALLY SENSITIVE polymers", that undergo abrupt reversible changes in mass and volume in response to minor changes in the gel's environment, are being probed worldwide as potential materials for novel applications such as drug delivery systems, mechano-chemical actuators in robotics, as artificial nerves and for concentrating protein/enzyme solutions near room temperature (1). Gels that undergo phase transition in response to change in their temperature are termed *temperature sensitive* and these shrink abruptly as temperature increases above a critical temperature. Crosslinked gels of poly (vinyl methyl ether) (PVME) and poly

(N-isopropyl acrylamide) (PNIPAm) when produced by thermocatalytic methods generally yield homogeneously crosslinked slow response gels that are unsuitable for many industrial uses. We have used EB irradiation to create non-homogeneously crosslinked temperature sensitive PVME gel which undergoes a phase transition at 37°C, and has a diffusion coefficient (D) value of $10^{-5} \text{ cm}^2 \text{ s}^{-1}$ compared to $1 \times 10^{-7} - 1 \times 10^{-8} \text{ cm}^2 \text{ s}^{-1}$, for conventional hydrogels (2). Development of such fast response temperature sensitive hydrogels will help to reduce the energy consumption levels of many processes such as concentrating dilute biological slurries. In the present work, the potential of utilizing EB crosslinked PVME gels to concentrate

dilute sewage sludge slurries has been demonstrated. The effect of process parameters such as solid content of sludge, swelling/deswelling cycle time and stirring rate has been studied. The results of these studies are reported in this paper.

Experimental

The PVME gels were synthesized by irradiating 30 wt% solution of PVME linear polymer using 2 MeV ILU-6 EB accelerator. The details have been published elsewhere (2). The sludge (2% solids) from input line of Sludge Hygienisation Research Irradiator (SHRI) was used.

Results and Discussion

Equilibrium swelling and swelling/deswelling behaviour of PVME gels: The linear polymer of PVME exhibits a lower critical solution at 307 K.

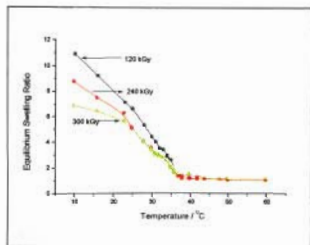


Fig. 1 Equilibrium swelling behaviour of EB crosslinked PVME hydrogels at different temperatures

Figure 1 shows the equilibrium swelling characteristics at different temperatures

for EB crosslinked PVME hydrogels. The swelling curves show the characteristic sharp discontinuity in the swollen mass at about 310 K, which is close to the LCST temperature of PVME in aqueous solution. Below this temperature, the strong interaction between the side chains of crosslinked polymer chains and water molecules, due to hydrogen bonding, result in swelling of the crosslinked polymer. At temperature > 310 K, the weak hydrogen bonds are broken and the structured water is eliminated, leading to the collapse of the hydrogel matrix.

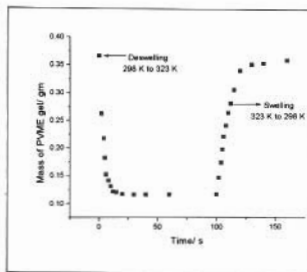


Fig. 2 Swelling and shrinking behaviour of EB crosslinked PVME hydrogel across LCST

Figure 2 shows results of the swelling/deswelling kinetics of a PVME hydrogel produced by irradiating to 300 kGy EB dose. The swelling and deswelling response of these hydrogels, shown in Fig.2, clearly indicates that the time required for these hydrogels to reach the equilibrium swelling is a few seconds as compared to hours required by conventional hydrogels. These materials could be beneficial in reducing the energy

requirements for applications, such as concentrating biological or coal slurries. We have studied the use of these hydrogels for concentrating dilute sewage sludge. The PVME gel equilibrated at 323 K was added to the sludge at 298 K and allowed to swell to equilibrium for varying lengths of time (15 s to 120 s). The gel samples were then taken out, equilibrated at 323 K for the same length of time as for swelling, so that they shrink and desorb water. The process was repeated for 10 cycles; the amount of water desorbed by the gel was estimated gravimetrically.

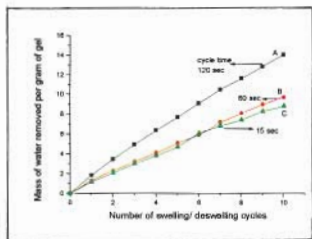


Fig. 3 Dewatering behaviour of sewage sludge slurry using PVME gels for various time cycles

The effects of swelling/deswelling time cycle on water removal characteristics of sludge slurry, shown in

Fig.3, indicate that the amount of water removed increased with the increasing cycle time. Therefore for investigations, a 120 s cycle time was selected. The effect of solid content of the sludge on the removal efficiency was also investigated. The comparative results of 2% and 4% solid content, presented in Fig.4, show that the removal efficiency of water is marginally reduced as the solid content of sludge increases. In conclusion, the results of this study have demonstrated that using a 1 g EB crosslinked PVME gel, about 9 to 12 g water can be removed from 25 g of sewage sludge by swelling the gel at room temperature and carrying out the deswelling at 323 K. Thus these hydrogels can be beneficial in reducing the energy requirements of processes such as dewatering of biological slurries.

References

1. A.S.Hoffman, A. Afrassiabi and L.C.Dong, *J.Controlled Release* 4, 174 (1986)
2. S.Sabharwal, H. Mohan, Y.K.Bhardwaj and A.B.Majali, *J. Chem.Soc.(Faraday Transactions)* 92, 4401 (1996)

This paper was adjudged as one of the two Best contributed papers at the International Conference on Applications of Radiation and Radioisotopes in Industrial Development (ICARID-98) held at Mumbai during February 4-6, 1998

"In the present work, the potential of utilizing EB crosslinked PVME gels to concentrate dilute sewage sludge slurries has been demonstrated."

About the authors



Dr. Sunil Sabharwal obtained his M.Sc. degree in Chemistry from Delhi University in 1978 and graduated from the BARC Training School in 1978-79. He obtained his Ph. D degree from Mumbai University. Presently he is working in the Radiation Technology Development Section of BARC. His main area of research are industrial application of radiation technology using electron beam irradiation, radiation effects on polymeric systems and pulse radiolysis studies of water soluble polymers.



Mr Y.K. Bhardwaj obtained his M.Sc. degree in Organic Chemistry from the University of Garhwal, Srinagar in 1988. He graduated from the BARC Training School in 1989 and started his research career in Radiation Technology Development Section. His research interests include development of radiation processed hydrogels for medical and pharmaceutical applications, synthesis of fast stimuli-responsive hydrogels and radiation crosslinking behaviour of water soluble polymers.



Mr A. B. Majali has over 25 years of experience in the application of radiation technology and industry. He was research associate at Atomic Energy Research Establishment UK and also served as an IAEA expert to the Government of Malaysia. Mr Majali's current research interest include radiation cross-linking, radiation vulcanization of natural rubber latex, depolymerization of poly tetrafluoroethylene and development of radiation cured controlled release systems for drugs and electron beam processing.

Evaluation of locally manufactured polyester film (Garfilm-EM) as a dosimeter in radiation processing

R.M.Bhat, U.R.Kini and B.L.Gupta

Radiation Standards and Instrumentation Division
Bhabha Atomic Research Centre

Abstract

Locally manufactured 250 μ m thick polyester film (Garfilm-EM) was evaluated spectrophotometrically for its dosimetric properties for use as a high dose radiation dosimeter. This film has good clarity, consistent thickness, scratch resistance and is easy to handle. Radiation induced changes in the absorption spectra were analyzed and 340 nm was chosen as the wavelength for absorption measurements. The reproducibility of the response for cobalt-60 gamma rays was found to be within $\pm 2\%$. The effect of post irradiation storage time on the response was also investigated. From the studies carried out, Garfilm-EM has been found to have a good potential as a dosimeter to measure absorbed doses in the range 20kGy-200kGy due to its linear dose - response relationship.

Introduction

SEVERAL POLYMERIC MATERIALS IN THE form of thin films like radiochromic dye films [1], clear perspex HX [2], and cellulose triacetate [3] find a wide application in radiation processing dosimetry. However, cost of these films, import procedures involved and their short shelf life make it necessary to look for locally available plastic films with good dosimetric properties. The aim of the present work was to investigate the dosimetric properties of locally manufactured Garfilm-EM to determine its suitability as a high dose dosimeter. This paper presents the results obtained during these investigations.

Experimental

Garfilm-EM films of the size 3.0 cm \times 1.0 cm were cut from the sheets to fit in

the holder of the spectrophotometer. Films were irradiated in a reproducible geometry at an ambient temperature (25-30 $^{\circ}$ C) using a cobalt-60 gamma chamber - 900 which was calibrated with Fricke dosimeter using ASTM protocol E 1026 [4]. Spectra of irradiated and unirradiated films were recorded on SHIMADZU UV 2101PC spectrophotometer. Minimum five films were irradiated for each dose to study reproducibility. Thickness of the films was measured using a digital micrometer screw gauge.

Results and discussion

The absorption spectra of Garfilm-EM before and after irradiation against air and

that of irradiated film against unirradiated are shown in Fig.1.

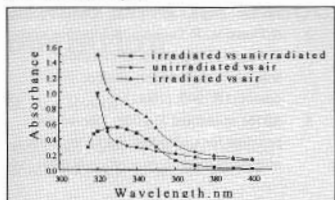


Fig. 1 Absorption spectra of Garfilm-EM

The radiation induced absorption maximum is at 330 nm. However, 340 nm was selected as the wavelength for absorption measurement as the error introduced due to the absorption of unirradiated films is comparatively smaller at this wavelength ($\Delta A/A$ is maximum at this wavelength). To investigate the post irradiation stability of these films, irradiated films were stored under controlled laboratory conditions. Absorbance of these films at 340 nm was read against air at different intervals of time. Fig.2 illustrates the results of post irradiation storage effect on these films. The radiation induced absorbance at various doses decreases rapidly for first 24 hr. Thereafter, it appears quite stable for a period of 10 days studied during this work. These results suggest that the absorbance of irradiated film should be measured at least 24 hrs after the irradiation. It was observed that the response of the films at various doses is reproducible within $\pm 2\%$. The dose-response relationship of these films, presented in the Fig.3, is linear upto 200 kGy.

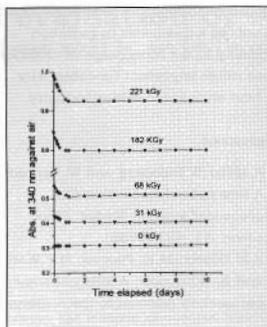


Fig. 2 Post-irradiation stability of Garfilm-EM

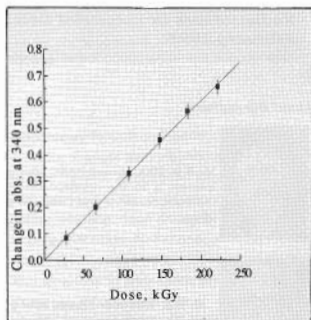


Fig. 3 Dose-absorbance relationship of Garfilm-EM

Conclusions

Garfilm-EM polyester films have useful dosimetric properties like reproducible response, good post-irradiation stability and linear dose-

response relationship. These films can be used as a dosimeter in radiation processing in the dose range 20-200kGy, a dose range important for cable/wire and heat shrinkable tubing industry.

References

1. A. Miller, W. Batsberg and W. Karman, A new radiochromic thin film dosimeter system. *Radiat. Phys. Chem.* 31, 491 (1988).
2. K.M. Glover, M.E. Plested, M.F. Watts and B. Whittaker, A study of some parameters relevant to the response of Harwell PMMA dosimeters to gamma and electron irradiation. *Radiat. Phys. Chem.* 42, 739 (1993).
3. N. Tamura, R. Tanaka, S. Mitomo and S. Nagai, Properties of cellulose triacetate dosimeter. *Radiat. Phys. Chem.* 18, 947 (1981).
4. ASTM standard E 1026, *Standard practice for using the Fricke reference standard dosimetry system* (1994).

This paper was adjudged as one of the two Best contributed papers at the International Conference on Applications of Radiation and Radioisotopes in Industrial Development (ICARID-98) held at Mumbai in February 1998.

About the authors



Mr R.M. Bhat joined BARC after graduating from 12th batch of Training School. His research interest is in the development of new chemical dosimetry systems for radiation therapy, radiation research and radiation processing covering a wide range of doses from a few Gy to kGy.



Mr U.R. Kini joined BARC after graduating from 9th batch of Training School. He has worked on the development of chemical dosimetry techniques for many years. Currently, he is looking after personnel monitoring using TLD systems.



A gold medalist from Roorkee University, Dr B.L. Gupta graduated from 7th batch of Training School. He is Head of Chemical Dosimetry Laboratory which maintains standards for high dose dosimetry in India. The techniques developed by him are widely used. He is a member of ASTM sub committee E10.01 - on Dosimetry for Radiation Processing and AERB Task Group on Food Irradiation Dosimetry.

Characterisation and evaluation of airborne dust associated with mining operation

D. K. Ghosh

Radiation Safety Systems Division
Bhabha Atomic Research Centre

Abstract

It has been well recognised since ancient times that inhalation and retention of excessive mineral dust in the lungs can pose a serious health hazard. In metalliferous mines, mining operations like drilling, mucking and dumping of ore are closely associated with the exposure to ubiquitous crystalline silica, commonly known as free silica. The advent of lung fibrosis and physiological potency to the health of miners arising out from the exposure to fibrogenic crystalline silica depend mainly on their particulate size-mass distribution, the nature of dust, their respirable mass concentration and duration of exposure.

The paper presents the results of a study conducted in the characterisation of airborne dust and subsequently in evaluating index of dust exposure according to job classification and outlines the control measures adopting in the mining operations.

Introduction

SILICA IS UBIQUITOUS AND IS predominantly associated in mining operations. In recent time, with the increase in scale of mechanisation and modernisation of mining activities, there is corresponding rise in dispersion of dust in the working atmosphere. In metalliferous mine, mining activities involve drilling, mucking, dumping, transportation of ore etc. and are closely associated with exposure of crystalline silica, commonly known as free silica. Inhalation and retention in excessive amount of such dust containing significant quantity of free silica over the length of time may lead to a serious

respiratory health problem¹. The advent of lung disease and physiological potency to the health of miners arising out of the exposure to fibrogenic crystalline silica bearing dust depend mainly on their particulate size-mass distribution, respirable mass concentration of dust and quantity of free silica present in it, duration of exposure and susceptibility of the exposed persons. Despite the existing potential hazards, it is possible to work safely in the mines by ensuring that the dust levels in the work atmosphere are within permissible limit and also adopting the prescribed control measures strictly. This paper presents the results of a study conducted in the characterisation of airborne dust and subsequently, estimated cumulative dust

exposure according to job classification and the control measures adopted in order to suppress the overall dust load in the mining environment.

Material and Methods

CHARACTERISATION OF SILICA BEARING DUST

Size-distribution

Size and its distribution of airborne dust vary mainly according to nature of operations. Physiological potency increases with the decrease of particle size below 3 microns. The deposition pattern of particulate dust in the human respiratory tract is dependent on the size-mass characteristics known as mass-median aerodynamic diameter (MMAD). This can be either obtained by Anderson Cascade Impactor² directly or based on microscope counting and sizing of particles using May's eye piece graticule. Distribution was observed to follow log-normal statistics. Figure 1 provides the typical particle size distribution during drilling operations. Count median diameter and geometric standard deviation of the particles were obtained directly from the plot and accordingly count median aerodynamic diameter (CMAD) and mass median aerodynamic diameter (MMAD) are calculated using following equations.

$$\text{CMAD (Dac)} (\mu\text{m}) = \frac{\text{CMD (mg)}}{D_p/D_{st}} \sqrt{\rho} \dots (1)$$

where D_p = projected area diameter
 D_{st} = Stokes diameter of the particle
 D_p/D_{st} = Shape factor for the irregularly shaped particle, quartz (1.53)

ρ = specific gravity of the particle
 (2.84 g/cc)

MMAD and pulmonary deposition from MMAD

$$\log(\text{MMAD}) = \log(\text{CMAD}) + 6.9078 \log^2 \sigma \dots (2)$$

σ is the geometric standard deviation which is unaltered for CMAD and MMAD.

The Task Group on Lung Dynamics³ has recommended a relation between MMAD with that of pulmonary deposition. This is represented graphically in Figure 2. Accordingly, Pulmonary deposition of particles are calculated from MMAD.

Free silica content

Biological significance of exposure to dust mostly depends upon the amount of free silica in the dust inhaled. Talvitie's⁴ method of analysis was adopted for analysis of free silica present in settled and airborne dust where as X-ray diffraction was adopted to estimate free silica in respirable dust.

Full-shift exposure to respirable dust

Respirable fraction of airborne silica bearing dust was collected over a shift from the breathing zone of the workers using gravimetric personal dust sampler⁵ operated through a cyclone separator at a flowrate of 1.9 l/min. The sampler was fitted on the lapel of the worker. The filter paper collects respirable fraction of airborne dust. The sample is weighed and exposure is calculated in terms of mg/m^3 of air.

Threshold Limit Value (TLV)

In India, Director General of Mine Safety⁶ recommended that the average concentration of respirable dust in mine

atmosphere during each shift to which each worker is exposed at any working point or place shall not exceed 3 mg/m³ where free silica in airborne dust is 5% or less and where the dust contains more than 5% quartz or free silica the limiting value is given as follows,

Threshold Limit Value for respirable dust (mg/m³) = 15 / p

where p is the percentage of free silica in respirable fraction of airborne dust

Average cumulative dust exposure (Annual)

Quantity of dust inhaled is directly related to the respiratory effect. Cumulative dust exposures with respect to operations were calculated knowing the duration of average hours of exposure per day and average working days in a year.

Results

Results of sizing of typical airborne dust samples, obtained during different operations and subsequent calculations of MMAD and pulmonary deposition are summarised in Table 1. Typical size distribution is shown in Figure 1.

MMAD is estimated from the size distribution analysis using equations (1) and (2) and accordingly pulmonary deposition from the figure 2.

Free silica present in the settled, airborne and respirable dust were analysed and are presented in Table 2.

Full-shift job exposure to respirable silica bearing dust with respect to different mining operations are summarised in Table 3. Based on this assessment average cumulative dust exposure to different category of workers have been evaluated and are shown in Table 4.

Table 1 : Size distribution, MMAD and pulmonary deposition in different mining operations

Operation	Gm	GSD	MMAD	PD (%)
Drilling	1.2	2.4	11.8±3.6	7.2±2.0
Mucking & Loading	1.5	1.9	3.4±1.4	11.4±1.8
Ore Dumping	1.3	2.1	7.0±1.7	9.6±1.3

Table 2 : Free silica content in different dust samples

Type of dust	No. of samples	Free silica (Mean ± S.D) (%)
Settled dust	45	45.4 ± 1.9
Airborne dust	22	30.5 ± 1.5
Respirable dust	12	17.3 ± 1.1

Table 3 : Full-shift exposure to respirable dust in different mining operation

Mining Operation	Geometric Mean (mg/m ²)	GSD
Drilling (100)	0.78	± 1.8
Mucking (109)	0.45	± 1.8
Ore dumping (146)	0.70	± 1.6
Timbering (62)	0.44	± 1.7
Loco Trammng(59)	0.54	± 1.8
Ore grading (23)	0.46	± 1.5
General (46)	0.39	± 1.4

() indicates No. of samples

Table 4 : Average annual cumulative dust exposure pertaining to different mining operation

Operation	Average duration of work per day (hrs/day)	Concentration Geo. Mean	Exposure Mg. H/m ² /y
Drilling (100)	5	0.78	975
Mucking (109)	6	0.45	675
Ore dumping (146)	6	0.70	1110
Timbering (62)	5	0.44	588
Loco Tamming (59)	5	0.54	688
Ore grading (23)	7	0.46	805
General (46)	8	0.39	620

() indicates No. of samples

Permissible Cumulative Exposure Works to be = 1920 Mg. h/m³ /y
 (TLV X 300 days X 8hrs/day = 0.8mg/m³ X 2400 = TLV X 2400hrs)

Discussion

The effect of particle size on the deposition and retention of particles in lungs is of great significance from the standpoint of pulmonary disease resulting from the inhalation of dust.

The size distribution was observed to follow log-normal distribution and provides information on geometric mean diameter and geometric standard deviation. The various physical

parameters of dust can be obtained from this distribution.

MMAD during drilling was observed to be high because of wide variation of dispersion from the mean value as evident from the geometric standard deviation of 2.4. Pulmonary depositions show 7.2 ± 2.0% lowest during drilling and the highest is 11.4 ± 1.8% during mucking & loading operations.

Threshold Limit Value for respirable silica bearing dust worked out to be 0.8

mg/m³ based on DGMS guide line. Permissible annual cumulative exposure worked out to be 1920 Mg. h/m³ /y based on working days of 300 in a year having 8 hours/day working period. Cumulative dust exposure as evident from the Table 4 appears to be within the limit .

Control measures such as ventilation, improvement in the performance of the dust extraction systems, better operations procedure, such as wetting of the ore after blasting and before mucking etc. and release of water during of the holes etc. are practised in reducing the dust concentration at the source.

Assessment of cumulative exposure with respect to mining operations is important for future comparison with the decrement of pulmonary functions and radiological abnormalities of the lungs.

Acknowledgement

Author wishes to acknowledge the encouragement received from Dr. U.C. Mishra, Director (H S&E Group) and Dr. S.K. Metha, Head, Radiation Safety Systems Division, BARC in presenting this paper. Substantive facilities provided by Mr J.L. Bhasin, Chairman and Managing Director, UCIL, Jaduguda, Bihar during the course of the work was greatly appreciated. Dr. D.D. Thorat is specially

thanked for the help in making transparencies required for OHP. Colleagues are thanked for various co-operation.

References

- 1 Exposure and Silicosis Among Ontario Hard Rock Miners: III Analysis and Risk Estimates., *Am. J. Ind. Med.*, 16, 29-43 (1989).
- 2 Anderson A.A , A Sampler For Respiratory Health Hazard Associates. *Am. Ind. Hyg. Asson. J.*, 27,160 (1965).
- 3 Task Group On Lung Dynamics (ICRP), Deposition and retention models for Internal Dosimetry of the human Respiratory Tract, *Health Physics*, 12, 173-207 (1966)
- 4 Talvite N.A. Determination of free silica, gravimetric and spectrophotometric procedure applicable to airborne and settled dust. *Amm. Inds. Hyg. Asson. Journ.* 1964, 25: 169-178.
- 5 Director General of Mines Safety(DGMS). Precautions against airborne dust. *Circular no.5 dated 29.7.1987, Ministry of Labour, Govt. of India.*
- 6 Casella C F and Co. Ltd., Personal Air Sampler Instruction Leaflet 3150/82, Regent House, Britannia Walk, London.

This paper presented at the International Conference on Occupational Health held at Mumbai in February 1998 was selected for "Britannia Award 1998". Dr Ghosh received the award at the 49th Annual Conference of Indian Association of Occupational Health, India, held at Hyderabad during February 5-7, 1999.

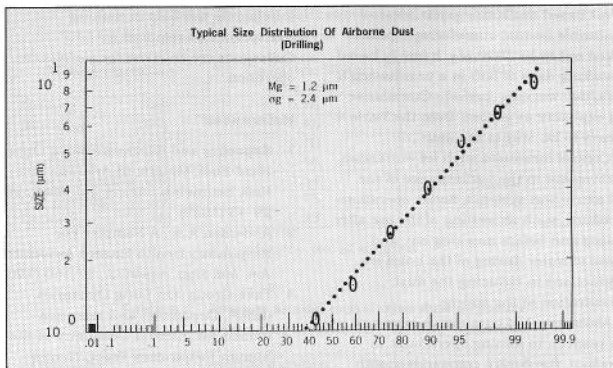


Fig. 1 Cumulative % less than stated size

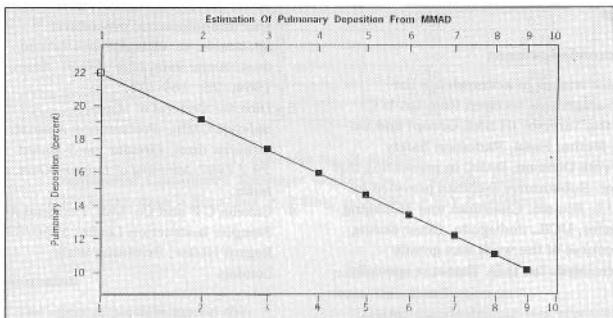


Fig. 2 Particle size, MMAD (μm)

About the author ...



Dr D.K. Ghosh has worked for more than twenty-five years in Industrial Hygiene aspects associated with mining and milling of Uranium ore at Uranium Corporation of India Ltd., Jaduguda, Bihar. At present, he is Officer-in-charge, Health Physics Units of Powder Metallurgy Division and Beryllium Machining Facility at Vashi and he is looking after health and safety work pertaining to processing and machining of Beryllium.

Measurement traceability in brachytherapy

K.N.Govinda Rajan, A.Shanta and B.C.Bhatt
Radiological Physics & Advisory Division
Bhabha Atomic Research Centre

S.P.Vinatha, A.T.Soman, A.Kannan and S.C.Misra
Radiation Standard & Instrumentation Division
Bhabha Atomic Research Centre

A.Shankar, S.Shirley, D.D.Deshpande and K.Dinshaw
Tata Memorial Hospital, Mumbai

W.F. Hanson
Radiological Physics Center, UTX, Houston, USA

Introduction

THE FIELD OF BRACHYTHERAPY DID NOT attract as much attention as External Beam Therapy because of exposures received by the Radiation Oncologists and the nursing staff in this modality of treatment. With the availability of afterloading equipment and development of afterloading procedures in the field, leading to considerable reduction in staff exposures, there was a revival of interest in brachytherapy. With the availability of modern Remote Afterloading Equipment that virtually eliminates all staff exposures, quite a few centres have come up in the recent past to practice this modality of treatment and many more are now coming up, in different parts of India. This development underlines the importance of improving the accuracy of brachytherapy dosimetry by developing appropriate chambers and source standardization and Calibration procedures, for establishing the

traceability of all brachytherapy source measurements to the SSDL of BARC.

Materials and Methods

While the accuracy of Co-60 external beam Standardization has been well established through International intercomparisons, the accuracy of *low* and *high* Air Kerma Rate(AKR) sources used in brachytherapy still remain to be established, through such International Intercomparisons. The first such intercomparison of a low Air Kerma Rate Cs-137 source was, therefore, carried out recently, between the SSDL, BARC and the SSDL, M.D. Anderson Cancer Research Institute, University of Texas (UTX), USA, at BARC, Mumbai. Both the SSDL of BARC and the SSDL of UTX used indigenously designed reentrant chambers as Reference chambers for this intercomparison. The intercomparison showed an agreement of better than 2%. This is an excellent agreement, for low

AKR sources, in a first intercomparison of this nature. By applying finer corrections such as source holder differences, source shape and size differences etc. better agreement can be expected.

This intercomparison thus assures us that the BARC Standard is consistent with another National Standard and that measurements being performed at various hospitals, in India, can be traced to the BARC Cs-137 Standard, to within the required level of accuracy.

Since the SSDL of BARC has not started the Standardization of HDR Ir-192 source it becomes important to check the accuracy of the AKR measurements at this energy, especially because many such units are increasingly coming into use in India.

Such a check was carried out at the Tata Memorial Cancer Centre, Bombay. A PTW reentrant chamber, traceable to the German National Standard, and in use at the Tata Memorial Centre, Mumbai, for measuring the Reference Air Kerma Rate of the HDR Ir-192 source, was compared against the Reference Standard of the SSDL of UTX, USA. (The SSDL of UTX,

USA made use of a commercial model of the reentrant chamber as the Reference Standard). The disagreement was more than 5%.

This paper would discuss the dosimetric characteristics of the Reference Standards used in the measurements, their calibration procedures, the intercomparison procedures and the significance of the results.

Conclusions

The intercomparison at Cs-137 has established the agreement between the two national standards, a prerequisite for ensuring measurement traceability for Cs-137 brachytherapy sources.

In the case of HDR Ir-192 calibration, the reason for the significant difference is being investigated, but it highlights the importance of establishing Primary Standardization and Calibration procedures in India, for the HDR Ir-192 source.

This paper was adjudged as one of the two Best Papers presented at the International Conference on Medical Physics, and the Nineteenth Annual Conference of the Association of Medical Physicists of India (AMPI), held at the All India Institute of Medical Sciences, New Delhi, during November 6-9, 1998. Only extended abstract of the paper is reproduced above.

Proposed quality assurance protocol for mammography X-ray system

Kanta Chhokra, U.B. Tripathi, C.P.R. Nair,
J.B. Sasane and B.C. Bhatt

Radiological Physics & Advisory Division
Bhabha Atomic Research Centre

Introduction

X-RAY MAMMOGRAPHY HAS PROVED TO BE quite effective in a number of screening programmes and in diagnosis of breast cancer. Consequently, it has contributed significantly in terms of reducing breast cancer mortality. The mammography units are increasing through out the world. There are about 200 units in the country. This necessitates the development of a Quality Assurance (QA) protocol so as to achieve a uniform and high standard of equipment performance and image quality in screening as well as in diagnosis. The implementation of protocol should ensure the success of diagnosis as well as the radiation safety of patients, workers and the general public. This paper describes the salient features of the protocol to achieve the above objective.

Materials and methods

Quality Assurance protocol of mammography X-ray systems can be divided into number of parts such as: electrical safety, mechanical safety, radiation safety measurements, automatic exposure control, screen film system, processing unit, breast dose, etc. as per requirements. However, in this paper the

quality assurance protocol has been divided into six main categories: 1) X-ray generator and control, 2) automatic exposure control, 3) compression device, 4) screen-film system and processor, 5) viewing conditions and 6) reference dose and image quality. It also differentiates between basic and desirable quality control level and proposes the frequency of the tests along with the relevant tolerance limits. Table I presents a summary of the tests together with the tolerance limits in case of film mammography. For xero-mammography, all the above parameters need to be performed in addition to the dark dusting of all the plates and cleaning of cassettes at least once a week. However, it is assumed that radiological protection survey of the installation is a part of the quality assurance programme.

Discussion and conclusions

The protocol for mammography X-ray technique/parameters lays down the procedures required to have a Quality Assurance programme in mammography ensuring that system produces the best diagnostic image with minimum radiation dose to the patient. Further, an important part of the protocol is the constraint on

the dose applied to the breast to achieve maximum benefit with minimum risk. It will also help in comparing the doses with that of reference values of *Entrance Skin Dose (ESD)* recommended in *Basic Safety Standard (BSS)*. Furthermore, it will also

serve as the criteria for the manufacturer to ensure that the mammography machines conforms to the national radiation protection rules as prescribed by the competent authority.

Table I: Quality assurance in mammography procedures

<i>Technique/Parameter</i>	<i>Limiting Value</i>
1. X-ray Generator and Control	
1.1 Radiation safety measurements	
- Tube leakage	<1 mGy in 1 hr
- Alignment of light & x-ray field	± 5 mm on all edges
1.2 X-ray measurements	
- focal spot size	
Large focus	< 0.5 mm at 5 cm from chest wall
Small focus	< 0.15 mm at 2 cm from chest wall
- grid system factor	< 2.5
2. Automatic Exposure Control	
- central optical density for 4.5 cm perspex	1.4 to 1.8
3. Compression Device	
- compression plate alignment	-
- compression force	160 to 250 Newton
4. Screen -Film System & processor	
4.1 Screen-film	
- cassette & screen identification	-
- characteristic curve of film	-
- artefacts	-
4.2 Processor	
- developer temp.(APU) (manufacturer specifications)	± 0.2° C
- processing time (manufacturer specifications)	± 5%
5. Viewing Conditions	
- visual check	-
- illumination light level	550 lux(±10%)
- ambient light level	≤ 86 lux
6. System Properties	
6.1 Reference breast dose	0.4 cGy
6.2 Image quality	-
- routine testing	-

This paper was adjudged as one of the two Best Papers presented at the International Conference on Medical Physics, and the Nineteenth Annual Conference of the Association of Medical Physicists of India (AMPI), held at the All India Institute of Medical Sciences, New Delhi, during November 6-9, 1998. Only extended abstract of the paper is reproduced above.

Tritium in Water Monitor for measurement of tritium activity in the process water

M. Rathnakaran, R.M. Ravetkar, M.C. Abani and S.K. Mehta

Radiation Safety Systems Division
Bhabha Atomic Research Centre

Abstract

This paper presents the evaluation of a Tritium in Water Monitor for measurement of tritium activity in the secondary coolant in Pressurised Heavy Water Reactor used for power generation. For this purpose, it uses a plastic scintillator flow cell detector in a continuous on-line mode. It is observed that the sensitivity of the system depends on the transparency of the detector, which gradually reduces with use because of the collection of dirt around the scintillator. A simple type of sample conditioner based on polypropylene candle filter and filter paper is developed and installed at RAPS along with Tritium in Water Monitor. The functioning of this system is reported here.

Introduction

HEAVY WATER IS USED AS PRIMARY coolant and moderator in heavy water type reactors. In fresh heavy water, tritium activity is negligible. But in course of time the tritium activity increases. Considering the radiological hazard of tritium and the cost of heavy water, its leak to the process water should be continuously monitored. It is a statutory requirement to have a continuous on line monitoring system for measurement of tritium leakage to the process water. The system normally used for monitoring of tritium leak is liquid scintillation counting. This system can measure a tritium leak rate of around 50 mCi/h. However, this system is not suitable for continuous on-line monitoring. In this system, the sample has to be collected manually and counted in the liquid scintillator system after mixing the sample with the liquid scintillation cocktail. This introduces time delay in

detecting any tritium leak to the process water. In addition, the manual sampling is time consuming. Though the use of liquid scintillation counting for continuous monitoring has been reported by some authors (1, 2), the system is not commercially available. Liquid scintillation counting for continuous monitoring will also involve an exorbitant cost. In addition, the disposal of large quantity of liquid scintillator will cause an additional environmental hazard.

Solid scintillators like anthracene, plastic scintillator, or calcium flouride filled flow cell can also be used for tritium measurement. Sensitivity of solid scintillator system is much less as compared to that of a liquid scintillator system. In the solid scintillator, since the range of the 18 keV tritium beta is very short (0.005 mm in water), only the tritium which is on the surface of the

scintillator will cause scintillation. Hence the efficiency and sensitivity for tritium with solid scintillator is low. But the system is very convenient to use for continuous monitoring of the process water activity. In this regard NPCIL has imported a tritium in water monitor from Technical Associates (U.S.A.), which is based on anthracene powder packed flow cell (3). The system does not have proper sample conditioning system.

Tritium in Water Monitor developed at BARC

The monitor is a prototype model developed for detection and measurement of tritium leakage from the primary coolant or moderator to the process water in PHWRs. The system is based on plastic scintillator flow cell detector developed at BARC (4). The sample water flows continuously through the flow cell detector and a continuous monitoring is done with the help of this instrument. The monitor consists of three parts namely, the sample conditioner, detector assembly and electronic system. Fig.1 shows the schematic of the Tritium in Water Monitor with sample conditioner.

Detector assembly

The detector assembly consists of plastic scintillator film packed flow cell coupled on either side with two EMI-9635 photomultiplier tubes. These tubes are connected in coincidence for increasing the sensitivity of the system. The flow cell is filled with 5 μm thick and 500 cm^2 area plastic scintillator films. Once packed with the films it behaves like a sponge and allows smooth flow of the sample through the flow cell. When the sample is passing through the

detector, it produces light photons proportional to the radioactivity contents in the flow cell at that instant. The light photons fall on the photo cathode surface of the photomultiplier and produce an electrical pulse output at the anode of photomultiplier tubes. This pulse is further processed by electronic system. Since the tritium beta range is very short, only those tritium betas which are just on the surface of the detector could be detected. To have a better sensitivity, the detector should have large surface area. Fig.2 shows the plot of count rate obtained, with varying number of films, with 100 nCi/ml of tritium activity. Maximum count rate obtained is with 10 films. For smooth flow of the sample six number of films, with a total surface area of 3000 cm^2 , are packed in the flow cell. Plastic scintillator material used in the flow cell weighs less than a gram. Since the quantity of scintillator is small the gamma response of the system is also poor, which is a desirable feature. Fig. 3 shows the tritium activity concentration versus the count rate with 6 number of films packed in the flow cell.

Sample conditioner

The process water contains impurities and particulate substances, which will be trapped in the flow cell detector during use. This will result in reduced transparency of the flow cell detector with use and cause in gradual reduction in sensitivity of the detector. Earlier model of tritium in water monitor uses activated charcoal, mixed column of ion exchange and glass fibre filter paper as sample conditioner. These components require frequent replacement. Even with these

replacements the detector does not work for a long time, which may be due to trapping of submicron sized particles in the flow cell detector. Replacement of different parts of this system is also cumbersome.

The present system of sample conditioner consists of polypropylene bag, polypropylene candle with activated charcoal and filter paper assembly. Except filter paper assembly all other parts are commercially available and are easy to replace. Polypropylene bag removes turbidity in the sample, polypropylene candle traps particulates above 10 μm size and activated charcoal absorbs organic compounds, free chlorine, fungus and turbidity. Filter papers are used for finer filtration. To filter submicron size particles a glass fibre filter paper sandwiched between two Whatman 541 filter papers is used.

Electronic system

Electronic system consists of EHT unit, coincidence amplifier, anti-coincidence analyzer, digital rate meter, alarm system and strip chart recorder. Fig.4 shows block diagram of the detector and electronic system. EHT unit provides the high voltage required for photomultiplier tubes. Background counts due to thermal noise of the photomultiplier tubes, which are a random phenomenon, are considerably reduced by using coincidence circuitry. The anti-coincidence analyzer provides energy discrimination against high energy radiation and enables counting in the window corresponding to tritium betas. Digital count rate meter gives the count rate due to tritium activity in the detector. Alarm level can be fixed as per the users requirements. A continuous

recording of the tritium level in the sample water is done with the help of recorder.

Discussion

Tritium in Water Monitor with the sample conditioner is tested at BARC for finding the suitability of the sample conditioner. First the background measurement is carried out. Tap water is connected to the inlet of the system as shown in Fig. 1. Sample water flow rate is adjusted to around 100 ml/minute through the flow cell detector. Detector sensitivity is found out at the beginning by passing 100 nCi/ml of tritium activity through the detector. Later, detector sensitivity is periodically found out after passing varying quantity of tap water through the detector. Fig.5 shows the plot of sensitivity versus the quantity of water passed through the detector. After passing around 2000 litres of water the sensitivity fall is found to be 25% of the original sensitivity. By keeping a flow rate of 50 ml/min through the detector, it will take more than a month for the sensitivity to fall to 50% of its original value. Afterwards the detector should be replaced.

The system is installed at RAPS. Background count rate at the site was varying between 4 and 5 cps. Minimum detectable activity concentration is around 10 nCi/ml. Presently the performance evaluation of the sample conditioner and the detector cum electronic system is being carried out. Efforts are being made to improve the sample conditioner. Performance study of the polypropylene candle of 5 μm pore size is being done. Use of lower pore size candle is also thought of. In addition, the

use of finer filter paper like Whatman 540 and 542 are also being carried out. We hope these studies will lead to an improved sample conditioner. Efforts are also being made to improve the sensitivity of the system. By making a large surface area flow cell, we hope of improving the detector sensitivity. Background of the system could be further reduced by additional shielding. In old system, count rate meter with a time constant of 10 second was used for counting. By providing microprocessor system in the new tritium in water monitor, the time of counting could be chosen to a longer timing, which will lead to better statistics of counting. Thus, by using the combination a sensitive detector, lower background and increased counting time, the minimum detectable activity value could be improved substantially. The problem faced earlier was with the sample conditioner. If this sample conditioner could solve the problem, it will be of great help for monitoring tritium leakage to the process water.

Acknowledgement

The authors express thanks to Mr M.P. Sharma, Head, C&I(RU), NPCIL, for his keen interest and encouragement

to carry out the work. We are thankful to Mr S.K. Sharma, SME(I) and Mr G.K. Tiwari, (CMU), RAPS 1&2 for their co-operation and help to carry out this work at RAPS. We are grateful to Mr J.V. Deo and Mr K.K. Narayan for useful discussions and help.

References

1. R.V. Osborn (1972) "Development of a monitor for tritiated water vapour in presence of noble gases", *Report, AECL-4303*.
2. R.A. Sigg, J.E. McCarty, R.R. Livingston, M.A. Sanders, "Real-time aqueous tritium monitor using liquid scintillation counting", *Nucl. Instr. and Meth in Physics Research*, A 353 (1994), 494-498.
3. Technical Associates Inc., (U.S.A.), *Operation Manual*.
4. A.N. Singh, M. Rathnakaran and K.G. Vohra, "An on-line tritium in water monitor", *Nucl. Instr. and Meth in Physics Research*, A 236 (1985) 159-164.

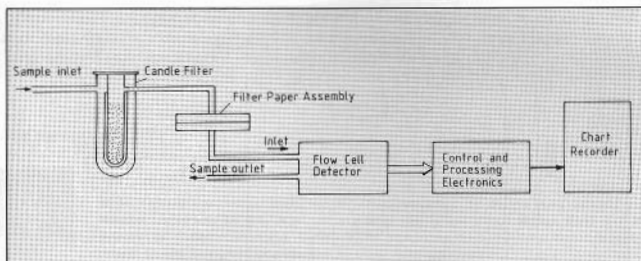


Fig. 1 Diagram of Tritium-in-Water Monitor with sample conditioner

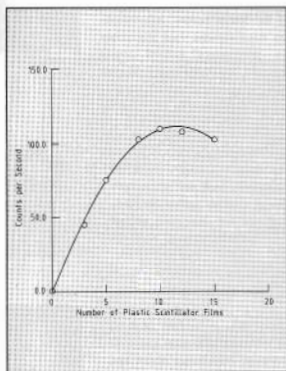


Fig. 2 Number of films versus count rate for 100 nCi/ml of tritiated water

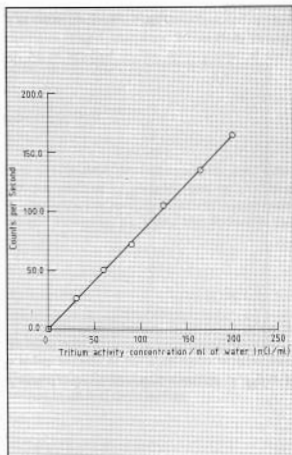


Fig. 3 Calibration curve

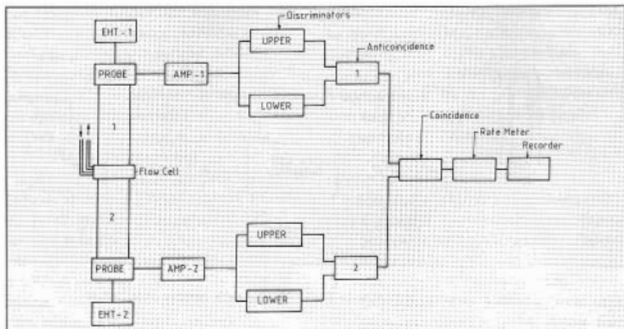


Fig. 4 Block diagram of detector and electronics

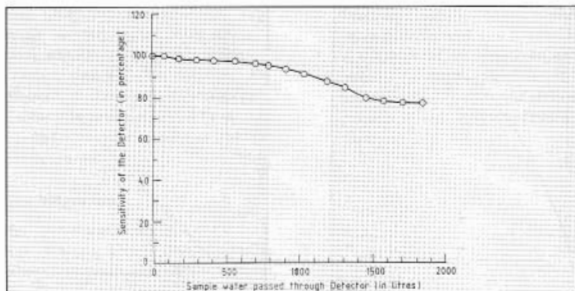


Fig. 5 Relation between sample water passed through the detector and sensitivity

This paper presented at the 24th IARP Annual Conference held at KAPS, Kakrapar, during January 20-22, 1999 was given the Best Paper award. This award was sponsored by Indian Nuclear Society.

About the authors



Mr M. Rathnakaran, joined BARC in 1967 after graduation. He did his M.Sc. in 1981 from Mumbai University. He has developed a special plastic scintillator sponge filled flow cell detector for tritium monitoring. Currently, he is working on continuous measurement of tritium activity leakage in air and water, in heavy water type reactor.



Mr R.M. Ravetkar, after completing graduation in science and post-graduate qualification in electronics, joined BARC in 1965. He is actively involved in the development of various electronic instruments such as Multichannel Pulse Height Analysers, Whole Body Scanners, Digital Pocket Dosimeters, etc. Presently, he is involved in the development of On-line monitoring of tritium in air and water at various reactor sites.



Dr M.C. Abani's main area of interests are gamma ray spectrometry and internal dosimetry. He has developed many codes for analysis of complex gamma ray spectra obtained using various types of detectors. An ultra low level radioactivity measurements facility has been set up by him at Trombay. Presently, he heads the Radiation Safety Systems Division, BARC.



Dr S.K. Mehta, former Head, Radiation Safety Systems Division, is recipient of Dr A.K. Ganguly Memorial Award - 1997 for outstanding contribution in Radiation Protection. He has made significant contributions in the safety aspects of the accelerator programmes of BARC and DAE. He has made pioneering work in Radiation Dosimetry. He has also contributed to Radiation Protection programmes in all fuel cycle facility.

Nondestructive characterisation of MOX fuel rods using gamma autoradiography (GAR)

J.P. Panakkal, D. Mukherjee, V. Manoharan and H.S. Kamath

Advanced Fuel Fabrication Facility
Bhabha Atomic Research Centre

Abstract

During the fabrication of mixed oxide uranium-plutonium oxide (MOX) fuel rods, two important characteristics to be checked in as-fabricated fuel pins are plutonium enrichment and plutonium dioxide agglomerates. The mixed oxide fuel pellets are made via mechanical mixing of uranium dioxide and plutonium dioxide powders by cold compaction and sintering. The chance of loading a wrong Pu enrichment pellet and having pellets with plutonium dioxide agglomerates in a fuel pin cannot be ruled out. A simple nondestructive evaluation technique is felt necessary to ensure at the last stage (in the welded pins) to check these two characteristics.

During the fabrication of MOX fuel rods for Boiling Water Reactors at Advanced Fuel Fabrication Facility of BARC at Tarapur, Gamma-auto-radiography was successfully used to evaluate composition of MOX pellets and to detect presence of PuO_2 agglomerates in the peripheral region. The fuel pins are allowed to be in contact with industrial X-ray films loaded in cassettes for a long time and the processed films are carefully evaluated. Experiments were made to standardise the conditions for distinguishing fuel pellets of different composition by gamma-auto-radiography of fuel pins loaded with pellets of different composition. Gamma-auto-radiography of fuel pins containing agglomerates of different sizes was also carried out. This paper describes the experimental details of the technique, results obtained and compare with other nondestructive evaluation techniques available.

Introduction

URANIUM-PLUTONIUM MIXED OXIDE (MOX) fuel has been developed as an alternative fuel for Boiling Water Reactors at Advanced Fuel Fabrication Facility, Bhabha Atomic Research Centre, Tarapur. MOX fuel rods are made by loading pellets of required enrichment and the plenum springs in thin zircaloy clad tubes and welding of the end-plugs by TIG welding (Fig. 1). It is necessary to ascertain the physical integrity, correct loading of pellets, maximum size of PuO_2 agglomerates present and plutonium enrichment in as-fabricated fuel pins. Experiments were carried out on specially

fabricated fuel pins containing mixed oxide pellets of different PuO_2 enrichment (0–3.25%) and PuO_2 agglomerates. The experimental conditions for distinguishing fuel pellets of different composition has been established. This paper describes the experimental details of gamma-auto-radiography (GAR) developed for this purpose, presents the results obtained, records our experience during the fabrication of MOX fuel assemblies and compare with other nondestructive evaluation techniques.

Mixed oxide fuel pellets are made from a mixture of uranium dioxide powder and varying percentage of plutonium dioxide powder by cold

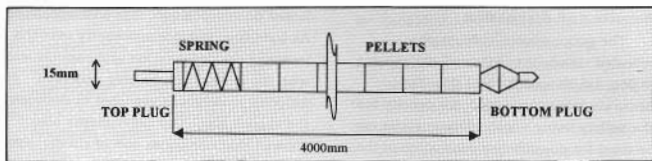


Fig 1. A typical BWR fuel pin (schematic).

compaction and sintering. The pellets (nominal diameter 12.26 mm) used for MOX assemblies are of three different enrichment (0.9%, 1.55% and 3.25%) [1]. The centreless ground pellets after inspection are loaded into long (4 m) zircaloy-2 tubes and welded. A mix-up of fuel pellets of different enrichment is avoided by fabricating the fuel pellets and pins of a particular enrichment a time. The probability of loading pellets of incorrect enrichment in a rod, however, cannot be ruled out completely.

Although $\text{UO}_2\text{-PuO}_2$ forms a complete solid-solution, there is a possibility of having isolated PuO_2 agglomerates in the sintered MOX pellets. Alpha-auto-radiography is the standard quality control check carried out on sample pellets to check the presence of such agglomerates [2]. A nondestructive testing technique capable of detecting PuO_2 agglomerate and verifying the composition of the pellets in the welded fuel pins is useful for quality control personnel. Neutron radiography with its unique characteristics can be used for this purpose [3, 4]. But it is not practical to carry out neutron radiography of all the pins. Gamma scanning gives information about the composition, fissile content and isotopic content, but the information about PuO_2 agglomerate is not reliable

because of poor signal to noise ratio. Gamma-auto-radiography (GAR) has been tried at AFFF on the MOX fuel rods on a large scale recently for BWR reactor fuel pins. Some studies had been reported earlier on low PuO_2 enriched fuel pins in the range of 0–6% [4, 5].

Experimental

Experimental fuel pins containing pellet of various PuO_2 loading (0.9%, 1.55% and 3.25%) were specially fabricated. The composition of representative pellets was checked by chemical analysis. Trial exposures using Agfa Structurix D7 film loaded in flexible cassette kept below the fuel pins were made. The radiation coming from the fuel pellets affect the film to different extent depending on the enrichment. It was observed that an exposure time of 14 hours was sufficient to distinguish the pellets of different composition.

The gamma-auto-radiographs with the same exposure time also revealed PuO_2 agglomerates lying in the periphery of the pellets. Experiments were made with specially fabricated fuel pellets containing agglomerates of size in the range 125–2000 microns to find out the minimum size of the agglomerate detectable in gamma-auto-radiograph.

Results and discussion

The gamma-auto-radiographs revealed clearly the pellets of enrichment (0.9%, 1.55% and 3.25%) [Fig. 2(A)]. Accurate measurement of the density over the pellets using a microdensitometer can be used for quantitative evaluation of the composition.

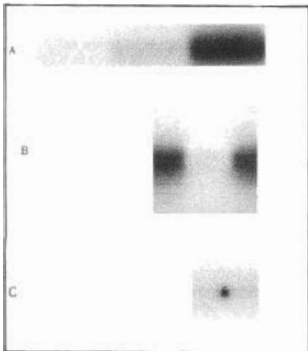


Fig. 2 Gamma autoradiographs
 A) Pellets of three enrichments
 (0.9%, 1.55%, 3.25%)
 B) Medium pellet in high
 enrichment pin
 C) PuO_2 agglomerate

Fig. 2(B) shows the presence of medium enrichment pellet in a stack of higher enrichment. Both the pins were subjected to gamma scanning also for comparison. The gamma-auto-radiographs also revealed the presence of agglomerates lying the periphery [Fig. 2(C)]. The exposure were made with an isolated agglomerates at different orientation and the data is being analysed. A theoretical model is also being developed to determine the limits

based on composition, size and distance. As a routine, microdensitometry over the image of the agglomerate and comparison with the density values over pellets of different enrichment are used to evaluate the cluster size. The experiments also showed that minimum size of cluster size detectable was 250 microns.

Additionally gamma-auto-radiography also revealed chipping of the pellets shown by lighter region caused by the absence of fuel material. The chipping was confirmed by X-radiography.

Conclusion

Use of gamma-auto-radiography for verifying the composition and detecting the presence of PuO_2 agglomerates and chipping of the pellets in welded MOX rods was demonstrated. The technique, however, suffers from the drawback that it provides information about the periphery of the pellets. The radiation coming from the centre of the pellets do not reach the film because of self-shielding. This technique being simple has been adopted as additional quality control check in our Quality Control Plan.

Acknowledgement

The authors would like to thank Fuel Manufacturing Section of Advanced Fuel Fabrication Facility for providing the fuel pins and their colleagues of Quality Control Section for their co-operation and help during this work. They would like to acknowledge the support and encouragement received from Mr M.S. Ramakumar, Director, Nuclear Fuels Group, BARC and Mr D.S.C. Purushotham, Head, AFFF & AFD, BARC.

References

1. "Specification for mixed oxide fuel pellets and fuel rods for All MOX assemblies", *BARC Internal Document*.
2. Wick O.J., "Plutonium Hand Book", *American Nuclear Society, Illinois*, 1980.
3. Panakkal J.P., Ghosh J.K. and Roy P.R., "Characterisation of uranium-plutonium mixed oxide nuclear fuel pins using neutron radiography", *British Journal of NDT 27* (1985), pp. 232-233.
4. Panakkal J.P., "Nondestructive evaluation of nuclear fuels by radiographic and ultrasonic techniques", *Ph.D. Thesis submitted to Kerala University*, 1992.
5. Ghosh J.K., Panakkal J.P. and Roy P.R., "Use of autoradiography for checking plutonium enrichment and agglomerates in mixed oxide fuel pellets inside welded fuel pins", *NDT Int.* 17 (1984), pp. 269-271

This paper was selected as 'Best Technical Paper in R&D' published in the Journal of Nondestructive Evaluation, an official journal of Indian Society for Nondestructive Testing during the period 1997-1998 and the award was presented on 10th December, 1998.

About the authors ...



Dr Jose P. Panakkal, Superintendent (Quality Control), Advanced Fuel Fabrication Facility, Tarapur (16th Batch of Training School, M.Sc. Physics, IIT, Madras 1992, Ph.D., Kerala University, 1992, National NDT Award in

R&D, ISNT, 1994, certified to ASNT Level-III in RT, UT and NRT, 1988). He was deputed to Fraunhofer Institute for NDT, Saarbrücken, Germany during 1987-1989. Working in the field of quality control of nuclear fuels, various NDE techniques and material characterisation. Associated with NDE of fuel pins constituting the first core of FBTR and responsible for quality control of BWR MOX fuel bundles for TAPS.



Mr D. Mukherjee, (32nd Batch of Training School, B.E. Metallurgy, Calcutta University, ISNT Level-III in UT). Joined AFFF in 1989. Working in the field of quality control of nuclear fuels, specialised in

various NDE techniques like radiography, ultrasonics and leak testing and microstructural evaluation of materials and welds. Responsible for NDE of MOX fuel pins and microstructural evaluation of MOX fuel.

Mr V. Manoharan, (B.Sc. Phy., Annamalai University, PG Diploma in Radiological Physics, ISNT Level-I in LPT). Joined AFFF in 1988. He has carried out radiograph inspection of MOX fuel pins and other fuel pins fabricated at AFFF. He has been transferred to IGCAR in 1996 and working in various NDE techniques.

Mr H.S. Kamath, Head, AFFF (13th Batch Training School, B.E. Met., REC, Suratkal University, 1969).



Working in the area of Pu bearing fuels for last 28 years starting with fuel for "PURNIMA" fast critical facility at Trombay to development of MOX fuels for BWRs at Tarapur. Associated with AFFF from conceptual stage to regulatory clearance. Major area of interest is development of high performance MOX fuel and new characterisation techniques. Plant Superintendent since 1991 and Head, AFFF since 1996.

Observation of double pulsing in a single mode TEA CO₂ laser caused by the effect of mode pulling and pushing

J. Padma Nilaya and Dhruba J. Biswas

Laser and Plasma Technology Division
Bhabha Atomic Research Centre

Abstract

We have discovered a mode pulling and pushing phenomenon of thermal origin in the operation of a single mode TEA CO₂ laser. This effect arises from the intra pulse temperature induced change of refractive index and can push the cavity mode, when appropriately located with respect to the center of transition, out of lasing even through condition of threshold population inversion is satisfied. Following the termination of lasing, the temperature equilibrates and the mode is pulled into the gain domain, causing thereby the emission of a second pulse. We have provided evidence in support of this mechanism. We also have discussed the possible uses of this double pulsing phenomenon.

THE HEAT DEPOSITED FROM THE vibrational transnational (V-T) energy relaxation during lasing is known to result in the frequency chirping in the operation of a pulsed CO₂ laser [1]. We report here, for the first time to our knowledge, that this intra pulse temperature induced change of refractive index can under certain conditions, lead to the emission of double pulse from the CO₂ laser when operated under single mode condition. As a result of the heat deposition, the change in the refractive index causes the frequency of the mode to increase and it can be pushed out of lasing bandwidth when detuned sufficiently away from the line center on its higher frequency side. This would cause premature termination of lasing even though condition of threshold population inversion is satisfied. Following this, as the

temperature equilibrates, the mode re-enters the gain domain causing thereby the emission of a second pulse, albeit, of lesser power. As expected the delay between the two pulses could be varied by varying the amount of detuning before the onset of lasing. The weakening of this double pulsing effect in the case of helium free operation for which V-T relaxation is greatly reduced further substantiates our above claim of its operating mechanism. The double pulsing phenomenon we report here can be put to many important applications such as measurement of frequency chirping and finding out the relaxation dynamics of the energy levels of any new additives.

The experiment was conducted on a mini TEA CO₂ laser (Fig. 1), detailed description of which can be found elsewhere[2]. The laser was first operated

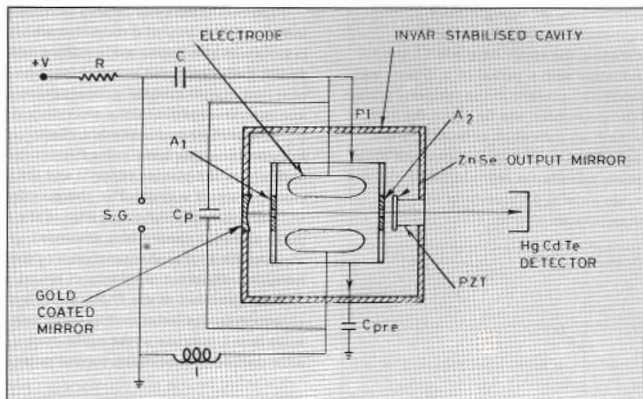


Fig. 1 The schematic of the experimental set-up. A_1 and A_2 are two intra-cavity apertures

in a short cavity (length $\cong 20$ cm) configuration with normal gas mixtures viz. $\text{CO}_2:\text{N}_2:\text{He}::1:1.5:4$. The single longitudinal mode nature of lasing was confirmed from the temporal profile of the pulse which contained no oscillation with period of cavity round trip time (t_R). It, instead, exhibited oscillation of a much larger period viz. $12t_R$ indicating the presence of two transverse modes. Introduction of appropriately shut apertures eliminated this oscillation yielding an absolutely clean temporal pulse. At this point we were intrigued by the premature termination of this pulse and there-emission of a second clean temporal pulse after a brief interval. On closer examination, it was revealed that this second pulse was emitted for some

specific range of cavity length conditions over which its temporal separation from the first pulse varied from almost 0 to 4.3 μsec (fig. 2, traces a to c). Using a CO_2 spectrum analyzer, we further confirmed that both the primary and secondary pulses originated from the same ro-vibrational transition. In order to eliminate the possibility of two excitation pulses well separated in time as a cause of this double pulsing phenomenon, we monitored the voltage and the corresponding current pulse. Their shapes were found to be reproducible and devoid of any second pulsing. The duration of the excitation pulse was $\cong 900$ nsec and the onset of lasing occurred at least 500 nsec after the beginning of this pulse. In order to confirm if the observed result of double lasing is indeed a single mode

phenomenon, we brought more longitudinal modes into lasing by increasing the cavity length to 75 cm. Oscillation with a period of ≈ 5 nsec was found to be present in the temporal profile of the pulse here (see fig 4 and the inset therein); an indication of beating of the longitudinal modes. In this case the pulse shapes was always reproducible and the double pulsing phenomenon was conspicuously absent.

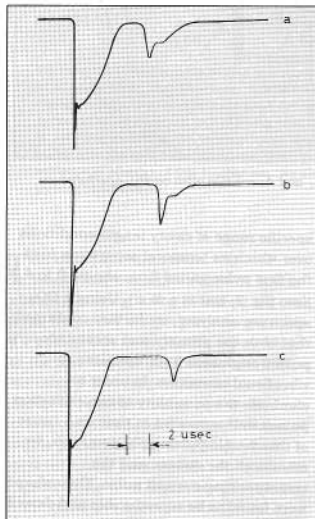


Fig. 2 The temporal profile of the laser pulse over the range of cavity lengths for which two pulses are emitted. The delay between the pulses increases from trace 'a' to trace 'c' as the mode is tuned to the line centre from the high frequency end.

The resonant behaviour of refractive index in the vicinity of a transition which is known to give rise to mode pulling and pushing effects cannot account for the observed cessation of the primary pulse and then re-emission of the secondary pulse. The other two important effects known to produce intra-pulse frequency shifting are the plasma effect[3] and the electrode shock wave[4]. The plasma effect will influence only the rising edge of the pulse and thus cannot be a dominant mechanism for the phenomenon we report here. Consideration of velocity of sound and the clearance of the TEM_{00} mode from either electrodes indicate that the shock wave is still to arrive at the mode even after the occurrence of the second pulse.

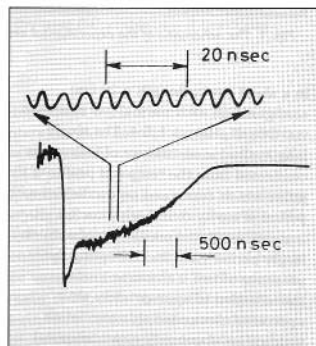


Fig 3 The time record of the multi-mode laser pulse. The inset shows the period of oscillation in a magnified scale.

The quantum efficiency of a CO_2 laser is 40% which means that 1.5 times the energy of the laser pulse appears as vibrational energy of the $O1^0$ level.

Assuming that all this energy is realized translationally in a Helium rich mixture[5], we have estimated a temperature rise of the gas mixture in the active volume as $\approx 15^\circ\text{K}$. This would result in an increase of the mode frequency of the short cavity laser by ≈ 175 MHz. If the cavity length is such that the mode is near to the end of the lasing band width on the higher frequency side, the change in the refractive index may then be sufficient to push the mode out of lasing. As the extra heat is conducted away, the mode is pulled inside the gain region causing the onset of the second pulse. If now the mode is slowly tuned away from the end towards the line centre, temperature rise will be higher and consequently the second pulse with lower energy would appear after an increasingly longer pause. A point will, however, come when the mode will be away from the higher frequency end by an amount, which is more than the maximum frequency shift caused by the change of temperature with the result that double pulsing is never observed in this region. All these aspects are amply demonstrated in the traces of fig.2. The maximum delay between the primary and the secondary pulse was found to be $4.3 \mu\text{sec}$.

In order to study this double pulsing behavior in a system where V-T relaxation is very slow we operated the laser utilizing Helium-free gas mixture with the help of low ionization potential additives[6]. As expected, the appearance of the second pulse here was found to be much restricted and its maximum delay with respect to the primary pulse was found to be $\approx 0.2 \mu\text{sec}$ (fig.4)

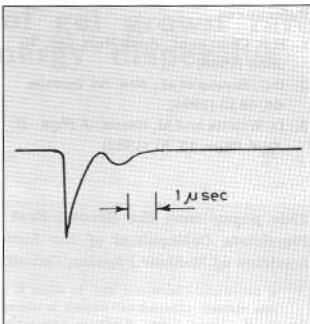


Fig. 4 The weakening of the two pulse effect when the laser is operated with very less helium.

In conclusion, we have shown that laser induced change of gas temperature may, under certain conditions, lead to the emission of two pulses separated in time in the operation of a single mode TEA CO_2 laser. The measurement of the delay between these two pulses can provide an indirect way of gauging the amount of frequency chirp the mode has undergone. The study of the dependence of the delay on the partial pressure of the gases normally used as well as any new additives may also provide valuable information with regard to the relaxation dynamics of the energy levels that participate in the lasing process. We finally note that this effect may not be specific to CO_2 lasers alone and may be observed in the single mode operation of any other lasers wherein onset of lasing will cause appreciable change in the temperature of the active region inside the pulse.

References

1. H.P. Chou et al., *Appl. Phys. Lett.* 56, 2086 (1980)
2. D.J. Biswas et al., *Rev. Sci. Instrum.* 66, 4813 (1995)
3. D. Willetts and M. Harris, *J. Phys. D: Appl. Phys.* 15, 51 (1982)
4. V.G. Roper et al., *Opt. Commun.* 25, 235 (19178)
5. L. Taylor and S. Bitteman, *Rev. Mod. Phys.* 41, 26 (1969)
6. A.K. Nath and D.J. Biswas, *J. Appl. Phys.* 53, 5469 (1982)

This paper won the Second Best presentation award at the XVII Young Physicists Colloquium of the Indian Physical Society, held at the Saha Institute of Nuclear Physics, Calcutta, during August 19-20, 1999

About the authors ...



J. Padma Nilaya, [B.Sc., Nagpur University, 1989; M.Sc(Physics), Nagpur University, 1991] graduated from the 35th batch of the Training School. She was recipient of the university gold medals for securing first position in both B.Sc and M.Sc. examinations. Her research interests include studies on continuous and pulsed CO₂ lasers. She has participated actively in the development of latch proof TEA laser pulsers and in understanding the role of spatial hole burning on the emission spectrum of gas lasers. She is also working towards her PhD on the development of a repetitive widely tunable single mode CO₂ laser and its application on optically pumped molecular lasers.



Dr Dhruba J. Biswas, [M.Sc, IIT Kharagpur, 1978; PhD, Edinburgh, 1986] graduated from the 22nd batch of the Training School. He was recipient of INSA young scientist award [Physics, 1987], A.K. Bose Memorial Award of INSA (Physical Science, 1989), N.S. Satyamurthy award of IPA(1991). His work, which mostly pertains to the research and development of gas and optically pumped molecular lasers and studies on optical chaos, has led to more than 60 research publications in international journals. He was awarded the

Associateship of the International Centre for Theoretical Physics, Italy (1994) and participates in the collaborative research work at the centre.

Elemental analysis of gel grown rare earth crystals by energy dispersive X-ray fluorescence

Daisy Joseph, Madan Lal and P.K.Patra

Nuclear Physics Division
Bhabha Atomic Research Centre

Abstract

Characterisation of gel grown rare earth crystals in terms of their elemental composition is important to assess their structural perfection. Crystals of Cerium-Lanthanum Oxalate and Cerium-Neodymium Oxalate were analysed by radio-isotope excited Energy Dispersive X-ray Fluorescence (EDXRF) to determine the rare earth elements La, Ce and Nd and impurities present in the samples. Based on the observed ratios of the rare earth elements, it is seen that the formulae assumed for some of the compounds may be incorrect or the elements were not added in right proportion during the growth process.

Introduction

CRYSTALS WITH FEWEST NUMBER OF imperfections are most suitable for use in scientific and technical applications^{1,2}. Quantitative estimation³ of the elemental concentrations is an important component of the physical and chemical properties of the crystals. The deviation of the determined ratios for the elements from that of the assumed chemical composition shows the inaccuracy of the chemical formulae. We have analysed a few crystals of Cerium Lanthanum Oxalate and Cerium Neodymium Oxalate obtained from M.G. University, Kottayam by EDXRF to determine the ratios of the elements of rare earth crystals to be able to verify the correctness of the formulae assumed.

Experimental method

Three samples each of Cerium-Lanthanum Oxalate and Cerium-

Neodymium Oxalate were ground to a fine powder and homogenised after adding an equal quantity of microcrystalline cellulose powder. The samples were pelletised under a pressure of 15 tons/sq. inch into thin pellets of 25mm diameter weighing around 350mg. The cellulose to sample ratio was 50% by weight. The experimental set-up consists of a lithium drifted silicon Si(Li) detector of 30 mm² x 3 mm size having an energy resolution of 170 eV at 5.9 keV Mn K α X-rays. An annular radio-isotope source of Am²⁴¹ (100 mCi) was used to excite the characteristic X-rays of the elements present in these crystals. (Fig 1)

The concentrations of the elements were calculated using the formula

$$I_j = I_0 G m_j k_j C_j$$

Where I_j = Intensity of the j^{th} X-ray line

I_0 = Intensity of the exciting source

G = Geometrical factor

m_j = Concentration of the j^{th} element

K_j = excitation cum detection factor.

C_j = absorption correction factor.

The geometrical factor I_0G was obtained from the Y-std (302 ppm) of the same diameter (25mm) using the measured values of I_j and C_j and the known values of K_i and M_j . In a separate experiment the mass absorption coefficients were determined by placing the sample in between the source and the detector and by measuring the transmission of X-rays energies of a known sample through the unknown sample. The intensity of X-rays were measured to obtain the absorption factors for each sample at these energies using the formula $I = I_0 e^{-\mu x}$ where μ is the mass absorption coefficient, and $C_j = 1 - e^{-\mu x} / (\mu_1 + \mu_2) x$ where μ_1 and μ_2 are the mass absorption coefficients for the incident and fluorescent energies respectively. Each pellet was run for a counting time of 2000 seconds. The spectrum obtained was stored in PC

based multichannel analyser and analysed in a PC/XT.

Results and discussion

Fig 1 shows a typical X-ray spectrum of Cerium-Lanthanum Oxalate crystal. It is seen that Ce, Nd and La are detected as major elements in the crystals. The concentrations of the elements were calculated using the above formula. Table-1 shows the elemental concentration ratios of Ce to Nd and La to Ce of the crystals and the same ratio calculated from the chemical formulae. The appreciable deviation in case of La:Ce may be due to wrong assumption of the chemical composition for the crystals. The deviation in case of Ce:Nd from the assumed formula is found to be less than 5%.

Table-1

Sample specification	Concentration ratios \pm error	
	Experimental	Theoretical
Ce:Nd		
Ce _{1.5} Nd _{0.5} (C ₂ O ₄) ₃ .10H ₂ O	2.87 \pm 0.02	2.91
Ce ₁ Nd ₁ (C ₂ O ₄) ₃ .10H ₂ O	0.99 \pm 0.01	0.97
Ce _{0.5} Nd _{1.5} (C ₂ O ₄) ₃ .10H ₂ O	0.35 \pm 0.002	0.32
La:Ce		
Ce _{1.5} La _{0.5} (C ₂ O ₄) ₃ .10H ₂ O	0.23 \pm 0.02	0.33
Ce ₁ La ₁ (C ₂ O ₄) ₃ .10H ₂ O	0.86 \pm 0.01	1.01
Ce _{0.5} La _{1.5} (C ₂ O ₄) ₃ .10H ₂ O	3.33 \pm 0.05	2.97

Conclusion

It is seen that constituents of rare earth crystals can be determined using a rapid and sensitive technique such as EDXRF. A study of its compositional formulae can also be made. The discrepancy in the concentration ratios could be the result of an incorrect assumption of crystal chemical composition.

References

1. M.O.Kuda, Anal.Chem. 45, 1578(193)
2. T.Seshhagiriand Y.Babu,Talanta 31 773(1984)
3. C.K.Bhatt,C.L.Bhatt,M.Lal, P.K. Pata, P.N.Kotru, X-ray Spectrometry,Vol23,247-250 (1994).

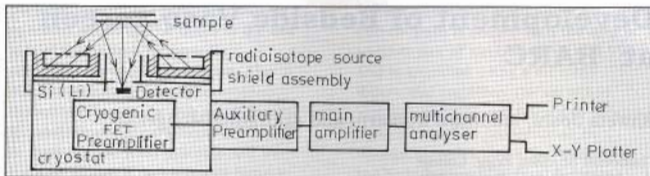


Fig. 1 Schematic diagram of X-ray spectrometer and experimental arrangement with radioisotope source excitation

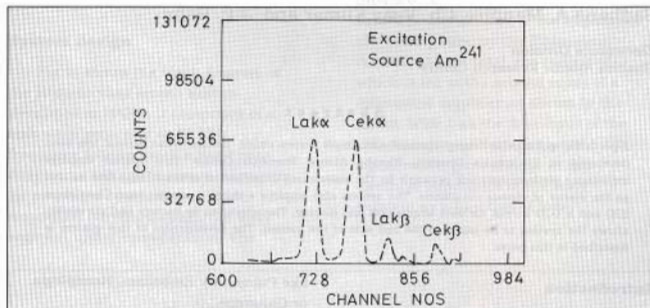


Fig. 2 X-ray spectrum of Cerium Lanthanum Oxalate crystal

This paper was adjudged as the best presentation at the Vith National Seminar on X-ray Spectrometry and Allied Areas, held at Post Graduate College of Arts and Science, Ratlam, Madhya Pradesh, during November 17-19,1997

About the author



Mrs. Daisy Joseph joined BARC in 1985 after completing M.Sc. (Phys.) from Mumbai University. She has been working in the field of Energy Dispersive X-ray Fluorescence (EDXRF) and Proton Induced X-ray Emission studies for the last 10 years.

(The other two authors are not presently working in BARC.)

Development of Bedside Vaso-screen at BARC

Shweta Joshi, Madhura Kulkarni and Anuradha Modgekar

Thadomal Shahani Engg. College
Bandra (West), Mumbai 400 050

and

Sadhana A. Mandlik, Ch. Vijay Kumar and J.P. Babu

Electronics Division
Bhabha Atomic Research Centre

Abstract

A portable, rechargeable battery operated and simple system called "Bedside Vaso Screen" has been developed at Electronics Division, Bhabha Atomic Research Centre. This system employs impedance plethysmographic principle for the assessment of peripheral arterial blood flow as well as the status of venous circulation. The system also employs a micro computer card Chameleon 220 and a LCD screen for data acquisition and display. The operation by battery and portability allows the system to be taken to the bed side of the patient. The development of this system is described in this paper.

Introduction

THE INCIDENCE OF PERIPHERAL vascular disease is very common in our country. Hypertensives, diabetics, smokers and tobacco chewers are at a high risk of developing peripheral arterial occlusive disease and often end up with gangrene demanding amputation of the limb. Sedentary habits, use of oral contraceptives, administration of intravenous fluids, injury to the vein and pregnancy are some of the causative factors of venous disorders. Particularly the patients on intravenous fluids, after abdominal surgery or those in ICCU following heart problem are at a high risk of developing Deep Vein Thrombosis which can lead to fatal consequences

like Pulmonary Embolism, Hemiplegia or Gangrene.

Peripheral Angiography is conventionally employed for the diagnosis of peripheral vascular disease. However it is an invasive procedure with inherent risk of mortality or morbidity and is therefore employed judiciously. Non-invasive procedures like vascular doppler, plethysmography etc. are routinely employed for screening the patients and selecting the patients for angiography. Most of the non-invasive modalities are available as laboratory equipments and the patient has to be ambulated to the laboratory for investigation.

Since the patients in ICU, ICCU etc. cannot be ambulated, it is therefore, necessary to develop a simple and

portable instrument preferably battery operated which can be taken to the bed side of the patient for periodic screening of venous circulation. Also clinicians dealing with hypertensives, diabetics etc. can use this small system for assessment of peripheral circulation in their clinics. With this objective we have developed a rechargeable battery operated simple and portable system at Electronics Division, BARC which is described in this paper.

System design

Fig. 1. shows the block diagram of the Bedside vaso screen system developed at BARC. It comprises of a sine wave generator at 50 KHz frequency followed with a band pass filter and a voltage to current converter for passing a constant amplitude sinusoidal current through the body segment under consideration. The

voltage signal developed along the current path is sensed with the help of another pair of electrodes (V1 and V2) and is amplified using a differential amplifier. The amplified signal is rectified and filtered to obtain Z signal which is proportional, in voltage, to the electrical impedance of the body segment confined between electrodes V1 and V2. This signal is connected to one of the multiplexed inputs of ADC in the Chameleon 220 card. The initial value of the impedance (Z_0) is outputted by the Chameleon card to a 12-bit DAC, the output of which is fed to the second input of a differential amplifier as shown in the figure. With Z as the first input of the differential amplifier, it outputs $\Delta Z(t)$ signal which gives change in the electrical impedance of the body segment as a function of time.

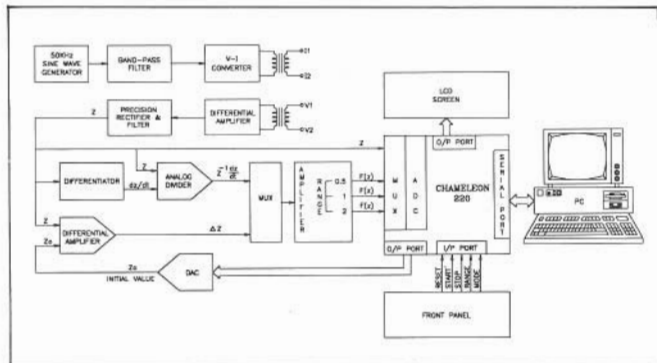


Fig. 1

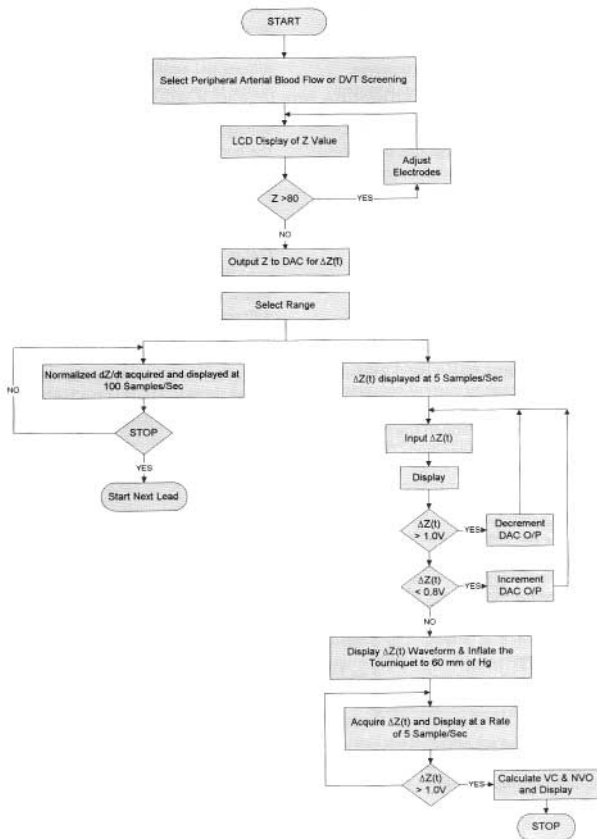


Fig. 2

The Z signal is also differentiated and divided by Z value to obtain normalized

dZ/dt waveform $\frac{1}{Z} \frac{dZ}{dt}$ as shown in the

figure. $\Delta Z(T)$ and normalized dZ/dt are fed to a multiplexer which outputs either of them depending upon the manual selection from the front panel of the instrument. The output of the multiplexer termed as $F(Z)$ is amplified and fed to the remaining three multiplexed inputs of ADC in the Chameleon card depending upon the range of measurement selected from the front panel of the instrument. There is also a start and stop input to the Chameleon card from the front panel. Serial port is also available from the Chameleon card for communication to a personal computer for development of software. The developed software can be loaded in the EPROM, resident in Chameleon card, and the communication with the PC is dispensed with.

To begin with, electrodes are applied to the desired body segment of the patient in supine position. The mode selection switch is used to select either the assessment of peripheral arterial blood flow or screening for Deep Vein Thrombosis. The Z value is sensed through AN13 and displayed on the screen. Z value higher than 80 ohms showed be lowered by adjusting the distance between sensing electrodes. The final Z value is outputted to DAC for obtaining $\Delta Z(t)$ signal. $F(z)$ input is read by the computer and simultaneously displayed on LCD screen at a rate of 100 or 5 samples per second for arterial or venous studies respectively. In case of venous studies, the Z value is adjusted by the computer on either side for bringing down the

$\Delta Z(t)$ trace on the LCD screen as shown in flow chart of figure 2.

In case of assessment of peripheral arterial blood flow normalized dZ/dt of value one is considered normal¹. The other distal locations can be similarly assessed by suitable placement of electrodes.

In case of assessment of venous circulation after stabilizing the $\Delta Z(t)$ trace proximal segment of the limb is pressurized with the help of a tourniquet to a pressure of 60 mm of Hg. The rise in the trace will be observed till it reaches a plateau when the tourniquet is deflated. After $\Delta Z(t)$ trace returns back to initial position the stop switch is pressed to stop the data acquisition. The difference between the plateau value and initial value of $\Delta Z(t)$, commonly known as venous capacitance (VC) is considered normal in the range of 0.75 ± 0.15 ohms. After deflation of the tourniquet the change in the $\Delta Z(t)$ value in first three seconds, commonly known as Maximum Venous Outflow (MVO₂), is considered normal in the range of 0.5 ± 0.1 ohms. Both the parameters are displayed on the LCD screen at the end of the procedure.

The power supply required for this system is +15V (100 mA), -15V (75 mA) and +5V (300 mA), which is derived from a 6V, 4 AH rechargeable battery. An astable multivibrator produces square wave of frequency around 15 KHz with the help of battery. This square wave is fed to a driver stage having ferrite core transformer. The secondary of the transformer is used to generate the required power supply for the system.

The system is under calibration and testing and will be shortly shifted to a hospital for clinical evaluation.

Acknowledgements

The authors express their gratitude to Dr. S.K. Kataria, Head, Electronics Division, for providing guidance and support for this development. The authors are also thankful to Mr S.P. Chaganty, Head, Reactor Instrumentation Section, and Mr Amitabh Das, Scientific Officer, Reactor Instrumentation Section, for their guidance and help. The first three authors are thankful to Mrs. Mita Bhowmick, Incharge, Biomedical Engineering Department, Thadomal Shahani Engineering College, for giving an opportunity to undergo Implant Training and carry out project work at BARC. The authors are also thankful to Mr A.R. Kini for helping in their day to day work.

References

1. Jindal G.D., Nerurkar Smita N., Pedhnekar Sadhana A., Babu J.P., Kelkar M.D., Deshpande Alaka K and Parulkar G.B. : Diagnosis of Peripheral Arterial Occlusive Diseases using Impedance Plethysmography, *Journal of Post graduate Medicine*, Vol. 36, 1990, pp147-153.
2. Jindal G.D., Nerurkar Smita N., Pedhnekar Sadhana A., Masand Kavita L., Gupta D.K., Deshmukh H.L., Babu J.P., and Parulkar G.B. : Diagnosis of Venous Disorders Using Impedance Plethysmography, *Journal of Post graduate Medicine*, Vol. 36, 1990, pp158-163.

This paper won the second prize in the student paper competition in the Conference on Biomedical Engineering, organised by Biomedical Engineering Society of India (Mumbai Chapter), on February 27, 1999

About the authors



Mrs. Sadhana A. Mandlik graduated in Engineering from Amravati University and has worked in Meltron as R&D Engineer from 1991 to 1996. She joined Electronics Division, BARC in 1996 and has been working in the field of Biomedical Instrumentation. She has made remarkable contribution in the development of Bedside Vaso Screen and Medical Analyzer for the screening of high risk patients of peripheral vascular disease and for the diagnosis of diseases of the internal organs of the body respectively.



Mr J.P. Babu joined BARC in the year 1969 after completing Diploma in Telecommunication from Government Polytechnic, Andhra Pradesh. He has made significant contribution in the development and production of control systems and power supplies for Variable Energy Cyclotron, Calcutta. He has been working in biomedical instrumentation for the past 17 years and has made remarkable contribution in the development of Microprocessor based Impedance Plethysmograph, PC Add on Card for Imaging in Nuclear Medicine, feasibility model of Electrical Impedance Tomograph and PC based Impedance Cardioasograph for the diagnosis of a variety of diseases of the human body.

Thermal investigations on N,N' dihexyl octanamide complex of uranyl nitrate

P.B.Ruikar, S. Sriram, P.C.Kalsi, M.S.Nagar and V.K.Manchanda

Radiochemistry Division
Bhabha Atomic Research Centre

Abstract

The thermal decomposition of uranyl dinitrate complex with N,N' dihexyl octanamide (DHOA) was studied which suggested that the decomposition proceeded in three TG stages with four exothermic DTA steps corresponding to release of two molecules of amides and two nitrate groups finally leading to U_3O_8 . Activation energy for each TG step was evaluated.

Introduction

N,N'-DIALKYL AMIDES HAVE BEEN proposed as alternate extractants to tri-n-butyl phosphate (TBP) for the reprocessing of nuclear fuels. Though organophosphorous compound TBP is a versatile extractant, amides have a distinct advantage of their incinerability leading to smaller amounts of secondary waste.

During recent past, our group has been investigating the solvent extraction behaviour of actinides as well as fission products employing N,N' dihexyl octanamide (DHOA). Physico-chemical studies on the complexes formed during the two phase reaction helps to understand the mechanism of extraction particularly under high loading conditions of the organic solvent. An attempt has been made in the present work to isolate

the ternary complex of uranyl nitrate with DHOA and investigate its thermoanalytical behaviour in air upto 850°C.

Experimental

Synthesis and characterisation of uranyl nitrate-DHOA Complex

DHOA used in the present study was synthesised in our laboratory [1,2] using octanoyl chloride and dihexyl amine, both of Merck-Schuchardt grade. The purity of distilled final product (DHOA) was ascertained by elemental analysis [%C: 76.6(77.1); %H:12.9(13.3); %N: 4.37(4.49)], IR spectra ($\nu_{C=O}$ = 1640 cm^{-1}) and non-aqueous potentiometric titration (amide content= 99.2%).

$UO_2(NO_3)_2$ -DHOA complex was prepared by solvent extraction method. 5ml of 3M HNO_3 containing 1mM of U

and 5ml of benzene containing 2mM of amide were equilibrated for 30 minutes. The benzene layer was separated, evaporated and dried and product recrystallised twice from n-hexane [2]. I.R spectrum was recorded as nujol mull in Pye-Unicam 9512 I.R spectrophotometer.

The thermal decomposition of $UO_2(NO_3)_2 \cdot 2DHOA$ was carried out in flowing air using differential thermal analysis (DTA) and thermogravimetry (TG). The thermogram was recorded at the heating rate of $5^\circ C/min$ upto $500^\circ C$ and $10^\circ C/min$ between $500^\circ C$ - $850^\circ C$ in a ULVAC thermoanalyser using sintered Al_2O_3 as the reference material for DTA.

Results and discussion

Analytical data of the complex conformed to the stoichiometry $UO_2(NO_3)_2 \cdot 2DHOA$. I.R spectrum of the complex clearly showed i) anhydrous nature of the product, ii) an absorption at $935cm^{-1}$, corresponding to the asymmetric stretch of the uranyl group and iii) a shift of $70 cm^{-1}$ in $\nu_{C=O}$ suggesting that DHOA moieties bind the uranyl ion through oxygen of the carbonyl group.

The thermal decomposition studies of $UO_2(NO_3)_2 \cdot 2DHOA$ in air showed three main stages in its decomposition (Table I). These three steps were clearly indicated by three arrests in the T.G curve. % Wt. loss at the end of first step agreed well (within 1.1%) with that expected from the release of two DHOA molecules. It was possible to correlate the weight loss in the second step to the formation of a polymeric uranyl nitrate complex of the type $U_2O_5(NO_3)_2$ [3]. Weight loss in the third step agreed well (within 1%) with that expected from the formation of U_3O_8 ,

which was reasonably constant in the temperature range 500 - $850^\circ C$. Whereas the first T.G step corresponded to two DTA exothermic peaks, each of second and third T.G steps corresponded to single DTA exothermic peaks.

The DTA data and TG temperatures for all three stages are also given in Table I. Occurrence of $220^\circ C$ DTA peak without any distinct step in TG suggested that the product formed is not stable under the experimental conditions chosen in the present work. The kinetics of the different stages of decomposition as seen from the TG curve was also investigated following various approaches reported in the literature [4,5]. TG data for all three steps were found to fit well to Horowitz-Metzger's method [6] for the kinetic analysis of non isothermal data of a first-order reaction. In this method $\log[\log(W_0/W)]$ was plotted versus θ where W_0 and W are the weights of the sample initially and at time t respectively and $\theta = T - T_s$ where T is the temperature corresponding to weight W of the sample and T_s is the peak temperature. The slope of the straight line thus obtained is given by $E/2.303RT_s^2$ where R is the gas constant and E is the energy of activation. The activation energy (E) values calculated from the TG curve by this method for the different stages of thermal decomposition of $UO_2(NO_3)_2 \cdot 2DHOA$ are also presented in table I.

Table 1: Thermal Decomposition Data for $\text{UO}_2(\text{NO}_3)_2 \cdot 2\text{DHOA}$

Sge No.	DTA peak temp. ($^{\circ}\text{C}$)	TG Temp ($^{\circ}\text{C}$)			Wt. loss (%)		Product formed	E (KJ mol^{-1})
		T_i	T_s	T_f	Expt	Theor		
1	220 (Exo) 290 (Exo)	200	285	295	61.9	61.2	$\text{UO}_2(\text{NO}_3)_2$	59.5
2	330 (Exo)	305	325	345	65.9	66.5	$\text{U}_2\text{O}_5(\text{NO}_3)_2$	35.5
3	470 (Exo)	355	470	500	73.1	72.4	U_3O_8	30.2

T_i =Initial decomposition temperature

T_s =Decomposition maxima temperature

T_f =Final decomposition temperature

References

1. K.K.Gupta, Ph.D Thesis, University of Mumbai (1997).
2. P.B.Ruikar, Ph.D Thesis, University of Mumbai (1992).
3. C.C.Addison, H.A.J.Champ, N.Hodge and A.H.Norbury, J.Chem. Soc; (1964) 2354.
4. A.W.Coats and J.P.Redfern, Nature, 68 (1964) 201.
5. E.S.Freeman and B.Carroll, J.Phys.Chem, 62 (1958) 394.
6. H.H.Horwitz and G.Metzer, Anal.Chem, 35 (1963)1464.

This paper was awarded the third prize in oral presentation at the Eleventh National Symposium on Thermal Analysis held at University of Jammu during March 2-5, 1998



Dr P.B. Ruikar joined Radiochemistry Division, BARC, in 1969, after graduating from Mumbai University in 1968. He obtained M.Sc. (Inorganic Chemistry) from University of Pune in 1987 and was awarded PhD (Chemistry) from Mumbai University in 1993. His special field of work is as follows: 1) Synthesis and characterisation of solid complexes of actinides with various novel extractants like TBP, CMP, CMPO, monoamides, diamides, sulphoxides, beta-diketones, etc, 2) Specification analysis of Pu fuels for metallic and non-metallic impurities, and 3) Effect of gamma radiolysis of various novel extractants on the extraction of actinides and fission products. 4) Recently, he is engaged with solvent

extraction studies of actinides with TBP using mixer settlers with respect to reprocessing and nuclear waste management. He is also involved in determining Limiting Organic Concentration (LOC) of plutonium with respect to DHOA.



After obtaining his M.Sc. (Analytical Chemistry) from Mumbai University, Mr S. Sriram joined Radiochemistry Division, BARC in 1996 as Junior Research Fellow under the BARC - Mumbai University Collaboration Scheme for Ph.D (Chemistry). His main area of research includes the studies on liquid - liquid extraction, synthesis and characterisation of solid actinide complexes, extraction chromatography and liquid membrane based separation of actinides and fission products using novel extractants like N,N'dialkyl amides and substituted malonamides relevant from the nuclear fuel reprocessing and waste management point of view.



Dr P.C.Kalsi after obtaining his M.Sc (1972) and Ph.D (1976) degrees from Jammu University joined as Post Doctoral Fellow of CSIR. He joined the Radiochemistry Division of BARC in 1978. His areas of interest include solid state nuclear track detectors, destructive and nondestructive assay techniques for nuclear materials accounting and thermal analysis of solid/ polymers. He is secretary of Nuclear Track Society of India (NTSI) and Indian Association of Solid State Chemists and Allied Scientists (ISCAS).



Dr. M.S.Nagar [M.Sc. (Inorganic Chemistry), 1964; Ph.D.(Chemistry), BHU,1968] was Senior Research Fellow (CSIR) until March 1968 when he joined Radiochemistry Division, BARC. His main area of research included the studies on radiation chemistry of actinides, radiolytic degradation of extractants in process chemistry of actinides, synthesis & characterization of novel extractants for actinides and solid actinide complexes. He was also involved in chemical quality control of FBTR fuels. His current interests include the separation and recovery techniques for actinides with organo-nitrogen (mono- & di-amides) and organo-phosphorous compounds (CMPO & substituted phosphonic acids) with respect to reprocessing & nuclear waste management.



Dr.V.K.Manchanda joined the Radiochemistry Division, BARC in 1969 after graduating from Delhi University and from 12th batch of Training School, BARC. He was awarded Ph.D. by Mumbai University in 1975 and he carried out Post-Doctoral work at UTEP, Texas, U.S.A. as Fulbright Scholar (1985-87). He was recognised as a Ph.D Guide in Chemistry by Mumbai University in 1993. He is working as Head, Actinide Chemistry Section, Radiochemistry Division since 1996. He has made original contributions in the following areas: i) Thermodynamics and kinetics of complexes of macrocyclic ligands with lanthanides and actinides, ii) Physico-chemical studies on actinide complexes, iii) Novel extractants of actinides, and iv) Chemical quality control of Pu based fuels.

Detection of blister formation and evaluation of pressure tube/calandria tube contact location by ultrasonic velocity ratio measurement technique

J.L Singh, Sunil Kumar, R. Keswani, S. Muralidhar,
A.K. Sengupta, H.N. Singh and K.C. Sahoo

Radiometallurgy Division
Bhabha Atomic Research Centre

Abstract

Presence of hydrogen in zircaloy pressure tube affects the velocity of ultrasound propagation. Both longitudinal wave velocity (V_L) and shear wave velocity (V_S) are affected depending on the concentration of hydrogen. Velocity ratio (V_L/V_S) changes as per the concentrations of hydrogen in different locations along the length of pressure tube. A hydride blister which forms at the pressure tube and calandria tube contact point is a distinct zone containing hydrogen 2-3 order of magnitude more than the parent matrix and hence, can be detected by sharp change in velocity ratio.

Introduction

WATER CORROSION OF ZIRCALOY PRESSURE tube produces hydrogen/deuterium (H/D) during reactor operation. Some fraction of this hydrogen is absorbed throughout the length of pressure tube. In case of contact between pressure tube (PT) and calandria tube (CT), hydrogen absorbed in the matrix migrates to the contact region (cold spot) under thermal and stress gradient. Over a length of time a point is reached when hydrogen concentration in the contact zone exceeds terminal solid solubility (TSS) limit and zirconium hydride

platelets begin to precipitate. The localised concentration of massive zirconium hydride is termed as "Blister". With time the blister grows in size and when it reaches a critical size it can crack. Presence of a cracked blister is a matter of concern for the safety of pressure tubes. Therefore, effort is to be made to detect the blisters using non-destructive technique before it grows to a critical size and cracks.

The measurement of ultrasonic velocity on pressure tube without accurate measurement of thickness can

be misleading. Thickness variations are present in the as manufactured pressure tubes. To avoid the effect of thickness variations, the velocity ratio (VR) technique have been adopted to detect blisters. This paper discusses the work carried out and result achieved at Radiometallurgy Division, BARC.

Ultrasonic testing technique

A 10 Mhz point focussed probe was used under normal incidence immersion condition to get 3-4 backwall echoes. A high frequency damped ultrasonic transducer which gives few oscillations is well suited for time of flight measurements. Normal incidence is achieved by maximising the signal coming from water/pressure tube interface. This is done by adjusting the probe and monitoring the signal on the screen. Fig.1 shows CRT screen photograph of typical ultrasonic echo pattern. The peaks A, B, & D are multiple backwall echoes produced by longitudinal wave trips. Peak C is by mode converted one way shear wave. The water column length between pressure tube surface and ultrasonic probe is adjusted such that shear wave peak C has maximum amplitude⁽¹⁾. The time of flight is measured with CRT screen fully expanded. The difference in time of flight (TOF) of C&B and D&B are measured in nanoseconds to calculate the ratio of the two velocities using derived correlation (1). The velocity ratio for unhydrided zircaloy is 2.05 and 2.8 for hydride blister.

$$\text{Velocity ratio } V_L/V_S = 1 + 2 \times (C-B)/(D-B) \quad \dots\dots\dots (1)$$

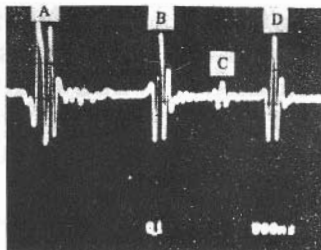


Fig.1 CRT screen echo pattern for velocity ratio measurement

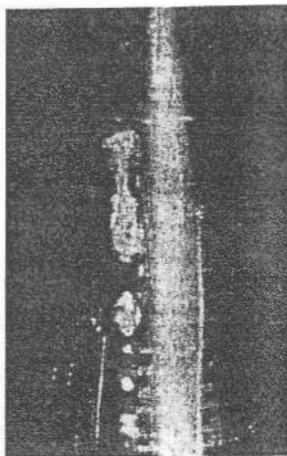
Scanning setup and measurement

The pressure tubes removed from the reactor are highly radioactive. A Lead shielded cell was constructed to carry out the velocity ratio measurement on irradiated pressure tube. A vertical water tank fitted with window was used to immerse pressure tube piece containing the pressure tube calandria tube contact locations. Perspex ring probe holder was fitted on a tripod inside the tank. A focussed normal probe was used for VR measurement. Two other probes were fitted for axial and circumferential flaw detection in the pressure tube wall. The pressure tube piece held by internal collet was translated up/down by a special pulley and drum arrangement with flexibility to rotate it by 360°. Counter weight was provided to balance the pressure tube piece weight for an easy and controlled movement. Interior of the cell was lightened by 100W electric bulbs. The visibility of contact locations was enhanced under immersion in water free from air bubbles. Through the window it

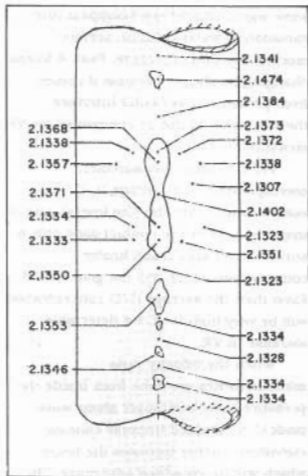
was possible to see the probe being accurately positioned on the contact locations while taking the measurements.

Fig.(2a) shows photograph of contact locations and Fig.(2b) shows the velocity ratios measured over different locations on the K-7 pressure tube. Measurements were taken in the centre of contact patches and on surrounding areas by moving the pressure tube both axially and circumferentially. As can be seen, velocity

ratios at contact locations are not different from that at surrounding areas which has about 30 ppm hydrogen/deuterium. This indicated that contact locations do not contain any blister. This was later confirmed by neutron radiography⁽²⁾ and metallography. Large number of measurements were taken but for brevity only few measured values are shown in the adjoining sketch Fig.2b.



(a)



(b)

Fig. 2a Contact locations of K-7 pressure tube; and Fig.2b Measured velocity ratios

Discussion

In a focussed beam peripheral longitudinal rays fall at an angle and get mode converted to shear wave. Shear wave signal appears separately due to its lower velocity. The amplitude of shear wave peak depends on crystal diameter and focal length. Wider the focussed beam cone, higher will be the amplitude of shear wave peak. Mode converted shear wave signals are normally weak. Shear wave signal should not disappear due to variation in water column, surface morphology and curvature. Peak A keeps changing its shape because it comes from pressure tube/water interface therefore should not be considered for VR measurements.

Velocity ratio measurement corresponds to the average H/D concentration over the (thickness) point of inspection. Over the contact zone only a surface layer may reach blister composition, which will not give VR 2.8. Even then the average H/D concentration will be very high to give a detectable increase in VR.

When the velocity ratio measurements are done from inside the pressure tube, a stronger shear wave peak C is obtained because concave curvature further focusses the beam which will be an added advantage. The disadvantage of carrying out VR measurement from inside is that it becomes a blind operation and further ID surface may have thick oxide with cracks and scratches which may affect signals.

Conclusion

The measurement carried out did not reveal any sharp change in velocity ratio at pressure tube and calandria tube contact zone compared to their surrounding areas. This indicates that no blisters have formed at the pressure tube calandria tube contact zone. This was also confirmed by neutron radiography and metallography. This technique will be refined by measurements on more number of pressure tubes removed from the reactor.

Acknowledgements

The authors would like to acknowledge the work done by the staff of Post Irradiation Examination Section for carrying out this work. The authors would like to thank Mr D.S.C. Purushottam, Director, Nuclear Fuels Group, for his encouragement and appreciation of this work.

References

1. Mair H.D., Moles M.D.C., and Dolbey M.P. The experience of uncracked blister detection in Bruce nuclear station, IAEA consultants meeting on the effect of hydride blisters on the integrity of PHWR pressure tubes, 25-29 July 1994 Vienna.
2. Gangotra S., et. al. Neutron radiography of contact location of irradiated zircaloy pressure tube from RAPS -II, 14th WCNDT Dec.8-13, 1996 New Delhi INDIA.

This paper received the Best Paper award in the technical session at the 14th World Conference on NDT & INTEXT NDT'96, New Delhi during December 8-13, 1996.



ISOMED-Plant for radiation sterilisation of medical products

*Edited and published by Dr. Viji Kaman, Head, Library & Information Services Division,
Bhabha Atomic Research Centre, Trombay, Mumbai-400 085.*

Editorial Management: T.C. Balan, Computer graphics & layout: P.A.S. Wariyar (For private circulation)

Available at URL: <http://www.barc.ernet.in>